DISSERTATION

A RESONANT ULTRASOUND SPECTROSCOPY STUDY OF HYDROGEN-ABSORBING INTERMETALLIC COMPOUNDS

Submitted by

Jennifer Eve Atteberry

Physics Department

In partial fulfillment of the requirements

for the degree of Doctor of Philosophy

Colorado State University

Fort Collins, Colorado

Spring 2004

COLORADO STATE UNIVERSITY

March 8, 2004

WE HEREBY RECOMMEND THAT THE DISSERTATION PREPARED UNDER OUR SUPERVISION BY JENNIFER EVE ATTEBERRY ENTITLED *A RESONANT ULTRASOUND SPECTROSCOPY STUDY OF HYDROGEN-ABSORBING INTERMETALLIC COMPOUNDS* BE ACCEPTED AS FULFILLING IN PART REQUIREMENTS FOR THE DEGREE OF DOCTOR OF PHILOSOPHY.

Committee on Graduate Work

Richard E. Eykholt

Carl E. Patton

Albert Migliori, Los Alamos National Lab

Gary E. Maciel, Chemistry Department

Adviser: Robert G. Leisure

Department Chair: David A. Krueger

ABSTRACT OF DISSERTATION

A RESONANT ULTRASOUND SPECTROSCOPY STUDY OF HYDROGEN-ABSORBING INTERMETALLIC COMPOUNDS

Resonant ultrasound spectroscopy (RUS) has been used to study four different hydrogen-absorbing intermetallic compounds. A fundamental study of the properties of hydrogen motion within a host metal lattice was undertaken on two different *C*15 Laves-phase compounds. These results have been obtained by determining the ultrasonic attenuation as a function of temperature from low temperatures (~0.5 K) up to room temperature and above. The hydrogen-absorbing intermetallic compounds, $TiCr_{1.8}$ and $LaNi_5$, were studied along with La-Al-Ni alloys. The temperature-dependence of the polycrystalline elastic moduli were determined from 3-410 K and used to calculate various elastic parameters.

Ultrasonic techniques have been used to study H(D) motion in $TaV_2H_{0.18}$, $TaV_2D_{0.17}$ and $TaV_2D_{0.50}$, providing strong evidence for the local quantum tunneling of hydrogen in Laves-phase materials, motion that remains extremely fast even at very low temperatures. For all three materials, a relatively large attenuation peak is observed near room temperature for measurement frequencies in the range of 1 MHz. This peak is associated with H(D) hopping between hexagons of *g* sites, the rate-limiting step for long-range diffusion. Much smaller attenuation peaks are observed for both H and D in each material at low temperatures and attributed to local motion

within a hexagon of g sites. These peaks exhibit totally non-classical behavior, with a large isotope effect on the H(D) motion. The relaxation rate is satisfactorily described by a non-classical expression, with a temperature-dependent mobile population of H(D). The parameters describing this motion for $TaV_2D_{0.50}$ are in agreement with NMR spin-lattice relaxation measurements at higher temperatures. The relaxation rate for $TaV_2D_{0.17}$ is somewhat faster than that for $TaV_2D_{0.50}$. Also, the relaxation rate for H is over an order of magnitude faster than that for D for similar concentrations. The value of 0.1 eV was found for the coupling parameter between intra-hexagon g sites and strain, a parameter for which no information was previously available. The low-temperature loss peak due to the local motion of hydrogen had not been seen prior to these measurements. Although this indicated a strong isotope effect, it was only possible to speculate as to why this peak was not observed. The current observation of the low-temperature peak for $TaV_2H_{0.18}$ provides convincing details concerning the local motion of hydrogen, including parameters for the extremely fast hydrogen motion and a consistent explanation of the strong isotope effect.

Previously undetected attenuation peaks, not associated with the local or long-range motion of H(D), are observed at an intermediate-temperature range as well, and are attributed to an order-disorder transition of H(D). It seems likely that this transition is related to the temperature-dependence of the mobile population.

Ultrasonic measurements also were made on the Laves-phase material $ZrCr_2H(D)_x$ with $x(H) = 0.09$, 0.15 and 0.31 and $x(D) = 0.12$. Attenuation peaks associated with H(D) motion between g-site hexagons are observed in all of these

materials for measurement frequencies of approximately 1.5 MHz. A large isotope effect is observed, which is interpreted in terms of quantum mechanical mechanisms of diffusion. In the temperature range of our measurements, the dominant mechanism appears to be tunneling transitions between ground states. This type of motion has been discussed theoretically. However, little evidence has been reported indicating the existence of this mechanism for motion. The current results provide strong evidence for this novel mode of hydrogen diffusion. The shear modulus of $ZrCr_2H_{0.09}$, $ZrCr_2H_{0.15}$ and $ZrCr_2D_{0.12}$ also has been measured. A small shift is observed in the modulus for each material at a temperature corresponding to the relevant peak in the ultrasonic loss, which is consistent with the interpretation that these peaks are due to H(D) relaxation.

In a more applied study, the elastic moduli of polycrystalline $TiCr_{1.8}$ have been measured over the temperature range of 3–410 K. The moduli display a normal temperature-dependence, approaching 0 K with zero slope and decreasing linearly with temperature at higher temperatures. The Debye temperature, calculated from the measured moduli, is found to be 500 K. An elastic energy contribution to the enthalpy of formation has been calculated from the present measurements and compared to the thermodynamic results. The comparison suggests that the electronic contribution to the enthalpy of formation is comparable in magnitude to the elastic contribution, but opposite in sign. Measurements such as these are useful to theorists for electronic structure calculations and for a complete understanding of hydrogen-metal materials.

Temperature-dependent measurements also have been made on poly-crystalline $LaAl_xNi_{5-x}$ with x ranging from 0 to 1. The elastic moduli have been determined and corrected for porosity so that values expected for the fully-dense material were found. The temperature-dependence in this case also resembles that of ordinary metals. Poisson's ratio is nearly temperature-independent with a value around 0.31. Our experimental values for the room-temperature shear and bulk moduli are in good agreement with theoretical values. The acoustic contribution to the low-temperature specific heat is calculated. The Debye temperatures, calculated from the 3 K moduli, are in good agreement with values reported from heat capacity measurements. The results of this work should prove useful in discerning trends or correlations that could help in the selection of new metal-hydride materials.

Jennifer Eve Atteberry
Physics Department
Colorado State University
Fort Collins, CO 80523
Spring 2004

Acknowledgements

I gratefully acknowledge the invaluable support of many people. First, I want to address the people in my personal life that have kept me going. I thank my husband for the love, patience, care and encouragement he has given me ever since we first knew each other. I thank my parents for loving me too, for supporting my dreams, and praying for me at all times. I thank my sister for keeping up with me when I am busy and helping me laugh. My incredible roommates and friends, Tina and Andrea, who kept me connected with the real world and made sure that I ate something other than cheese. And my larger circle of friends, who prayed for me, asked about my research and put up with my excitement and complaints about physics.

Next, I want to address the people in my professional life who cross over into my personal life as well, my physics friends. Special thanks go to Keir for training me as a new student in our lab and to Dennis for keeping me sane throughout all the long days taking data. I thank my original group of classmates (Sangita, Bob, Andy, etc.) for helping me survive the coursework. And the new guys (Kevin, Tony, Elijah, etc.) for making my life a bit more lively.

On the professional side, I would like to thank my advisor, Bob Leisure. There could never be his equal! I have benefited immensely from his expertise, advice, example and attitude. Also, I am grateful for the many fruitful collaborations

I have enjoyed during my work. Alexander Skripov (Urals Branch of the Academy of Sciences, Ekaterinburg, Russia) and Isaac Jacob (Ben-Gurion University of the Negev, Beer Sheva, Israel) have provided excellent samples to study and, along with Albert Migliori (National High Magnetic Field Lab, Los Alamos National Lab) and many others, have provided helpful insights on various topics.

Finally, I would like to express my incredible sense of blessing at being able to enjoy this much education. I have always loved to learn. It is a great privilege to live in a society that values education and opens doors for those who desire to learn. I intend always to pursue greater understanding, and through that understanding, to appreciate science, beauty, family, and the love of God even more.

Contents

Chapter 1: Introduction

1.1 Motivation for Study 1

1.2 Hydrogen-Absorbing Intermetallic Compounds 2

1.3 Review of Elasticity
- 1.3.1 A Brief History 4
- 1.3.2 Theoretical Background 5

References 13

Chapter 2: Experimental Details

2.1 History of Resonant Ultrasound Spectroscopy (RUS) 15

2.2 RUS Measurement Technique 16

2.3 Resonance Peak Analysis 23

2.4 Elastic Constants from RUS 26

2.5 Temperature-Dependent Measurements 32

References 39

Chapter 3: A Resonant Ultrasound Spectroscopy Study of Hydrogen Motion in the *C*15 Laves-Phase Compounds TaV_2 and $ZrCr_2$.

3.1 Background 41

3.2 Ultrasonic Evidence for Hydrogen Tunneling in a Laves-Phase Material: $TaV_2H(D)_x$.
- 3.2.1 Introduction and Experimental Details 49
- 3.2.2 Results and Discussion 52
- 3.2.3 Conclusions 66

3.3 Ultrasonic Measurements of H(D) Effects on the Laves-Phase Material $ZrCr_2H(D)_x$.
3.3.1 Introduction and Experimental Details 68
3.3.2 Results and Discussion 70
3.3.3 Conclusions 76

References 78

Chapter 4: A Resonant Ultrasound Spectroscopy Study of the Elastic Properties of the Hydrogen-Absorbing Compounds $TiCr_{1.8}$ and $LaAl_xNi_{5-x}$.

4.1 Background 81

4.2 Temperature Dependence of the Elastic Moduli of Polycrystalline $TiCr_{1.8}$.
4.2.1 Introduction and Experimental Details 85
4.2.2 Results and Discussion 87
4.2.3 Conclusions 95

4.3 Temperature Dependence of the Elastic Moduli of Polycrystalline $LaAl_xNi_{5-x}$.
4.3.1 Introduction and Experimental Details 96
4.3.2 Results and Discussion 99
4.3.3 Conclusions 108

References 109

Chapter 5: Conclusions 112

Chapter 1

Introduction

- 1.1 Motivation for Study
- 1.2 Hydrogen-Absorbing Intermetallic Compounds
- 1.3 Review of Elasticity
- References

1.1 Motivation for Study

The elastic constants that describe the response of a material to a small applied stress are dependent on the nature of the interatomic potentials.[1] Because of this, any physical property of the material that is related to the lattice can affect the elastic properties. Also, properties that interact with sound waves or with phonons in the material can change the elastic response or the elastic energy dissipation. For example, the free electrons in a metal can interact with the propagation of sound waves, causing elastic energy dissipation. With the onset of superconductivity the electrons pair up, dramatically decreasing the energy loss, resulting in a measurable effect on the ultrasonic loss of a metal due to superconductivity.[2]

The presence of a light interstitial atom within the host lattice can affect the elastic constants in several ways, including through expansion of the lattice,[3] through electronic effects,[4] and through re-orientation under the application of a strain.[3] An example of measurement of this type of change will be discussed in Section 3.3 for

$ZrCr_2$ upon the addition of hydrogen and deuterium. The motion of a light interstitial atom or defect within the host lattice can also affect the elastic energy absorption of the host material, most noticeably through the attenuation of sound within the sample. Examples of these types of measurements will be discussed in Section 3.2 for TaV_2 with hydrogen and deuterium motion among interstitial sites and in Section 3.3 for similar motion within $ZrCr_2$. The energy necessary to introduce hydrogen into a metal lattice is directly dependent on the elastic moduli. Therefore, elastic properties of potential hydrogen-storage materials or battery materials are important for material characterization. An example of the application of these measurements will be described in Section 4.2 for $TiCr_{1.8}$ and in Section 4.3 for La-Al-Ni alloys.

The connection of elastic properties to thermal properties is made through the Debye theory.[5] The Debye temperature and the acoustic contribution to the low-temperature specific heat can be calculated from the elastic moduli. Also, the anharmonic nature of the lattice results in temperature-dependence of the elastic constants.[6] Temperature-dependent studies can reveal phase transitions,[7,8] unusual electronic effects[9,10] and evidence for the anharmonic nature of the interatomic potentials.

1.2 Hydrogen-Absorbing Intermetallic Compounds

Metal-hydrogen materials are important for a number of technological reasons, primarily related to energy storage and battery applications. Interest in intermetallic compounds has grown due to their ability to absorb considerable quantities of hydrogen. This work reports studies on intermetallic AB_5 compounds and C15 Laves-phase AB_2 compounds. In these formulas, A represents an early

transition or rare-earth metal that has a strong affinity for hydrogen and B represents a later transition metal with a weaker affinity for hydrogen. All of these materials are able to absorb fairly large amounts of hydrogen reversibly. In particular, the Laves-phase compound $TaV_2H(D)_x$ forms stable homogeneous solid solutions with H(D) up to a maximum concentration of $x = 1.7$.[11]

Among other interesting topics of theoretical significance, the diffusion of a light interstitial atom such as hydrogen poses challenging theoretical problems.[12] The local environment of hydrogen in intermetallic compounds is often complex due to the large variety of interstitial sites in these compounds. Studies of the diffusion of H throughout the host lattice along with quantum-mechanical effects seen in this motion have been active areas of scientific inquiry.[13] Information about the diffusion of hydrogen within two Laves-phase intermetallic compounds has been determined through ultrasonic techniques and will be presented in Chapter 3.

Materials that can store such large amounts of hydrogen are also of interest in the new focus on a hydrogen economy, particularly for application to automobile power. Peter Hoffman notes, "The difficulty lies in how to carry hydrogen onboard a vehicle... Will hydrogen be carried in a metal hydride...? As a compressed gas in tanks...? As a cryogenic liquid...? Or will it be extracted from a carbonaceous fuel such as gasoline..., or from methanol...?"[14] Although the large weight of metal-hydrides limits their applicability, the advantages related to safety and capacity keep these materials among the list of possible solutions to the hydrogen storage problem.

Being able to move hydrogen easily in and out of host intermetallic compounds is important also for battery applications. Rechargeable Nickel-Metal-

Hydride (Ni-M-H) batteries are used extensively today[15] to power laptop computers, digital cameras, cellular phones and other weight-limited devices. One important property in the process of hydrogenation is the plateau pressure, the hydrogen pressure in the relatively flat region of the pressure-composition isotherm. Alloys such as LaM_xNi_{5-x} where M represents a metal atom that substitutes for Ni, are commonly used in applications because they exhibit a decrease in plateau pressure as compared to $LaNi_5$.[15] Elastic studies on these materials, such as those reported here, are useful for an evaluation of the elastic contribution to the hydrogen-hydrogen interaction energy[12] and the elastic energy associated with the precipitation of hydrides.[16,17] The lattice constants of the hydride are usually different than those of the host material resulting in misfit strains. These strains result in an elastic energy that affects the formation and decomposition of hydrides.[18,19,20,21,22] Information about the elasticity of the technologically important hydrogen-absorbing compounds $LaAl_xNi_{5-x}$ will be presented in Chapter 4.

1.3 Review of Elasticity

1.3.1 A Brief History

The elastic properties of materials provide the basis for understanding many of their physical characteristics. The beginning of this understanding occurred when someone first asked the question, "What happens when you apply a force to a material?" Does it bend? Does it break? How does it bend? How can we describe the bending? Galileo Galilei gets the credit for being the first person in recorded history to ask any such elasticity question in a meaningful way.[23] He proposed what is now known as Galilei's problem, in which he asked, "At what point will a beam

fracture under the force of its weight?" As the magnitude of the applied force increases, the type of deformation of the beam changes. In the elastic region of deformation, the object returns to its original form after the applied force is removed. Therefore, an elastic body is defined as one in which every point in the material returns to its equilibrium position after being subjected to a small stress. This type of elastic deformation is described by Hooke's Law. Expressed in 1-D, the displacement from equilibrium, x, is proportional to the applied force, F, in the following way:

$$F = -kx \tag{1}$$

where k is the constant of proportionality. Robert Hooke first published his law in 1678.[23] Many of the years following Hooke's statement of proportionality saw experiments performed using his law and theories propounded attempting to ground the law in mathematics. George Gabriel Stokes' memoir of 1845 is given credit[23] for the physical basis of generalizing Hooke's law for a solid body.

1.3.2 Theoretical Background

The generalization of Eq. (1) in 3-D also results in a description of the elastic body by elastic constants. The resulting generalized Hooke's Law has the form,

$$\sigma_{ij} = \sum_{i,j,k,l} C_{ijkl}\varepsilon_{kl}, \tag{2}$$

where σ_{ij} is an element of the stress tensor, ε_{kl} is an element of the strain tensor, and the C_{ijkl} make up a fourth-rank elastic constant tensor. The stress tensor can be defined by a force per unit area in the i direction on a plane of atoms with the normal to the surface in the j direction, in the following way,[24]

$$\sigma_{ij} = \lim_{\Delta A_j \to 0} \frac{\Delta F_i}{\Delta A_j}. \tag{3}$$

The strain tensor describes the deformation of the solid as a differential displacement with respect to direction, in the following way,[24]

$$\varepsilon_{ij} = \frac{1}{2}\left(\frac{\partial u_i}{\partial x_j} + \frac{\partial u_j}{\partial x_i} \right), \tag{4}$$

where the u_i are components of the displacement vector for a point with position x_i. The elastic constant tensor has 81 possible elements. General constraints, such as no external body torques and equality under an exchange of subscripts, reduce the number of elements to 21. This is the number of moduli necessary to describe a triclinic material, with the maximum amount of elastic anisotropy. Increasing the symmetry of a solid reduces the number of independent elements further.[24] In fact, for a material having maximum symmetry (an elastically isotropic material) there are only two independent elements of C_{ijkl}.[25] Two different constants are necessary because a solid will resist a change in volume and a change in shape.

Different representations of the elastic moduli of an isotropic material may be chosen. The polycrystalline materials studied in this report are elastically isotropic and are primarily described by the shear modulus (G) and the bulk modulus (B). The bulk modulus describes a change in volume without a change in shape, as pictured in Fig. 1.1. This type of deformation is called a dilatation. The shear modulus describes a change in shape without a change in volume, as pictured in Fig. 1.2. Any general body deformation can be factored into a dilatation and a shear. Therefore, B and G form a fundamental elastic-constant pair.[25]

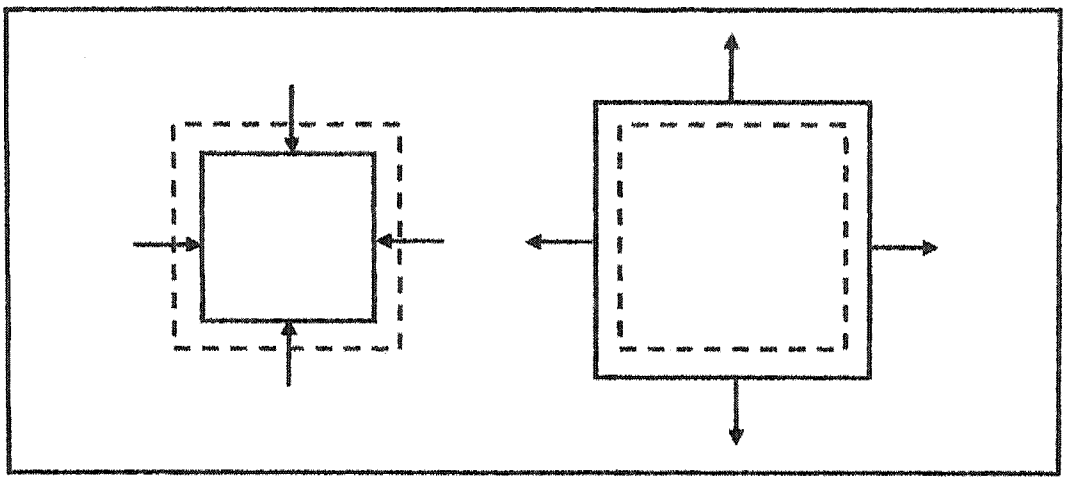

Figure 1.1 Representation of preserving shape while changing volume. This type of deformation is described by the bulk modulus.

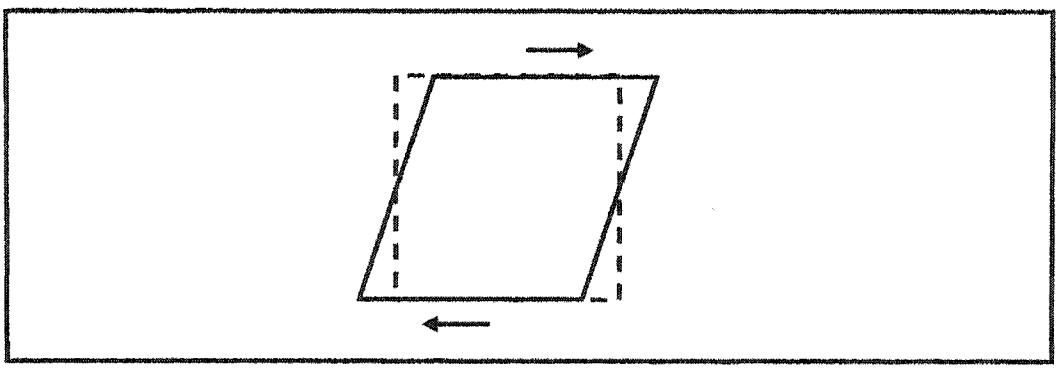

Figure 1.2 Representation of preserving volume while changing shape. This type of deformation is described by the shear modulus.

The measurement technique of resonant ultrasound spectroscopy, described in detail in Chapter 2, determines the aggregate elastic moduli, C_{11} and C_{44}. C_{44} is the normal shear modulus, G, described above. From C_{11} and C_{44}, the polycrystalline shear modulus (G), bulk modulus (B), Young's modulus (E) and Poisson's ratio (ν) can be computed using the equations

$$
\begin{aligned}
G &= C_{44}, \\
B &= \frac{3C_{11} - 4C_{44}}{3}, \\
E &= C_{44}\frac{3C_{11} - 4C_{44}}{C_{11} - C_{44}}, \\
\nu &= \frac{C_{11} - 2C_{44}}{2(C_{11} - C_{44})}.
\end{aligned}
\tag{5}
$$

Young's modulus, E, is defined as the ratio of the stress to the strain in the direction of an applied, uniaxial stress. An example of the deformation associated with E is shown in Fig. 1.3(a). Poisson's ratio can also be defined by such a situation, shown in Fig. 1.3(b), where ν is the negative ratio of the transverse and longitudinal strains (ε_2 and ε_1 respectively).

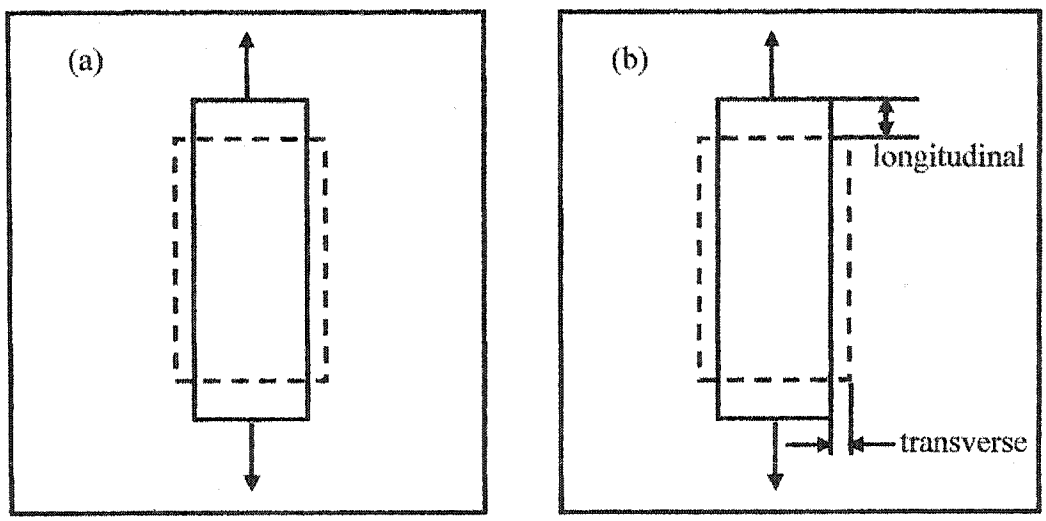

Fig. 1.3 (a) Representation of the type of deformation described by Young's modulus. (b) Illustration of deformation associated with Poisson's ratio.

In a real material, vibrations damp out over time due to intrinsic losses. We can take this into account by introducing a complex elastic constant into Hooke's Law.[26] A complex force constant represents one way to introduce loss. The following discussion corresponds to the arguments in Ref. 26. For the damped,

driven oscillator in 1-D, the resulting equation of motion is

$$m\frac{d^2x}{dt^2} = -k^* x + F_0 e^{i\omega t}, \tag{6}$$

where m is the mass, x is the displacement from equilibrium, $k^* = k_1 + ik_2$ is the new complex elastic constant, and $F_0 e^{i\omega t}$ is the driving term. The steady-state solution to Eq. (6) is $x = L(\omega)e^{-i\theta}e^{i\omega t}$, where θ is a phase shift and

$$\left|L(\omega)\right| = \frac{(F_0/m)}{\left(\left(\omega_0^2 - \omega^2\right)^2 + (k_2/m)^2\right)^{1/2}}. \tag{7}$$

This equation exhibits a resonant response centered around the undamped resonance frequency, ω_0. Near resonance, the width of the lineshape[26] is approximately $\Delta\omega = \omega_0 k_2 / k_1$. The loss is related to the width through the factor, Q, by the definition of the loss as $1/Q$ where $Q = \omega_0 / \Delta\omega$. Therefore, the loss is the ratio of the imaginary part to the real part of the elastic constant,

$$Q^{-1} = \frac{k_2}{k_1}. \tag{8}$$

A significant contribution to the ultrasonic loss is due to the time delay between the application of a stress and the response of the material to the value of stress applied. This time delay can be due to the reorientation of a light interstitial atom in the host material. For example, hydrogen hopping has been studied by use of ultrasonic attenuation in many systems. The motion of a hydrogen isotope between neighboring sites can be affected by the application of a time-dependent stress. Anelastic relaxation[27] occurs when nearby interstitial sites are affected differently by this applied stress causing the hydrogen to relocate to sites of lower energy. When

the applied ultrasonic frequency is comparable to the hydrogen hopping rate, the net effect is dissipation of the input energy. Modifying the stress-strain relation to include simple exponential relaxation with a single relaxation time, τ, yields

$$\sigma + \tau \frac{d\sigma}{dt} = C_R \varepsilon + \tau C_U \frac{d\varepsilon}{dt}, \tag{9}$$

where C_R and C_U are the relaxed and unrelaxed elastic constants, respectively. In our measurements, we apply an oscillating voltage (with ultrasonic frequency, $f = \omega / 2\pi$) to a transducer. The transducer oscillates mechanically in response to the oscillating voltage. As a result, stresses and strains are induced in our samples that can be represented by the following expressions

$$\sigma(\omega, t) = \sigma(\omega) e^{i\omega t}, \tag{10}$$

$$\varepsilon(\omega, t) = \varepsilon(\omega) e^{i\omega t}. \tag{11}$$

Substituting Eqs. (10) and (11) into Eq. (9) yields $\sigma(\omega) = C^*(\omega)\varepsilon(\omega)$ where C^*, the complex elastic constant is given by,

$$C^* = C_U + \frac{C_R - C_U}{1 + \omega^2 \tau^2} + i(C_U - C_R)\frac{\omega\tau}{1 + \omega^2 \tau^2}. \tag{12}$$

This is a complex elastic constant of the form $C^* = C_1 + iC_2$. Therefore, we have shown that including a non-zero response time for the material results in a complex, frequency-dependent elastic constant. Using the analogy with Eq. (8) we find that the loss due to relaxation (relaxation-attenuation) is

$$Q^{-1} = \frac{\Delta c}{c} \frac{\omega\tau}{1 + \omega^2 \tau^2}, \tag{13}$$

where we have ignored both the second term in Eq. (12) as compared to the first as well as the distinction between C_U and C_R in the denominator. The quantity $\Delta c / c$ is

usually referred to as the relaxation strength, where $\Delta c = C_U - C_R$. It can be seen from Eq. (13) that there will be a peak in the loss when the ultrasonic frequency is approximately equal to the relaxation rate. In other words, the amplitude of the loss is a maximum when the quantity $\omega\tau \approx 1$. The relaxation causes an associated change in the real part of the elastic constant, found from the first two terms of Eq. (12), which is

$$\delta c = \Delta c \frac{\omega^2\tau^2}{1+\omega^2\tau^2}. \tag{14}$$

This is seen as a step in the elastic constant (and resonance frequency) as a function of temperature when the quantity $\omega\tau \approx 1$. An example of a peak in the loss accompanied by dispersion in the resonance frequency, due to anelastic relaxation of deuterium, is shown in Fig. 1.4 for $TaV_2D_{0.50}$.

The procedure for determining Q from our measurements is described in Section 2.3. Chapter 3 describes two different materials in which the ultrasonic loss provides significant information about physical processes of hydrogen and deuterium motion within the host structure. Different expressions are discussed for the relaxation times and fit parameters are found for the H(D) motion. Evidence of dispersion in the resonant frequencies and the shear modulus is given. Chapter 3 also discusses an expression for the relaxation strength, including its dependence on hydrogen or deuterium concentration.

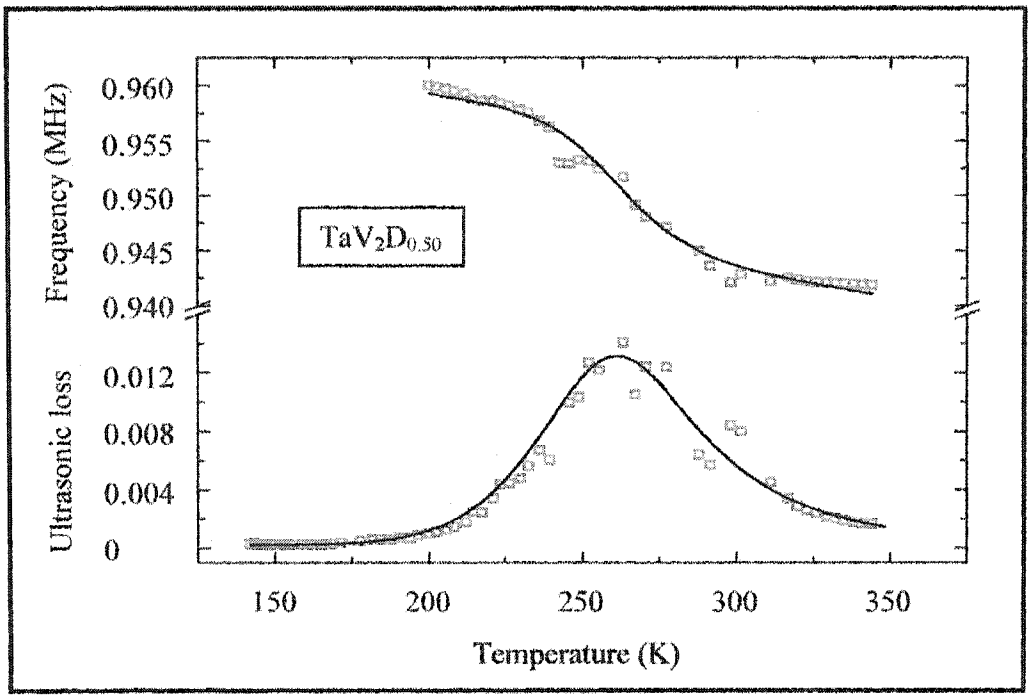

Figure 1.4 Temperature dependence of the resonant frequency and attenuation of a mechanical eigenmode in $TaV_2D_{0.50}$. The attenuation and dispersion are due to the anelastic relaxation of deuterium.

References

[1] J. S. Blakemore, *Solid State Physics* (Cambridge Univ. Press, Cambridge, 1985).

[2] A. B. Bhatia, *Ultrasonic Absorption: An Introduction to the Theory of Sound Absorption and Dispersion in Gases, Liquids and Solids* (Oxford Univ. Press, London, 1967).

[3] A. Magerl, B. Berre and G. Alefeld, Phys. Stat. Sol. A **36**, 161 (1976).

[4] A. C. Switendick in *Hydrogen in Metals I, Topics in Applied Physics* **28**, G. Alefeld and J. Volkl, eds., 101 (Springer, Berlin, 1978).

[5] N. W. Ashcroft and N. D. Mermin, *Solid State Physics* (Saunders College Publishing, USA, 1976).

[6] J. A. Garber and A. V. Granato, Phys. Rev. B **11**, 3990 (1975).

[7] W. L. Rehwald, Adv. Phys. **22**, 721 (1973).

[8] F. Willis and R. G. Leisure, Phys. Rev. B **54**, 9077 (1996).

[9] C. Weinmann and S. Steinemann, Solid State Commun. **15**, 281 (1974).

[10] K. Foster, J. E. Hightower, R. G. Leisure and A. V. Skripov, Phil. Mag. B **80**, 1667 (2000).

[11] J. F. Lynch, J. Phys. Chem. Solids **42**, 411 (1981).

[12] Y. Fukai, *The Hydrogen-Metal System* (Springer, Berlin, 1993).

[13] A. V. Skripov, Defect and Diffusion Forum **224-225**, 75 (2004).

[14] P. Hoffmann, *Tomorrow's Energy: Hydrogen, Fuel Cells, and the Prospects for a Cleaner Planet*, 103 (MIT Press, Cambridge, MA, 2001).

[15] F. Cuevas, J. –M. Joubert, M. Latroche and A. Percheron-Guégan, Appl. Phys. A **72**, 225 (2001).

[16] J. D. Eshelby, Proc. R. Soc. A **241**, 376 (1957).

[17] J. D. Eshelby in *Progress in Solid Mechanics*, I. N. Sneddon and R. Hill, eds. (North-Holland, Amsterdam, 1961).

[18] J. K. Lee, D. M. Barnett and H. I. Aaronson, Metall. Trans. A **8**, 963 (1977).

[19] J. K. Lee and W. C. Johnson, Acta Metall. **26**, 541 (1978).

[20] M. P. Puls, Acta Metall. **32**, 1259 (1984).

[21] B. J. Heuser and J. W. Althauser, J. Phys.: Condens. Matter **9**, 8945 (1997).

[22] B. J. Heuser and W. C. Chen, J. Phys.: Condens. Matter **11**, 7195 (1999).

[23] I. Todhunter and K. Pearson, *A History of the Theory of Elasticity and the Strength of Materials* (Dover Publications, Inc., New York, 1960).

[24] H. B. Huntington, *The Elastic Constants of Crystals* (Academic Press, New York, 1958).

[25] H. M. Ledbetter in *Materials at Low Temperatures*, 1 (American Society for Metals, Metals Park, OH, 1983).

[26] R. G. Leisure in *Resonant Ultrasound Spectroscopy*, 137 (Wiley, New York, 1997).

[27] A. S. Nowick and B. S. Berry, *Anelastic Relaxation in Solids* (Academic, New York, 1972).

Chapter 2

Experimental Details

- 2.1 History of Resonant Ultrasound Spectroscopy (RUS)
- 2.2 RUS Measurement Technique
- 2.3 Resonance Peak Analysis
- 2.4 Elastic Constants from RUS
- 2.5 Temperature-Dependent Measurements
- References

2.1 History of Resonant Ultrasound Spectroscopy (RUS)

Resonant ultrasound spectroscopy (RUS) measures vibrational eigenmode frequencies for solid samples of well-defined shapes.[1,2,3] From a small number (20 – 50) of the lowest of these frequencies, the full set of elastic constants for the solid can be determined.[4,5] By analyzing the resonance peak lineshapes, the quality values (Qs) can be measured to derive the ultrasonic loss.[6] Details of the RUS technique and analysis will be discussed in Sections 2.2 – 2.4.

A short 37 years after the theoretical grounding of a generalized Hooke's Law, Horace Lamb tackled, and solved, the analytical solution to the vibration of an elastically isotropic sphere.[7] Pioneers in the application of this solution (and in the development of RUS) hail from the field of geophysics, in which the vibrations of the earth, modeled as a sphere, are of great interest. As the theory developed and

computers became faster and more powerful, RUS expanded and evolved.[8] Currently, crystalline, polycrystalline, quasi-crystalline and amorphous materials with a variety of possible shapes (parallelepipeds, spheres, cylinders, cones, ellipsoids) and a variety of elastic symmetries (isotropic to monoclinic) have been measured with RUS to determine the material's full elastic constant tensor.

2.2 RUS Measurement Technique

Over the course of my studies in the Ultrasonics Laboratory at Colorado State University, I have made RUS measurements on samples shaped as rectangular parallelepipeds (RPs), right circular cylinders (cylinders), and approximately spherical solid droplets (spheres). Different experimental difficulties are associated with each type of sample. All of the materials we study in the Ultrasonics Lab are the result of collaborations with others who fabricate the materials using their own facilities. Early in my graduate work, we received cylindrical copper alloy samples from Ansonia Copper and Brass, hoping to investigate the results of extrusion on the elastic properties of a metal. Although the results were inconclusive, it gave me an opportunity to experience dealing with cylindrical samples. The major difficulty encountered was due to the degeneracy of modes from the circular cross-section. If the sample is not perfectly circular, degeneracies may split, confusing the determination of resonance peaks. Also early in my graduate work, we received semi-spherical solid droplets of Ti-Zr-Ni quasi-crystals from Washington University in St. Louis, Missouri. Our lab is not currently set up to polish spherical samples accurately. The resulting difficulties were similar to those with the cylindrical samples. Since the samples were not perfectly spherical, modes that should be

degenerate were in fact split. However, determining which modes were split and which modes were degenerate was an intractable problem. The majority of samples that we receive from collaborators arrive in the form of button ingots. Therefore, the majority of our samples are cut and polished into highly accurate RPs, with each of the three dimensions different from the other two. This eliminates most of the problems with degenerate modes and with error accumulation due to inaccurate shape. Sample preparation begins with a measurement of the mass and rough measurement of the dimensions of the irregularly-shaped ingot. The sample is then cut into an approximate RP using a low-speed diamond saw, shown in Fig. 2.1.

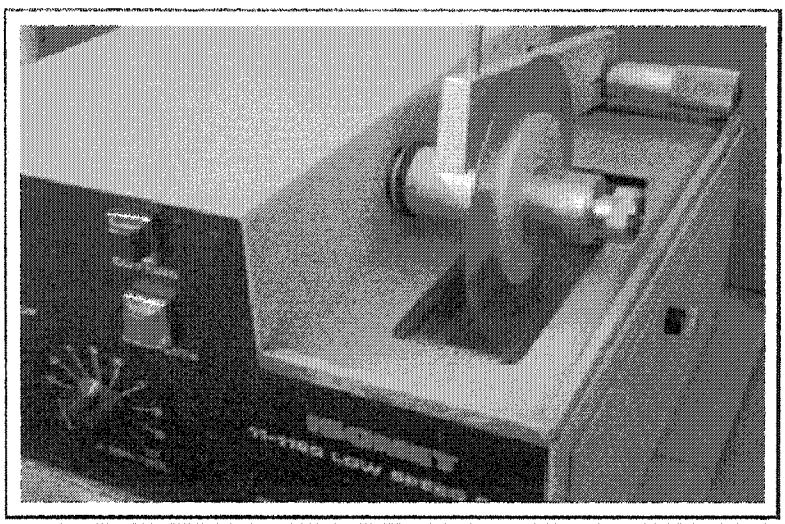

Figure 2.1 Low-speed diamond saw used to cut an approximately parallelepiped-shaped sample.

Using steel shims mounted around the sample on an optically flat surface,[1] as shown in Fig. 2.2, the top surface of the sample is ground and polished down to the dimension of the shims. Choosing a set of shims with a smaller dimension, the sample is turned over and again ground and polished down. These two opposing, parallel sides are then held tightly between the next set of shims in order to polish an

adjacent side in a perpendicular orientation. The process continues until all six sides are smooth, with opposing sides parallel and adjacent sides perpendicular, producing a highly accurate RP. The accuracy is judged visually by examining the sample under a microscope. The accuracy is also judged in the RUS fitting procedure by observing the effects on the fitting parameters when the dimensions are allowed to vary. This particular procedure will be described in more detail in Section 2.3. Finished sample dimensions are usually 1 – 2 mm on a side.

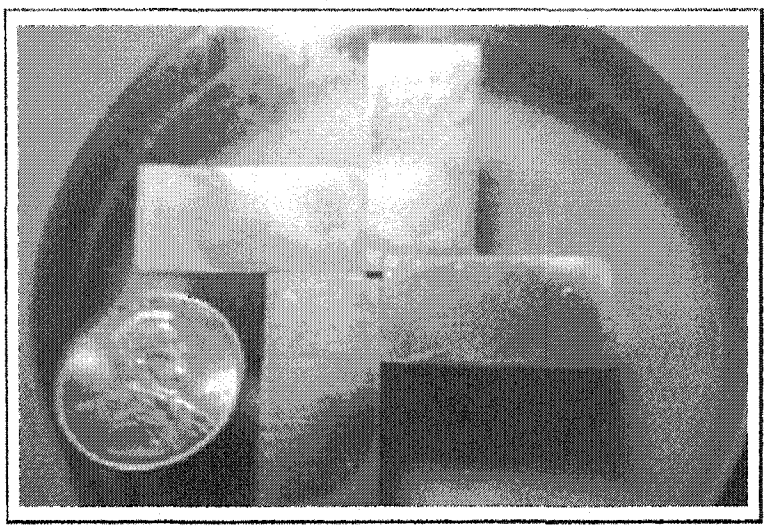

Figure 2.2 Arrangement of sample, shown in center, and steel shims on an optical flat used for polishing.

Polished samples are placed between two piezoelectric transducers in order to carry out the RUS measurements. One of the transducers is used to excite the mechanical resonances of the sample. The other transducer is used to detect these resonances. Depending on the assembly structure of the transducers and electronics, the sample is either mounted corner-to-corner, as sketched in Fig. 2.3 and pictured in Fig. 2.4, or placed with one face flat on the bottom transducer, as pictured in Fig. 2.5.

The key reason for the difference in the sample configuration pictured in Fig. 2.5 is that the entire face of the transducer is available for direct contact with the sample.

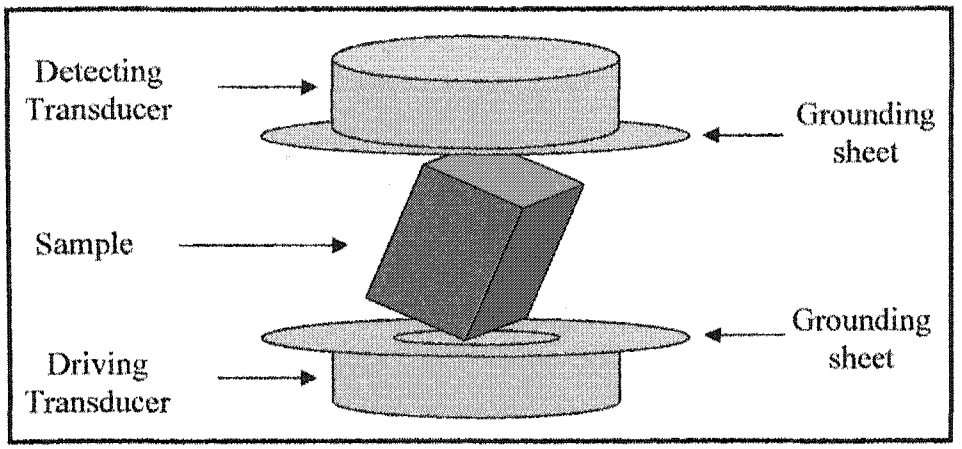

Figure 2.3 Schematic representation of sample-transducer arrangement.

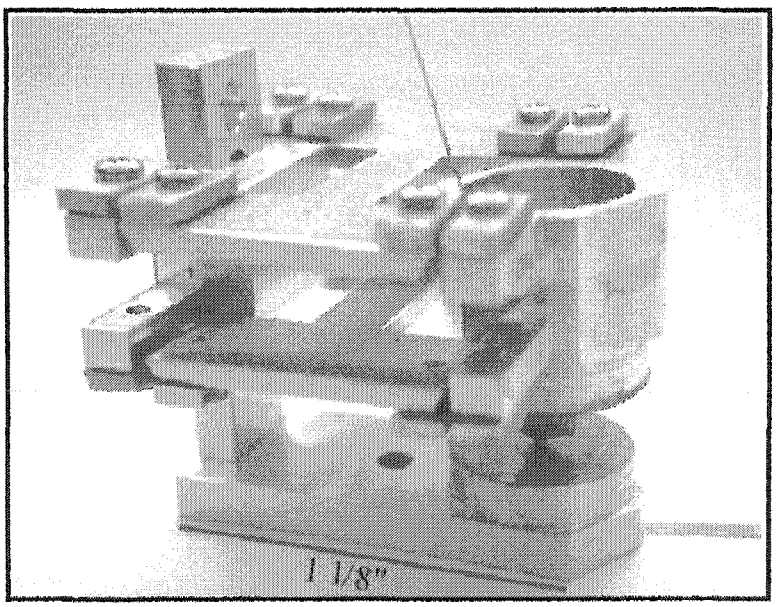

Figure 2.4 Picture of sample-transducer assembly previously used in the cryostat.

The new assembly, pictured in Fig. 2.5, has many advantages over the assembly we used previously. The RUS experimental station at the National High Magnetic Field Lab (NHMFL) at Los Alamos National Lab (LANL) first developed

and implemented the design. We received a picture of their setup that I used to draft plans for our own version. I machined the structure of the assembly from Stycast Epoxy (#1266) that was cast in our lab in the form of a solid tube. This epoxy is known to absorb sound at low temperatures. This is one of the distinct advantages gained from the new assembly. We always seek ways to cut down on sound transmission through the supporting structure of our assembly. Using this epoxy instead of a metal decreases noise levels in our low-temperature measurements.

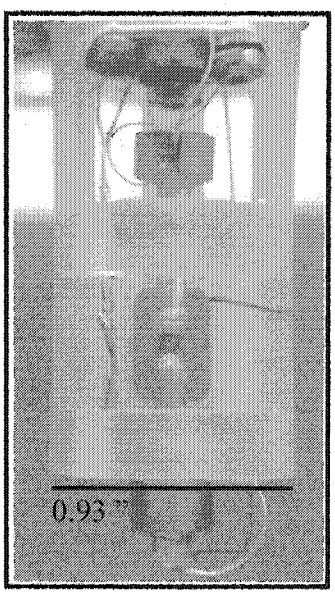

Figure 2.5 Picture of sample-transducer assembly currently used in the cryostat.

Wiring for the drive and detect transducers was changed to a gortex-insulated flexible coaxial cable. Grounding has proven to be a significant issue for reliable, clean measurements. Figure 2.6 is a sketch of the details for one transducer, wired as shown in Fig. 2.5. The outer coaxial conductor, which is grounded, serves to shield the inner conductor. This grounded conductor is also electrically connected to the faces of the transducers that are in contact with the sample. Since all of the samples I studied were metallic, it is important to have these faces electrically grounded.

Figure 2.7 is a schematic representation of the electrical setup including a section of wire representing a metallic sample.

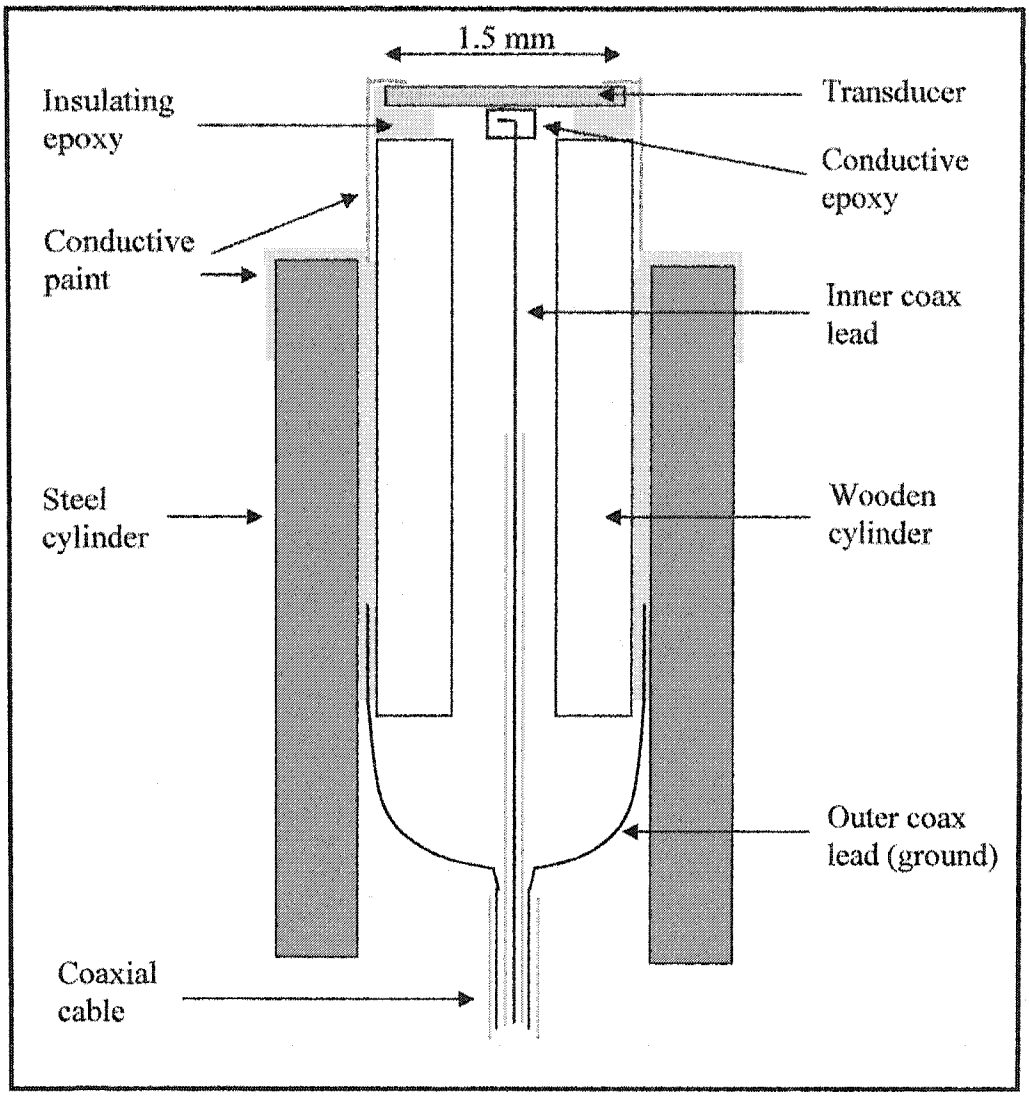

Figure 2.6 Sketch of the details for one transducer setup.

Another advantage of the new assembly is the flat-faced arrangement of the sample between the transducers. As mentioned above, we formerly mounted samples in a corner-to-corner configuration. It was thought that this arrangement was necessary in order to excite all the different mechanical modes of resonance for the sample. However, we are still able to detect all of the same modes with the new

arrangement. We have concluded that the important factor for the corner-to-corner arrangement was actually that the sample be in direct contact with the transducer. Positioning a millimeter-sized sample on a corner between two lightly contacting transducers was a difficult experimental task. The new face-to-face arrangement has significantly streamlined our experimental process. It also allows us to expand our range of sizes for samples. Previously, a sample could be too small to maneuver it into the corner-to-corner arrangement required, or too large to be stable in such a position.

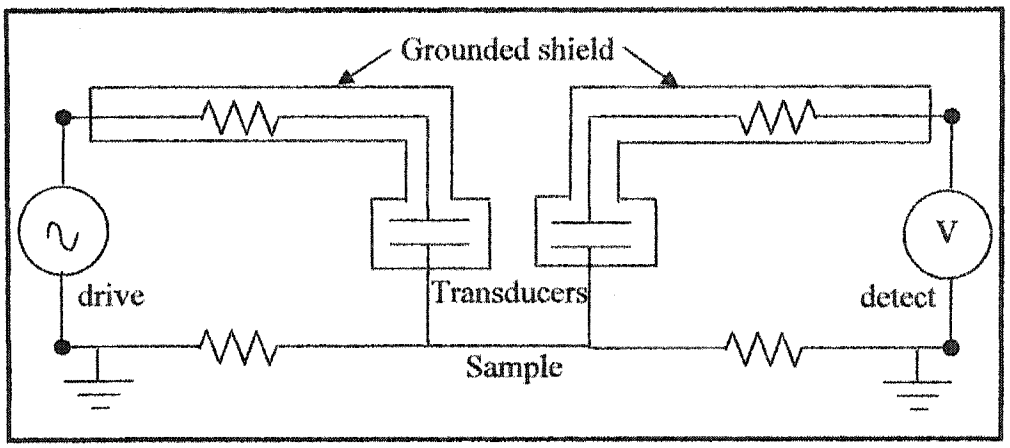

Figure 2.7 Schematic representation of the electrical setup.

The drive and detect transducers are electrically connected to a commercial spectrometer from Dynamic Resonance Systems, Inc. (DRS). The drive signal is swept through an ultrasonic frequency range, typically 400 kHz to 4 MHz, and the output is amplified in the detection stage. At frequencies corresponding to the natural resonances of the sample, a strong peak is recorded in the output signal. The various software programs that we use to record and analyze the data allow us to change the drive voltage, the gain of the output, the number of data points per sweep, the frequency range of each sweep, the number of averages for each data point taken, and

the time delay between each measurement step. Typical output for a high-Q sample is shown in Fig. 2.8. The spectrometer is able to record the part of the output signal that is in-phase with the driving signal as well as the part that is out-of-phase with the driving signal. In power units, the shape of each resonance peak is Lorentzian. Each peak is analyzed to determine the center point frequency and Q-value. Section 2.3 describes the resonance peak analysis. From the center-point frequencies, the elastic constants can be determined. This procedure is described in Section 2.4.

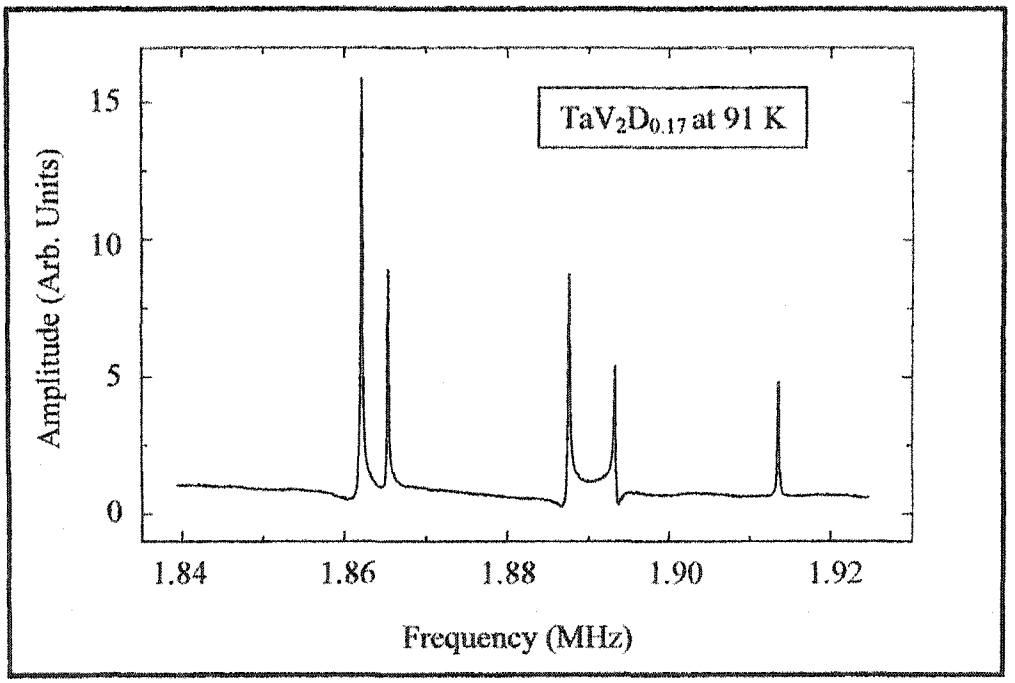

Figure 2.8 Section of a typical RUS scan for a high-Q sample. Five modes are observed. This spectrum was taken at CSU on the C15 Laves-phase material, $TaV_2D_{0.17}$.

2.3 Resonance Peak Analysis

Two pieces of information are important to glean from the resonance peaks: the center-point frequency, f_0, which is related to the determination of elastic constants, and the quality value, Q, which is related to the ultrasonic loss. As

mentioned in Section 2.2, the RUS technique is a phase-sensitive measurement. Therefore, the detected signal includes an in-phase and a quadrature part. In some measurement situations, this signal may be mixed with interfering signals that give an unwanted background to the RUS spectrum. Interference may be due to electrical grounding problems, vibrational noise from outside the system, or sound transmission through the gas surrounding the sample and through the sample-transducer assembly. In order to use all of the information generated from our measurements, we find it best to fit both the in-phase and the quadrature parts of our signal as well as the background to a theoretical expression that yields the desired parameters, f_0 and Q. From Section 1.3 we showed that for a damped, driven oscillator near a resonance frequency, the signal has the form,

$$x(f,t) = L(f)e^{-i2\pi ft} \tag{1}$$

where

$$L(f) = A\frac{e^{-i\theta}}{(f_0^2 - f^2) - i(f_0 f/Q)} \tag{2}$$

is a Lorentzian lineshape written in complex notation. In Eq. (2), A represents an amplitude, θ represents a phase shift, usually unknown (due to unknown shifts from electronics, transducers, etc.), between the drive voltage and the detected signal, and f is the frequency. The background is represented in terms of an expansion in frequency,[6,9]

$$g(f,t) = B(f)e^{-i2\pi ft} \tag{3}$$

with

$$B(f) = b_1 + ib_2 + \frac{(c_1 + ic_2)(f - f_0)}{f_0} + \ldots \tag{4}$$

where b_1, b_2, c_1, and c_2 are parameters characterizing the background signal. We do not keep terms higher in order than linear in frequency for Eq. (4). The sum of the Lorentzian, L, and the background, B, is written as

$$w(f) = u(f) - iv(f). \tag{5}$$

The detected signal is given by the real part of the total theoretical expression, $w(f)e^{-i2\pi ft}$, which is

$$s(f,t) = u(f)\cos(2\pi ft) - v(f)\sin(2\pi ft) \tag{6}$$

where $u(f)$ and $v(f)$ are used to fit the in-phase and quadrature signals, respectively. The expressions for these quantities are

$$u(f) = a\left(\frac{f_0^2}{Q}\right)\frac{(f_0^2 - f^2)\cos\theta + (f_0 f/Q)\sin\theta}{(f_0^2 - f^2)^2 + (f_0 f/Q)^2} + b_1 + \frac{c_1(f - f_0)}{f_0} \tag{7}$$

and

$$v(f) = -\left[a\left(\frac{f_0^2}{Q}\right)\frac{(f_0 f/Q)\cos\theta - (f_0^2 - f^2)\sin\theta}{(f_0^2 - f^2)^2 + (f_0 f/Q)^2} + b_2 + \frac{c_2(f - f_0)}{f_0}\right] \tag{8}$$

where $a = A(Q/f_0^2)$. Using these expressions, we are able to fit the entire set of data available to us, both the in-phase and the quadrature signals, to obtain the same parameters, f_0 and Q. An example of this type of fitting procedure is shown in Fig. 2.9 for a Ti-Zr-Ni *w*-phase crystalline approximant material obtained from Washington University in St. Louis. This sample has a relatively low Q; the sample has relatively high ultrasonic attenuation at this temperature.[10] Currently we have two options available to us for fitting the data: a non-linear least-squares algorithm used in Microcal Origin and a semi-automated non-linear least-squares algorithm that was written by Albert Migliori and Frank Willis and modified by Dennis Agosta.

The semi-automated program is able to compute an initial guess for the fitting parameters, by analyzing the input data. This feature, along with several others in the automated program, greatly increases the speed at which Q analysis is performed.

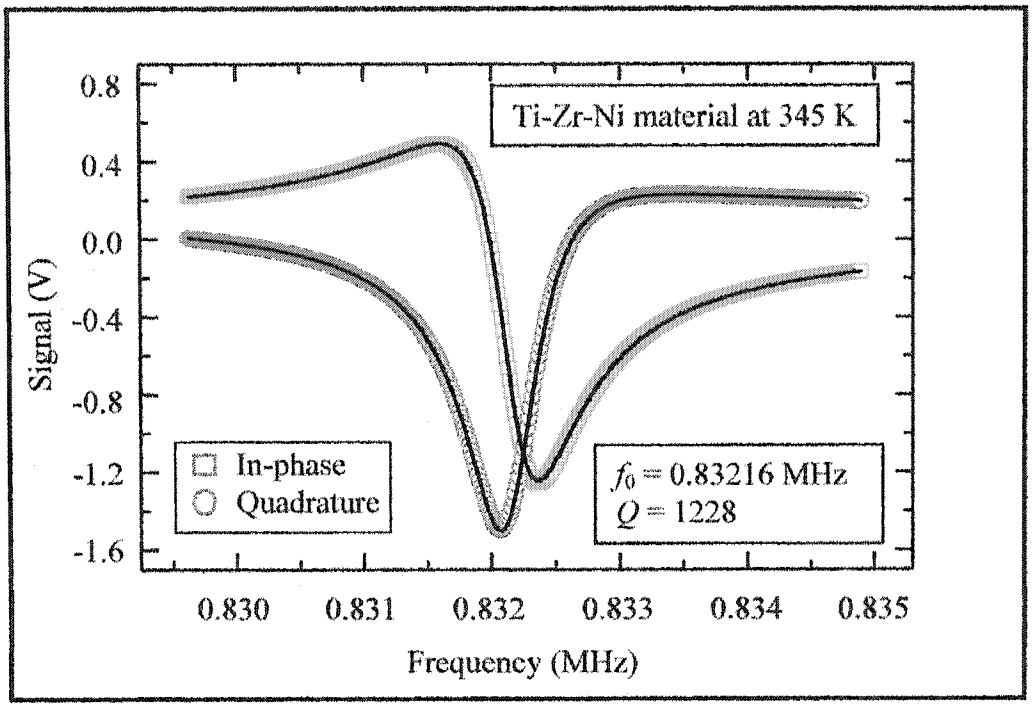

Figure 2.9 The in-phase and quadrature parts of an RUS signal with a background. These data were taken on a Ti-Zr-Ni *w*-phase cyrstalline approximant. The solid lines are the fits of Eqs. (7) and (8) to the data, yielding the parameters Q and f_0.

2.4 Elastic Constants from RUS

One of the major strengths of RUS is its capability to determine the complete elastic constant tensor, even for low-symmetry crystals, from a spectrum on a single, small sample. To determine the elastic constants, a number (dependent on the symmetry of the crystal) of the lower resonance frequencies are measured. For samples that are elastically isotropic, with only two independent elastic constants, 20 to 30 frequencies are generally sufficient. The center-point frequencies are

determined by the procedure described in Section 2.3. These frequencies are compared with computed ones that are calculated based on an initial set of elastic constants. The initial values are then varied in an iterative procedure to minimize the difference between the measured and computed frequencies. The computational methods for different sample shapes and different elastic symmetries have been developed and implemented by others.[1,2,4,5,11,12,13] A generalized approach appropriate for all geometries and crystal symmetries is described by Migliori and Sarrao[1] and is based on the technique of Lagrangian minimization. The discussion below follows their arguments.

The Lagrange expression, L, for a 1-D simple harmonic oscillator is

$$L = KE - PE = \frac{1}{2}m\dot{x}^2 - \frac{1}{2}kx^2, \tag{9}$$

where we have the usual expressions for the kinetic and potential energies, with m being the mass of the oscillator, x the displacement from equilibrium and k the elastic constant. Generalizing this Lagrangian for an elastic solid with volume V, density ρ, displacement vector $\bar{u}$, and linear elastic tensor c_{ijkl}, we obtain

$$L = \int_V (KE - PE)dV = \int_V \left(\frac{1}{2}\sum_i \rho\omega^2 u_i^2 - \frac{1}{2}\sum_{i,j,k,l} c_{ijkl}\frac{\partial u_i}{\partial x_j}\frac{\partial u_k}{\partial x_l} \right) dV, \tag{10}$$

where ω is the angular frequency. Here i, j, k, and l run from 1 to 3, corresponding to the three directions of space, and the components of the displacement vector are assumed to have harmonic time dependence, given by

$$u_i(t) = u_{i,0}e^{i\omega t}. \tag{11}$$

In order to find the equations of motion for the elastic solid, we wish to set the variation of the Lagrangian equal to zero. Allowing the displacements to vary in the following way,

$$u_m \rightarrow u_m + \delta u_m, \tag{12}$$

where m is a general subscript, we can find δL. Breaking Eq. (10) back down into kinetic and potential energy terms and making the substitution of Eq. (12) yields

$$KE + \delta KE = \frac{1}{2}\sum_i \rho\omega^2 (u_i^2 + 2u_i \delta u_i), \tag{13}$$

and

$$PE + \delta PE = \frac{1}{2}\sum_{i,j,k,l} c_{ijkl}\left[\frac{\partial u_i}{\partial x_j}\frac{\partial u_k}{\partial x_l} + \frac{\partial u_i}{\partial x_j}\frac{\partial(\delta u_k)}{\partial x_l} + \frac{\partial(\delta u_i)}{\partial x_j}\frac{\partial u_k}{\partial x_l}\right] \tag{14}$$

to first order in δu_m. The second and third terms of Eq. (14) are equivalent, giving

$$\delta L = \int_V \left[\sum_i \rho\omega^2 u_i \delta u_i - \sum_{i,j,k,l} c_{ijkl}\frac{\partial(\delta u_i)}{\partial x_j}\frac{\partial u_k}{\partial x_l}\right] dV \tag{15}$$

for the variation in the Lagrangian. To simplify this further, an integration by parts is performed on the second term, which results in

$$\begin{aligned}\int_V \left[\sum_{i,j,k,l} c_{ijkl}\frac{1}{\partial x_j}\partial(\delta u_i)\frac{\partial u_k}{\partial x_l}\right] dV = &-\int_V \left[\sum_{i,j,k,l} c_{ijkl}\frac{\partial^2 u_k}{\partial x_j \partial x_l}\delta u_i\right] dV \\ &+ \int_V \left[\sum_{i,j,k,l} c_{ijkl}\frac{\partial}{\partial x_j}\left(\frac{\partial u_k}{\partial x_l}\right)\delta u_i\right] dV.\end{aligned} \tag{16}$$

Using a combination of the divergence theorem and Stokes' theorem, the second term on the right hand side of Eq. (16) becomes

$$\int_S \left[\sum_{i,j,k,l} c_{ijkl}\bar{n}_j \frac{\partial u_k}{\partial x_l}\delta u_i\right] dS, \tag{17}$$

where $\bar{n}_j$ is the unit vector normal to the free surface, S. Putting Eqs. (16) and (17) into Eq. (15) results in

$$\delta L = \int_V \left[\sum_i \left(\rho\omega^2 u_i + \sum_{j,k,l} c_{ijkl} \frac{\partial^2 u_k}{\partial x_j \partial x_l} \right) \delta u_i \right] dV - \int_S \left[\sum_i \left(\sum_{j,k,l} c_{ijkl} \bar{n}_j \frac{\partial u_k}{\partial x_l} \right) \delta u_i \right] dS. \quad (18)$$

The expressions in parenthesis in Eq. (18) are equal to zero yielding two important pieces of information. The first expression yields the elastic wave equation. The second expresses boundary conditions for a freely vibrating surface. Therefore, the u_i that satisfy Eq. (18) are those that have normal modes of free oscillation with frequency ω. The Ritz method expands the u_i in an appropriate set of basis functions, with the result that the resonance frequencies can be calculated numerically. Following the lead of Visscher,[5] Migliori and Sarrao[1] suggest using powers of Cartesian coordinates,

$$u_i = \sum_{l,m,n} a_{ilmn} x^l y^m z^n, \quad (19)$$

where l, m, and n are three nonnegative integers. Eq. (19) is put into Eq. (10) and the derivatives of the Lagrangian with respect to the a_{ilmn} are set equal to zero. This results in an eigenvalue problem which can be solved numerically to determine the resonance frequencies (eigenvalues) and the displacements (eigenvectors) for a particular shape. This method is flexible enough to accommodate many different sample shapes (ranging from spheres to parallelepipeds). The basis functions can also be expressed in cylindrical coordinates,[14,15] which is particularly useful for crystals with trigonal symmetry. The technique described above considers a simple linear elastic body, without allowing for external electric or magnetic fields. Others[4,12,16] have applied the Ritz method using a different set of basis functions

(Legendre polynomials). Piezoelectric materials have been looked at closely in these terms,[11,16,17,18] determining not only the second-order elastic constants, c_{ijkl}, but also the piezoelectric constants from resonance frequency values.

In our lab, we have used the formulation of Migliori and Sarrao[1] to determine the second-order elastic constants for linear elastic motion of rectangular parallelepipeds (RPs) from a single frequency spectrum. The measured frequencies are compared with those calculated using the above technique. The initial values used to compute frequency are then iterated to provide a better match between measurement and calculation. An example of the output from this type of fit for an elastically isotropic sample, having only two independent elastic constants, is shown in Fig. 2.10. The red boxes enclose the free parameters (those that the fitting procedure determines): in this case, c_{11} and c_{44}. All of the other constants are dependent on these two. The blue circles enclose the input parameters for the sample: the mass and the RP's three dimensions. The column labeled "fex" contains the measured values of the resonance frequencies, determined from fitting the Lorentzian lineshapes (described in Section 2.3). The column labeled "fr" contains the calculated resonance frequencies, determined from applying the Ritz method (described above). The column labeled "%err" contains the percent difference between the measured and computed frequencies. The column labeled "wt" shows what weight, between 0 and 1, was assigned to each measured frequency. The columns, "k", "i", and "df/d(moduli)" contain information about the particular resonance mode and its dependence on the two free moduli.

$LaAl_{0.5}Ni_{4.5}$ 270 K
free moduli are *c11, c44*
using 10 order polynomials mass= 0.0431 gm

n	fex	fr	%err	wt	k	i	df/d(moduli)	
1	0.539170	0.535040	-0.77	0.00	4	1	0.00	1.00
2	0.723734	0.722624	-0.15	1.00	1	2	0.08	0.92
3	0.791660	0.792047	0.05	1.00	7	2	0.11	0.89
4	0.818088	0.815200	-0.35	1.00	4	2	0.00	1.00
5	0.829192	0.829515	0.04	1.00	8	2	0.01	0.99
6	0.921582	0.923919	0.25	1.00	5	1	0.02	0.98
7	0.932704	0.932696	0.00	1.00	1	3	0.26	0.74
8	0.937439	0.937431	0.00	1.00	2	2	0.01	0.99
9	0.950654	0.951926	0.13	1.00	6	2	0.09	0.91
10	0.967942	0.964295	-0.38	1.00	3	2	0.04	0.96
11	1.020700	1.023653	0.29	1.00	3	3	0.07	0.93
12	1.030720	1.028200	-0.24	1.00	5	2	0.06	0.94
13	1.054420	1.053587	-0.08	1.00	2	3	0.12	0.88
14	1.112180	1.118033	0.53	1.00	5	3	0.06	0.94
15	1.174950	1.169931	-0.43	1.00	3	4	0.03	0.97
16	1.253130	1.254637	0.12	1.00	7	3	0.09	0.91
17	1.293940	1.294829	0.07	1.00	6	3	0.07	0.93
18	1.295350	1.297793	0.19	1.00	4	3	0.06	0.94
19	1.313790	1.315926	0.16	1.00	8	3	0.10	0.90
20	1.317110	1.319004	0.14	1.00	2	4	0.03	0.97

Bulk Modulus= 129.4 GPa

c11	c22	c33	c23	c13	c12	*c44*	c55	c66 (GPa)
200.97	200.97	200.97	93.69	93.69	93.69	*53.64*	53.64	53.64

d1	d2	d3 (cm)
0.14143	0.17969	0.20545

loop# 4 rms error= 0.2213 %, changed by -.0000009 %

chisquare increased 2% by the following % changes in
independent parameters
0.75 -0.07
0.00 0.07

Figure 2.10 Portion of the output from an RUS fit for $LaAl_{0.5}Ni_{4.5}$. Circled values are input parameters for the sample. Boxed values are output elastic parameters determined from the fit.

Several factors that indicate the reliability of an RUS fit appear in Fig. 2.10. The root mean square error (rms) of 0.2213 % is one indication of a good fit. We generally do not trust a fit with an rms error of > 0.4 %. Another requirement for a reliable fit is that the absolute value of all the numbers in the column labeled "%err" is less than one. Although not explicitly shown in Fig. 2.10, another indication of reliability is the effect on the fit of allowing the sample dimensions to vary. If the fit is good, allowing the dimensions to vary should result in values for the dimensions that lie within the measurement error, and values of c_{11}, c_{44} and rms error that do not change dramatically. The last section of the output is an error matrix. The biggest entry in the first column is the approximate error bar for c_{11}. The biggest entry in the second column is for c_{44}. These errors are calculated based on the steepness of the surface of parameter space surrounding the minimum. The shear moduli usually seem to fit better and have smaller error bars, which is due to the fact that the lower frequency modes are more dependent on shear. Typical error bars for a good fit of our moduli are ~ 0.8 % for c_{11} and ~ 0.15 % for c_{44}. If all of these factors indicate a good fit, we generally proceed with confidence, calculating other values of interest from the elastic parameters given in the fit, or continuing our measurements over a range of temperatures.

2.5 Temperature-Dependent Measurements

Ultrasonic measurements determine the second-order adiabatic elastic constants. They are adiabatic because there is essentially no exchange of heat between different parts of the sample during a vibration period. The second-order elastic constants of materials are given by the second derivative of a thermodynamic

potential with respect to strain.[19] For samples in which entropy is held constant, the adiabatic elastic constants are determined from the internal energy, U. For an elastic material, in which displacements from equilibrium may be considered to be small, the state function may be expanded in the following way,

$$\frac{1}{V_0}U(X,\varepsilon_{ij},S)=\frac{1}{V_0}U(x,0,S)+\sigma_{ij}\varepsilon_{ij}+\frac{1}{2}C_{ijkl}\varepsilon_{ij}\varepsilon_{kl}+... \tag{20}$$

where V_0, X, and σ_{ij} are, respectively, the volume, position, and stress of the material in an initial configuration, x is the final position, S is the entropy and ε_{ij} is the strain. From Eq. (20) we see that the second-order adiabatic elastic constants are given by[20]

$$C_{ijkl}=\frac{1}{V_0}\left(\frac{\partial^2 U}{\partial\varepsilon_{ij}\partial\varepsilon_{kl}}\right)_S. \tag{21}$$

The internal energy, U, for an elastic solid consisting of N particles, vibrating with small amplitude may be expressed as[20,21]

$$U=U_0+\sum_{\alpha=1}^{3N}\left(\frac{1}{2}+n_\alpha\right)\hbar\omega_\alpha, \tag{22}$$

where U_0 is the equilibrium potential energy, ω_α is an angular frequency associated with one of the $3N$ normal modes of vibration of the system and n_α is the average number of phonons at frequency ω_α. This expression is based on the *harmonic approximation*,[21] in which both U_0 and ω_α are independent of temperature and ω_α is independent of strain. Therefore, the elastic constants are determined from the second derivatives of U_0 with respect to strain, and are also independent of temperature.

In order to take into account the temperature-dependence of the elastic constants, the anharmonic nature of the lattice vibrations must be included. Garber and Granato[20] have included an indirect temperature-dependence for U_0 and ω_α through the temperature-dependence of the lattice dimensions. This results in a term linear in temperature at higher temperatures, with the intercept at 0 K being the value of the elastic constant for a static lattice. At low temperature, there is a T^4 term, with the intercept at 0 K being at a lower value for the elastic constant (softer) because of zero-point effects. In metals there is also a contribution from the conduction electrons. For simple metals the electrons contribute a T^2 term at low temperatures.[22] These effects are shown schematically in Fig. 2.11, along with a curve with normal temperature-dependence for a metal. The overall result, for typical materials, is that the elastic moduli approach 0 K with zero slope and decrease monotonically with increasing temperature. This simple picture is not applicable to materials undergoing phase transitions[23,24] or to materials with more complicated electronic structures.[25,26,27]

This work reports temperature-dependent RUS measurements over a range of 0.5 K to 415 K. Low-temperature data (from 0.5K to 40 K) reported in Chapter 3 were taken in a ^{3}He cryostat at LANL-NHMFL under the presence of a 1 Tesla magnetic field. All other measurements were performed at Colorado State University in the Ultrasonics Lab. Measurements from 3.2 K to just above room temperature were made in a commercial ^{4}He cryostat built by Oxford Instruments, using a commercial temperature controller by Conductus and a home-built sample-transducer assembly, described in Section 2.2. Measurements above room temperature were

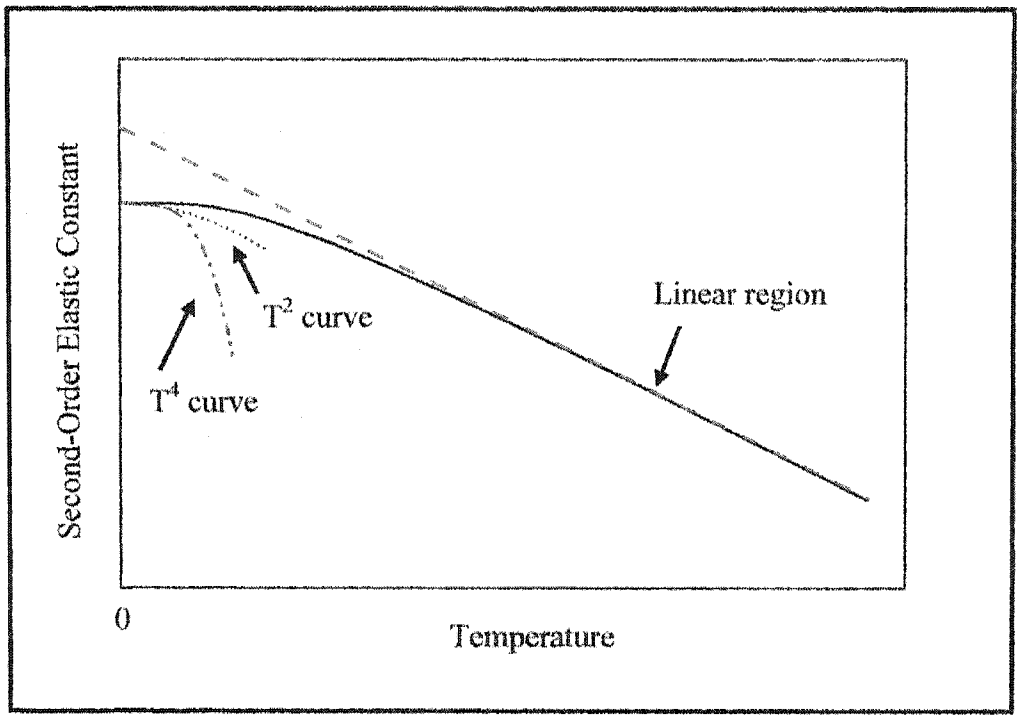

Fig. 2.11 Effects on the temperature-dependence of the second-order elastic constant. The solid black line is typical behavior for a simple metal.

made using a commercial oven and temperature controller from Lindberg. Many of the materials studied showed a normal temperature-dependence,[26,28,29,30] including $TiCr_{1.8}$ and alloyed samples of $LaAl_xNi_{5-x}$. Fig. 2.12 shows shear modulus data for $LaAl_xNi_{5-x}$ with $x = 0$, 0.25, 0.50, and 1.00 over the temperature range of 3 K to 415 K. These data follow the expected behavior for normal metals, approaching 0 K with zero slope and decreasing monotonically with increasing temperature.

Details of the operation of the ^{4}He cryostat have been reported elsewhere.[31] Only one important aspect for successful operation will be discussed here, and that is the isolation of the cryostat and sample from vibrational and electrical interference. The cryostat itself is a "static bath" system, in which the sample space is isolated from the gas-flow region. This allows the sample space to be kept at a low pressure

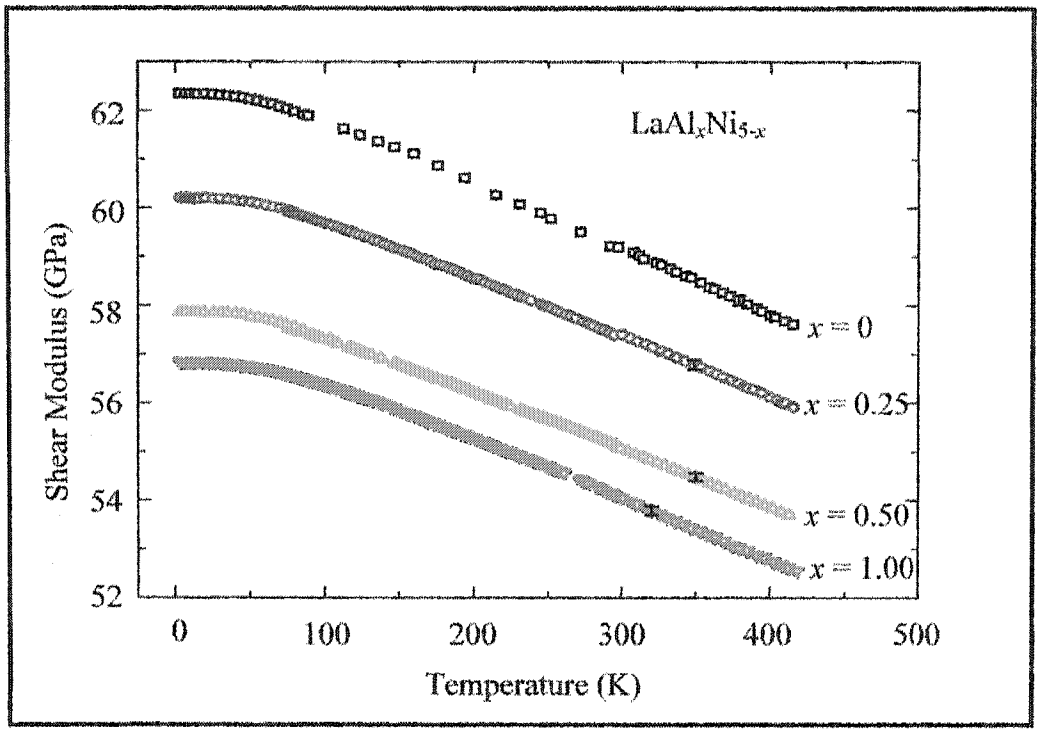

Fig. 2.12 Shear modulus of polycrystalline $LaAl_xNi_{5-x}$ versus temperature. The temperature-dependence is characteristic of simple materials.

of helium gas. For our experiments this pressure was kept around 3 Torr, allowing heat exchange between the walls and the sample, but cutting down on any ultrasonic coupling through vibrational modes of the surrounding gas. Another source of vibrational interference is transmission of sound through the sample-transducer assembly. As mentioned in Section 2.2 this interference has been reduced by changing the material of the support assembly from a metal to a plastic. The plastic, an epoxy, is known to absorb sound at low temperatures. Any vibrations of the cryostat itself also may contribute to signal noise and interference. These sources of noise may be due to pump connections, cryogen transfer ports, vibrations of the air in the room, vibrations through the floor or support structure, etc. Considerable effort was put into reducing any background noise and interference from these sources. A

sound-absorbing box was built and insulated in which the entire structure of the cryostat was placed. All access ports for pumping were connected via flexible tubing. The pumping line for cooling the cryostat was immersed in a sandbox, in order to damp any transverse or longitudinal vibrations of the line. And finally, the cryostat was placed on 5 Sorbothane feet. The Sorbothane helped to isolate the system from floor vibrations. In terms of electrical issues, ground loops and any major fluctuations in temperature during measurement can contribute to an electrical offset or electrical noise. Grounding considerations have been discussed in Section 2.2. In order to acquire clean data, it has been found that the temperature must be stable during frequency sweeps. When taking measurements over a large range of temperature, allowing the temperature to stabilize becomes a limiting factor in the quality and amount of data that can be acquired. Partially in order to address problems of temperature control, I have modified an automated data acquisition program originally developed by Jon Betts at LANL-NHMFL. This program allows the user to set temperature stability parameters for the entire temperature range and leave the system to run. Being able to run the system overnight has allowed us both to increase the temperature stabilization time between temperature steps and to take data at smaller temperature increments than was feasible when data was taken manually. Implementation of the data automation program has resulted in less noise due to better temperature stability and greater certainty in our data due to the larger number of data points acquired. All of the steps that have been taken to address the concerns of signal interference resulted in cleaner resonance signals and lower overall background sound attenuation and scatter as compared to our earlier work.

These considerations are particularly important in measurements of ultrasonic attenuation. For many of our experiments, the temperature-dependence of the ultrasonic loss reveals interesting aspects of the physics in our materials. For example, for a material with a Debye-type relaxation (as described in Section 1.3) a peak occurs in the ultrasonic loss at a temperature corresponding to the point at which the measurement frequency is approximately equal to the relaxation frequency. Determination of the ultrasonic loss as a function of temperature can result in the determination of the hopping frequency of an interstitial atom, such as hydrogen, between available sites.[6,32,33] Temperature-dependent studies of ultrasonic loss and of elastic moduli will be described in detail in the following chapters.

References

[1] A. Migliori and J. L. Sarrao, *Resonant Ultrasound Spectroscopy* (Wiley, New York, 1997).

[2] A. Migliori, J. L. Sarrao, W. M. Visscher, T. M. Bell, L. Ming, Z. Fisk and R. G. Leisure, Physica B **183**, 1 (1993).

[3] R. G. Leisure and F. A. Willis, J. Phys.: Condens. Matter **9**, 6001 (1997).

[4] I. Ohno, J. Phys. Earth **24**, 355 (1976).

[5] W. M. Visscher, A. Migliori, T. M. Bell, R. A. Reinert, J. Acoust. Soc. Am. **90** 2154 (1991).

[6] R. G. Leisure, K. Foster, J. E. Hightower and D. S. Agosta, Mat. Sci. and Eng. A, to be published.

[7] H. Lamb, Proc. London Math. Soc. **13**, 189 (1882).

[8] O. L. Anderson in *Resonant Ultrasound Spectroscopy*, 153 (Wiley, New York, 1997).

[9] J. B. Mehl, J. Acoust. Soc. Am. **64**, 1532 (1978).

[10] K. Foster, R. G. Leisure, J. B. Shaklee, J. Y. Kim and K. F. Kelton, Phys. Rev. B **61**, 241 (2000).

[11] R. Holland, J. Acoust. Soc. Am. **43**, 988 (1968).

[12] H. H. Demarest, J. Acoust. Soc. Am. **49**, 768 (1971).

[13] I. Ohno, S. Yamamoto, O. L. Anderson and J. Noda, J. Phys. Chem. Solids **47**, 1103 (1986).

[14] W. Johnson and P. Heyliger, J. Acoust. Soc. Am. **113**, 1826 (2003).

[15] P. Heyliger and W. Johnson, J. Acoust. Soc. Am. **113**, 1812 (2003).

[16] H. Ogi, Y. Kawasaki, M. Hirao and H. Ledbetter, J. Appl. Phys. **92**, 2451 (2002).

[17] I. Ohno, Phys. Chem. Minerals **17**, 371 (1990).

[18] H. Ogi, N. Nakamura, K. Sato, M. Hirao and S. Uda, IEEE Trans. Ultrason., Ferroelect., Freq. Contr. **50**, 553 (2003).

[19] D. C. Wallace, Phys. Rev. **162**, B776 (1967).

[20] J. A. Garber and A. V. Granato, Phys. Rev. B **11**, 3990 (1975).

[21] D. Chandler, *Introduction to Modern Statistical Mechanics* (Oxford Univ. Press, New York, 1987).

[22] G. A. Alers in *Physical Acoustics* Vol. IV, pt. A, W. P. Mason, ed. (Academic, New York, 1966).

[23] W. L. Rehwald, Adv. Phys. **22**, 721 (1973).

[24] F. Willis and R. G. Leisure, Phys. Rev. B **54**, 9077 (1996).

[25] C. Weinmann and S. Steinemann, Solid State Commun. **15**, 281 (1974).

[26] K. Foster, J. E. Hightower, R. G. Leisure and A. V. Skripov, Phil. Mag. B **80**, 1667 (2000).

[27] K. Foster, J. E. Hightower, R. G. Leisure and A. V. Skripov, Phys. Rev. B **65**, 094108 (2002).

[28] D. S. Agosta, J. E. Hightower, K. Foster, R. G. Leisure and Z. Gavra, J. Alloys Comp. **346**, 1 (2002).

[29] J. E. Atteberry, D. S. Agosta, R. G. Leisure, O. Beeri and M. H. Mintz, J. Alloys Comp. (to be published).

[30] J. E. Atteberry, D. S. Agosta, C. E. Nattrass, R. G. Leisure, I. Jacob, R. C. Bowman, Jr., and O. Yeheskel, (to be submitted).

[31] K. Foster, Ph.D. Dissertation, Colorado State University, unpublished (2001).

[32] R. G. Leisure in *Resonant Ultrasound Spectroscopy*, 137 (Wiley, New York, 1997).

[33] K. Foster, J. E. Hightower, R. G. Leisure and A. V. Skripov, J. Phys.: Condens. Matter **13**, 7327 (2001).

Chapter 3

A Resonant Ultrasound Spectroscopy Study of Hydrogen Motion in the *C*15 Laves-Phase Compounds TaV_2 and $ZrCr_2$.

- 3.1 Background
- 3.2 Ultrasonic Evidence for Hydrogen Tunneling in a Laves-Phase Material: $TaV_2H(D)_x$.
- 3.3 Ultrasonic Measurements of H(D) Effects on the Laves-Phase Material $ZrCr_2H(D)_x$.
- References

3.1 Background

Recently, much interest has been shown in the study of hydrogen diffusion in Laves-phase materials.[1] There are many binary Laves-phase materials with the AB_2 stoichiometry, forming with three different symmetries: the *C*15 cubic, the *C*14 hexagonal and the mixed *C*36 structure. Many of these compounds can absorb considerable amounts of hydrogen.[2,3,4,5,6,7] This work focuses on the cubic (*C*15-type) Laves-phase compounds. In contrast to elemental metals, the number and variety of interstitial sites in these materials leads to unusual features for the interstitial motion of hydrogen isotopes. Nuclear magnetic resonance (NMR) and quasielastic neutron scattering (QENS) experiments give strong evidence for two frequencies of H(D) motion among interstitial sites.[7,8,9,10,11,12,13,14,15]

The structure of the *C*15 Laves-phases is shown in Figure 3.1. The A atoms are shown in green and the B atoms in red. The Laves-phase compounds are topologically close-packed (TCP) with the structure primarily determined by the ratio of the atomic sizes of the two components such that they can fill space most efficiently.[16] The ideal ratio for the *C*15 materials is $R_A / R_B = 1.225$. The structure is based on a face centered cubic (f.c.c.) lattice with the basis including two A atoms and 4 B atoms, as shown in Fig. 3.1. There are three different types of tetrahedral

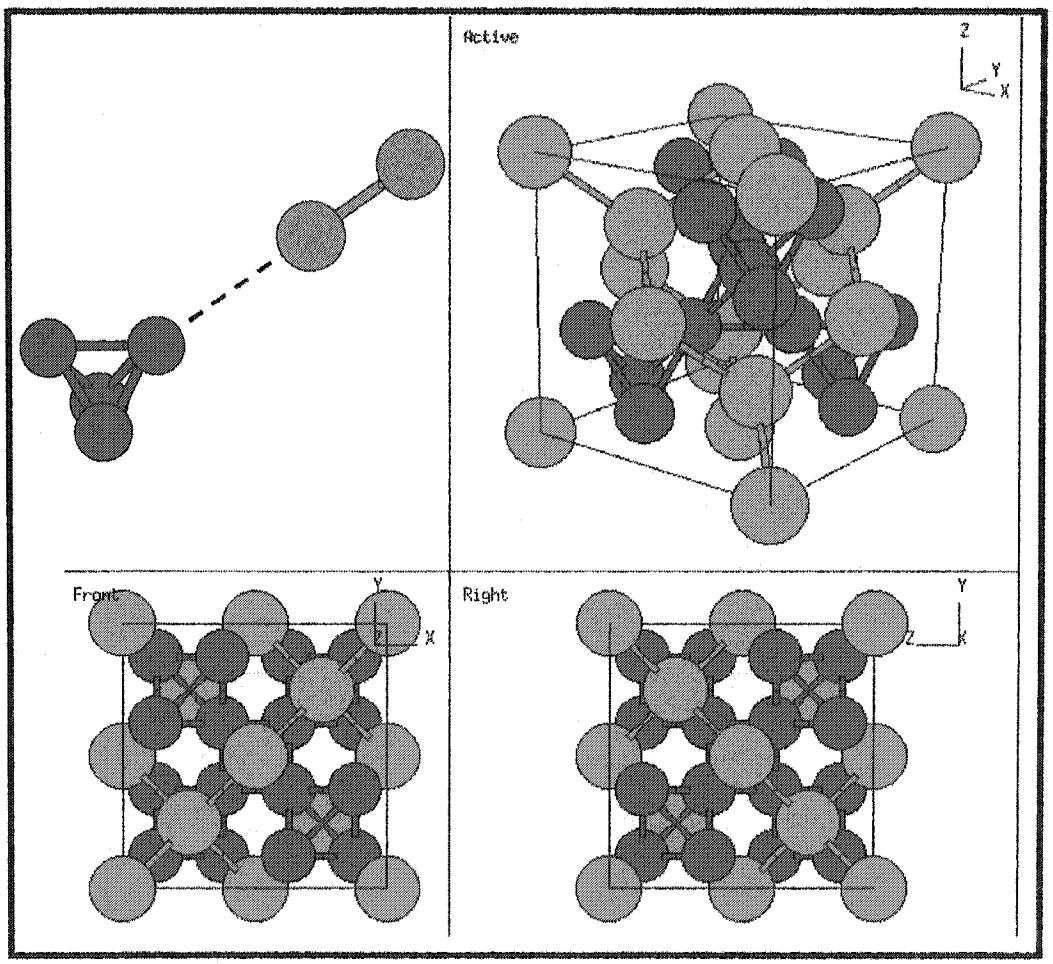

Figure 3.1 The f.c.c. C15 Laves-phase AB_2 structure. The larger, green circles represent A atoms. Smaller, red circles represent B atoms. The basis of two A atoms and 4 B atoms is shown on the top left. The other pictures, showing different views of the structure, are taken from http://cst-www.nrl.navy.mil/lattice/mainpage.html.

interstitial sites, determined by the surrounding atoms. Interstitials surrounded by 2 A and 2 B atoms are *g* sites; those surrounded by 1 A and 3 B atoms are *e* sites; and those surrounded by 4 B atoms are *b* sites. Hydrogen isotopes usually occupy the *g*-type interstitial sites in the *C*15 structure. The 96 *g* sites per unit cell (12 per AB_2 formula unit) form a series of linked hexagons. The *g*-*g* distance for neighboring sites within a hexagon is usually shorter than the distance for neighboring sites on different hexagons. Figure 3.2 shows the *e* and *g* type interstitial sites in the *C*15 Laves-phases. Several of the hexagons of *g* sites are outlined in black. A 2-D representation of these interlinked hexagons is shown in Figure 3.3. The two

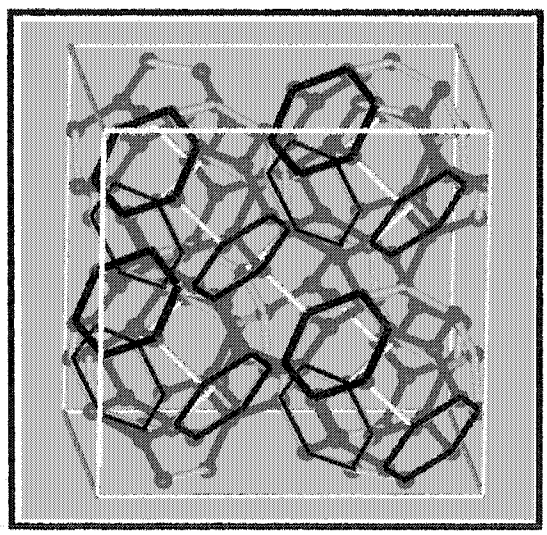

Figure 3.2 The *e*-type and *g*-type interstitial sites in the *C*15 Laves-phase AB_2 structure. Blue circles represent *e* sites. Red circles represent *g* sites. The *g* sites form a series of interlinked hexagons, several of which are highlighted in black in the figure. (Picture courtesy of G. Majer, Max Planck Institute for Metal Physics, Stuttgart, Germany.)

frequencies of H(D) motion that have been observed correspond to hopping within a hexagon of *g* sites, with distance r_1, and between hexagons, with distance r_2, where $r_2 > r_1$. This difference between the inter-hexagon and intra-hexagon *g*-*g* distances is

related to the ratio of the radii R_A/R_B of the elements A and B forming a cubic Laves-phase AB_2 material. As the ratio of the metallic radii decreases, the ratio of r_2 to r_1 increases. The two materials studied in this work have R_A to R_B ratios at the far ends of values for these intermetallic compounds. In particular, TaV_2 has $R_A / R_B = 1.09$, whereas $ZrCr_2$ has $R_A / R_B = 1.25$.

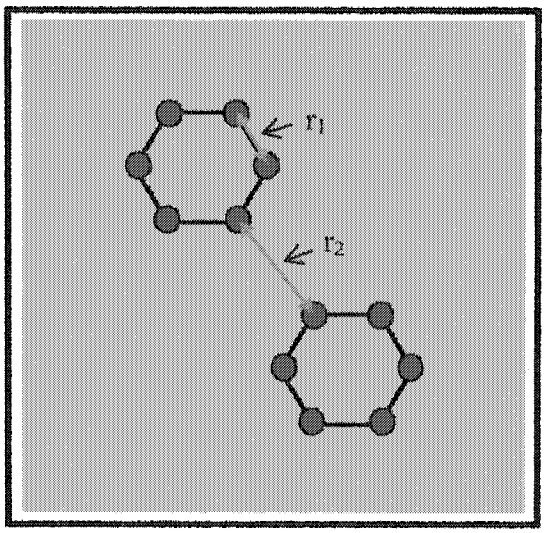

Figure 3.3 A 2-D representation of the *g*-type interstitial sites in the C15 Laves-phase AB_2 structure. The *g* sites, shown as red circles, form hexagons. The distance between g sites on different hexagons, r_2, is usually longer than the distance between g sites within hexagons, r_1.

The tetrahedral *g* sites have a lower symmetry than the C15 lattice. Therefore, selection rules for anelastic relaxation[17] permit a non-zero relaxation strength for hydrogen atoms moving between neighboring *g* sites. An explicit expression for the relaxation strength can be calculated for a two-level system, which is an appropriate description of an interstitial atom such as hydrogen occupying either of two nearby sites. A sketch of the two-level system is shown in Figure 3.4. The neighboring sites are represented as two adjacent potential wells with an energy difference of $2A$, the site asymmetry energy. The two wells can be described by the wavefunctions, φ_1 and

φ_2 with energies A and $-A$. In the case where there is no overlap of the two wavefunctions, these energies are the energies of the system. However, it is possible that the two wavefunctions may overlap, resulting in a modification to the Hamiltonian for the system. The new Hamiltonian will have off-diagonal elements, E_T, representing the adjustment to the energy levels due to tunneling. In this case, the

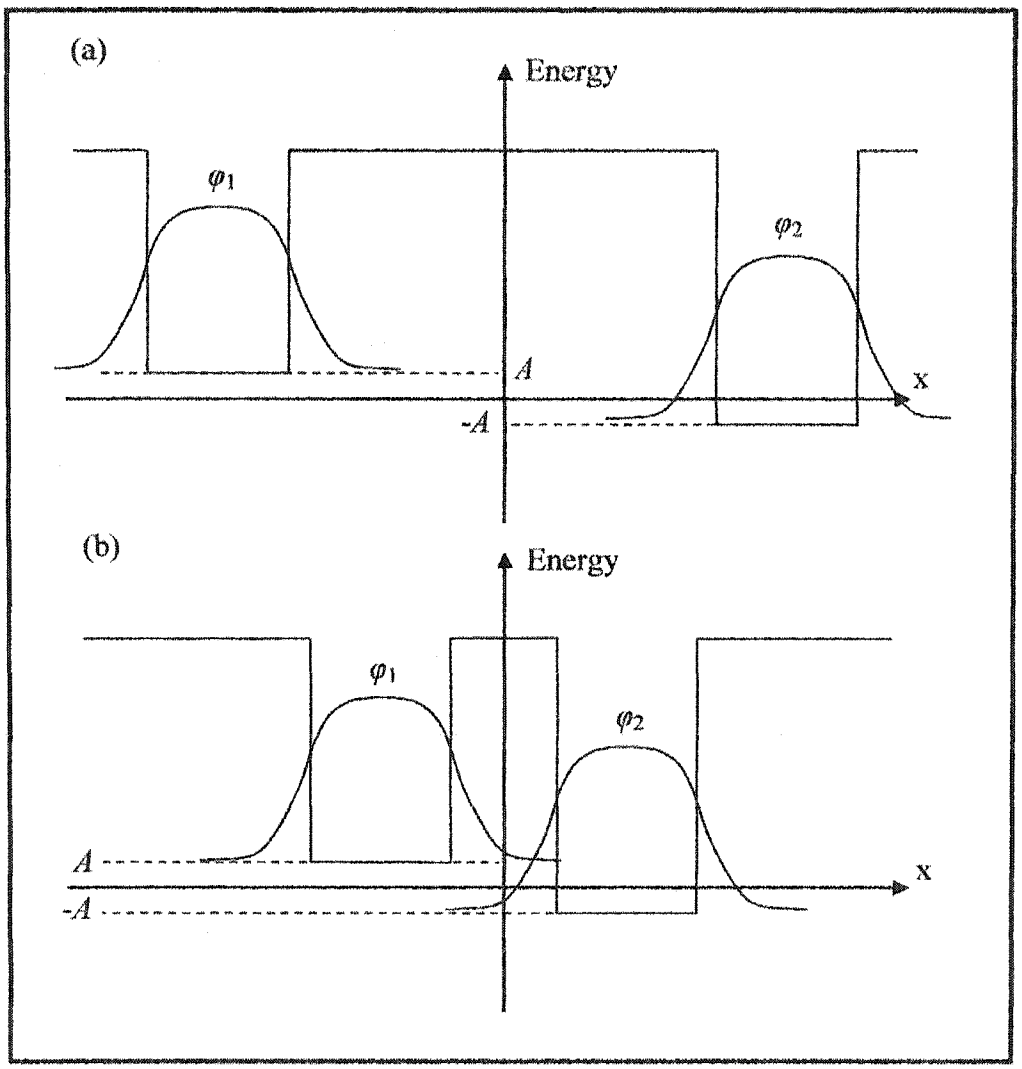

Fig. 3.4 Sketch of a two-level system with (a) no overlap of the wavefunctions, φ_1 and φ_2 and (b) some overlap of the wavefunctions. The two-level system is an appropriate description of hydrogen occupying either of two adjacent sites.

energies of the system are $E_{\pm} = \pm E$, with

$$E = (E_T^2 + A^2)^{1/2}, \tag{1}$$

where $2E_T$ is the tunnel splitting, which will be non-zero for overlapping wave-functions.

From Chapter 1 we found that the relaxation strength is given by $\Delta c / c$, where Δc is the difference between the relaxed and unrelaxed elastic moduli. From Chapter 2 we saw that the elastic moduli are given by the second derivative of the internal energy, U, with respect to strain, ε. Following the discussion of Migliori and Sarrao,[18] we can calculate the effect of the two-level system (TLS) on the elastic constant at zero frequency from this fundamental definition. We start by modifying the energy with an extra term due to the TLS, $U(\varepsilon) = U_0(\varepsilon) + U_{TLS}(\varepsilon)$, where $U_0(\varepsilon)$ includes all the interactions except those due to the two-level system. From basic statistical mechanics,

$$U_{TLS}(\varepsilon) = -nk_B T \ln[Z(\varepsilon)], \tag{2}$$

where n is the density of states, k_B is Boltzmann's constant, T is the temperature and $Z(\varepsilon)$ is the partition function given by

$$Z(\varepsilon) = 2\cosh\left(\frac{E}{k_B T}\right). \tag{3}$$

For the modulus, we calculate $\partial^2 U(\varepsilon)/\partial\varepsilon^2$, which results in

$$c = c_0 - \frac{nD^2 E_T^2}{E^3}\tanh\left(\frac{E}{k_B T}\right) - \frac{nD^2}{k_B T}\left(\frac{A}{E}\right)^2 \operatorname{sech}^2\left(\frac{E}{k_B T}\right) \tag{4}$$

where c_0 is the usual elastic constant, $D = \partial A/\partial\varepsilon$, and $\partial^2 A/\partial\varepsilon^2$ is considered to be negligibly small. The second term is zero when the tunneling matrix element is zero.

This purely quantum-mechanical effect is related to resonant transitions between levels.[19] In the frequency range of our ultrasonic measurements, this term may contribute to the elastic constant but has a minimal affect on the attenuation. The last term in Eq. (4) is associated with relaxation. This term arises due to the repopulation of sites in response to an applied strain. In the limit of very high frequencies, the system does not have time to adjust and there is no effect due to relaxation. The difference between the zero frequency limit (given by Eq. (4)) and the high frequency limit (given by Ref. (19)) gives us Δc for the two-level system. Therefore, we have for the relaxation strength,

$$\frac{\Delta c}{c} = \frac{n\Gamma^2}{k_B T c}\operatorname{sech}^2\left(\frac{E}{k_B T}\right) \tag{5}$$

where $\Gamma = \partial E / \partial \varepsilon$ is the variation of the energy level splitting with respect to the ultrasonic strain (the deformation potential). Except at very low temperatures, $k_B T >> E$. Therefore, for the case of a metal-hydrogen system, the relaxation strength is of the following form[18]

$$\frac{\Delta c}{c} = \frac{n\Gamma^2}{k_B T c}, \tag{6}$$

where n is taken to be the concentration of hydrogen atoms participating in the relaxation.

The particular mechanisms of motion of a light interstitial atom from site to site can be quite complicated.[20,21] At high enough temperatures, the particle may hop between sites in a classical manner, with a thermally activated energy that is greater than the potential barrier height. At moderate temperatures, the particle is more likely

to undergo phonon-assisted tunneling. Depending on the measurement temperature and the particulars of the system, this motion may be dominated by tunneling through coincident ground states (generally at low temperatures) or by tunneling through excited states. Each of these mechanisms for motion requires thermal energy. For an activation-type process such as this, the relaxation time, τ_R, is of the Arrhenius form, given by

$$\tau_R = \left[\sum_i \tau_{R0,i}^{-1} \exp\left(\frac{-E_{a,i}}{k_B T} \right) \right]^{-1}. \qquad (7)$$

In this expression, the $\tau_{R0,i}$ and $E_{a,i}$ are generally considered to be attempt times and activation energies, respectively. The long-range diffusive motion of H(D) in TaV_2 (from previous work[24,25]) and $ZrCr_2$ (present work) has been studied by means of ultrasonic attenuation and dispersion and has been found to follow an Arrhenius-type process such as this. In the temperature range of our measurements, it is very unlikely that these peaks are due to over-barrier hops. The motion appears to be well-described by phonon-assisted tunneling between ground states along with tunneling between excited states. Details of the results on these systems will be reported in the following sections of Chapter 3.

Non-Arrhenius mechanisms for H motion are also possible. In particular, at very low temperatures, there is not enough thermal energy to activate processes such as those described above. Tunneling still may occur, perhaps due to some type of barrier fluctuation.[22] Variations in the potential barriers seen by the H atoms may lead to a non-zero relaxation rate. The exact form of the relaxation time for low-temperature relaxation such as this is not well-known. We have evidence of such

relaxation for the short-range motion of H(D) in TaV_2 at low temperatures. These results are discussed in detail, along with the form of the relaxation time, in the next section.

3.2 Ultrasonic Evidence for Hydrogen Tunneling in a Laves-Phase Material: $TaV_2H(D)_x$.

3.2.1 Introduction and Experimental Details

For TaV_2 the ratio of the metallic radii, R_A to R_B, is anomalously low, resulting in a large difference between the fast jump rate and the slow jump rate for hydrogen isotopes in this material.[11] The fast motion is of particular fundamental interest because it appears to be dominated by non-classical effects, including a non-Arrhenius relaxation time and a temperature-dependent H population, $n(T)$, participating in the motion.[11] The exact form of this temperature dependence and the origin of the effect are not well known. Recent ultrasonic measurements[23,24,25] have indicated a strong isotope effect on the fast, localized motion. A low-temperature attenuation peak was observed for D in TaV_2, but not for H. Two possibilities were suggested[25] for the lack of a peak for H: the absence of a mobile H population at the low temperatures of the experiment; or, the H motion remained much faster than the approximately 1 MHz frequency of the ultrasound down to helium temperatures. The aim of the present work was to further explore this intriguing low-temperature motion using improved ultrasonic methods. Ultrasonic experiments are ideal for probing the isotope effect because H and D couple to the ultrasound in the same way, in contrast to other probes such as NMR and neutron scattering.

TaV_2 exhibits other interesting behavior that can be investigated by ultrasonic techniques. Previous studies[26,27] on the $TaV_2H(D)_x$ system with $x(D) \geq 1.30$ and $x(H) \geq 1.15$ have indicated an order-disorder transition below 150 K associated with the long-range ordering of H(D) on the *g* sites. It has been suggested that for lower concentrations, some ordering – perhaps on a local scale – would still exist.[1,28] It is possible that this ordering is connected with the low-temperature, local motion by contributing to the decrease of the mobile population as the temperature is lowered.

The present work is an extension of earlier studies of ultrasonic attenuation in $TaV_2H(D)_x$.[24,25] As described in Chapter 2, improvements were made in the equipment that have allowed higher sensitivity in the attenuation measurements. We report new ultrasonic attenuation measurements of $TaV_2H_{0.18}$ over the range of 0.5-100 K and of $TaV_2D_{0.17}$ over the range of 3-100 K. Also reported are results for $TaV_2D_{0.50}$ over the temperature range of 3-340 K. Measurements from 0.5-40 K on $TaV_2H_{0.18}$ were made in a 1 Tesla magnetic field. A large attenuation peak near room temperature was observed previously[24,25] in TaV_2H_x and $TaV_2D_{0.17}$, and is associated with the slower hexagon to hexagon hopping of H and D atoms. The present work reports a similar peak for $TaV_2D_{0.50}$. A second, much weaker attenuation peak is observed at low temperature in the deuterated materials and is attributed to the fast, local motion of D. Such a peak was previously seen in $TaV_2D_{0.17}$, although there was too much scatter in the data to permit a quantitative analysis. Newly seen in the current measurements is an even weaker peak (an order of magnitude smaller than the low-temperature peak in the deuterated materials) at low temperature in the hydrogenated material. The current measurements also indicate a small attenuation peak at

intermediate temperatures. This latter peak is consistent with the phenomenology of an ordering transition.

Polycrystalline ingots of TaV_2 were prepared by A. V. Skripov *et al.*[29] by arc melting appropriate mixtures of the high-purity constituent elements in an argon atmosphere followed by various annealing procedures. The TaV_2 material was then loaded to varying concentrations of H or D to form $TaV_2H(D)_x$ as has been described previously.[29]

Using the experimental technique of Resonant Ultrasound Spectroscopy[18,30,31] (RUS) the ultrasonic attenuation and resonant frequencies were measured for $TaV_2H_{0.18}$, $TaV_2D_{0.17}$ and $TaV_2D_{0.50}$. As described in detail in Chapter 2, with the RUS technique, piezoelectric transducers are used to excite a large number of the lowest-frequency vibrational eigenmodes in samples of well-defined shapes, such as rectangular parallelepipeds. Samples were prepared by cutting approximate parallelepipeds from the button ingots using a low-speed diamond saw. These were then hand-polished into accurate rectangular parallelepipeds suitable for the ultrasonic measurements. Sample edge dimensions and masses were 1-1.8 mm and 16 to 22 mg respectively. Lithium-niobate compressional-mode transducers were used to excite and detect the mechanical resonances. Measurements on $TaV_2D_{0.17}$ from 3-100 K, on $TaV_2D_{0.50}$ from 3-300 K and on $TaV_2H_{0.18}$ from 40-100 K were made using a commercial cryostat and temperature controller, with the sample in a low vacuum (3 Torr) environment of helium gas. As described in Sections 2.2 and 2.5, the sample mounting stage was redesigned for this experiment and care was taken in isolating the entire system from vibrational interference. These steps resulted in lower overall

background attenuation and scatter as compared to our earlier work. Measurements on $TaV_2H_{0.18}$ from 0.5-40 K were made using a ^{3}He cryostat at the National High Magnetic Field Laboratory at Los Alamos National Laboratory. Measurements on this sample were also made in a 1 Tesla magnetic field from 0.5-40 K. The presence of a magnetic field is known to reduce the background of the ultrasonic attenuation in metals.[32] Measurements above room temperature were made at atmospheric pressure using a commercial oven and temperature controller. The ultrasonic attenuation in the materials was found by fitting the Lorentzian lineshapes of the resonant peaks to determine the quality factor, Q. This procedure was explained in Section 2.3. The ultrasonic loss is then given simply by $1/Q$.

3.2.2 Results and Discussion

Figure 3.5 shows the ultrasonic loss versus temperature over the range of 3–340 K for $TaV_2D_{0.50}$. As Fig. 3.5 shows, a relatively large attenuation peak, centered at about 260 K, is observed for the measurement frequency of approximately 1.3 MHz. Similar peaks are observed for $TaV_2H_{0.18}$ and $TaV_2D_{0.17}$ as reported previously.[24,25] These peaks have been attributed to H(D) hopping between hexagons, the relatively slow rate responsible for long-range diffusion. The dependence of this peak on H concentration was reported previously.[24] For D, the amplitude of the peak increases with an increase in concentration, from approximately 0.008 for $x = 0.17$ (Ref. 24) to approximately 0.014 for $x = 0.50$ (Fig. 3.5). The dependence of the ultrasonic loss on deuterium concentration for this peak will be discussed in more detail below.

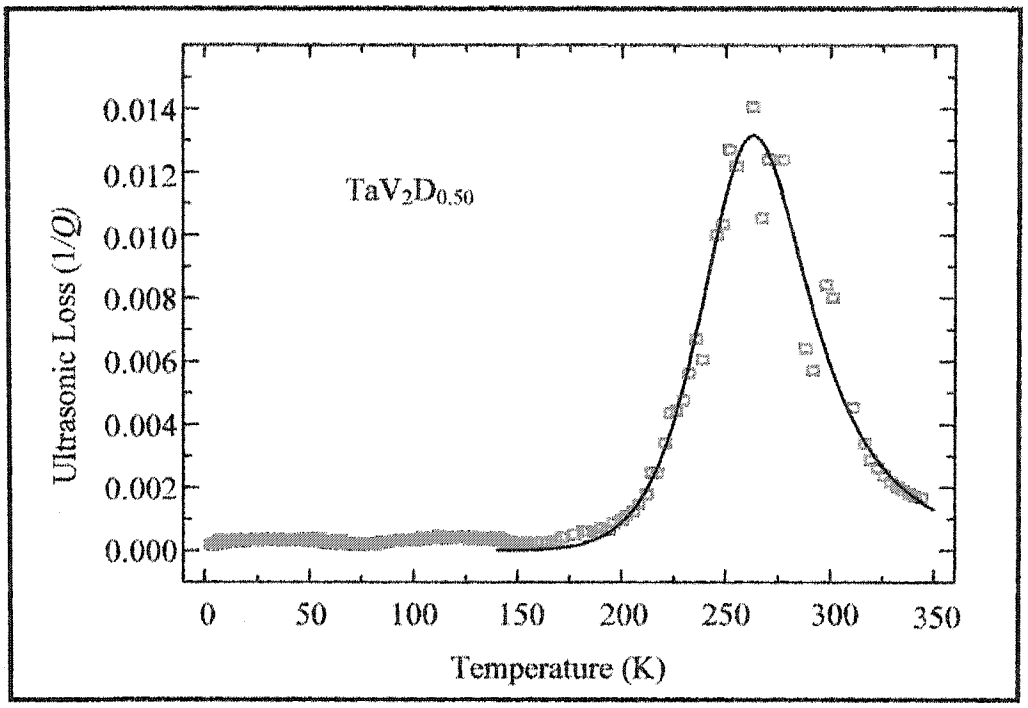

Fig. 3.5 Ultrasonic loss versus temperature for $TaV_2D_{0.50}$ over the range of 3-340 K. The solid line through the high-temperature peak represents a fit to the data using Eqs. (6), (8) and (9).

Figure 3.6 shows the ultrasonic loss at low temperatures for $TaV_2D_{0.50}$ on a greatly expanded vertical scale. Two additional peaks, hardly apparent in Fig. 3.5, are seen in Fig. 3.6. Similarly, Fig. 3.7 shows the low-temperature ultrasonic loss in $TaV_2D_{0.17}$ and $TaV_2H_{0.18}$. Note that the vertical scale for Fig. 3.7(b) ($TaV_2H_{0.18}$) is greatly expanded as compared to Fig. 3.7(a) ($TaV_2D_{0.17}$). In a previous report[25] the low-temperature peaks in $TaV_2H_{0.18}$ could not be observed, the scatter in the data was too great. The data of Fig. 3.7(b) from 0.5-40 K were taken in a 1 T magnetic field, which has the effect of decreasing the overall background attenuation in a metal.[32] This lowered background attenuation permitted the observation of the small peaks in Fig. 3.7(b). As previously reported, H-free TaV_2 exhibited no rise in the ultrasonic

attenuation at low temperatures, remaining relatively constant at about 4 x 10^{-5} up to 100 K, and increasing slightly from this value with increasing temperature.

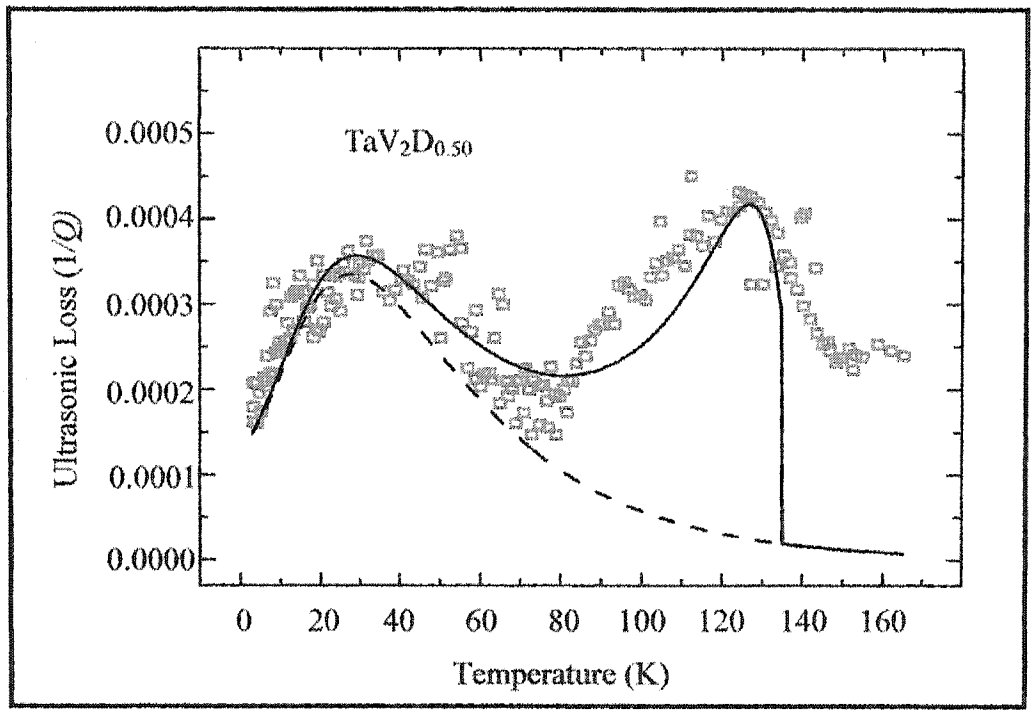

Fig. 3.6 Expanded view of the low-temperature ultrasonic loss for $TaV_2D_{0.50}$. The dashed line represents a model of the data using Eqs. (6), (8), (11) and (12) with a distribution of mobilization energies. The solid line shows contributions from all of the effects we have modeled.

Figures 3.5 – 3.7, in combination with previous work,[24] indicate several features for the ultrasonic attenuation in $TaV_2H(D)_x$. 1. There is a relatively large loss peak near room temperature for measurement frequencies near 1 MHz. This peak is well-explained as H(D) hopping between hexagons of *g* sites. The present work provides additional information about this peak for deuterium. 2. There is a peak at low temperatures. This peak shows a large isotope effect. It appears at about 20 K for deuterium, but at about 1 K for hydrogen. Furthermore, this peak is much weaker for H as compared to D. We will interpret these peaks as H(D) motion within

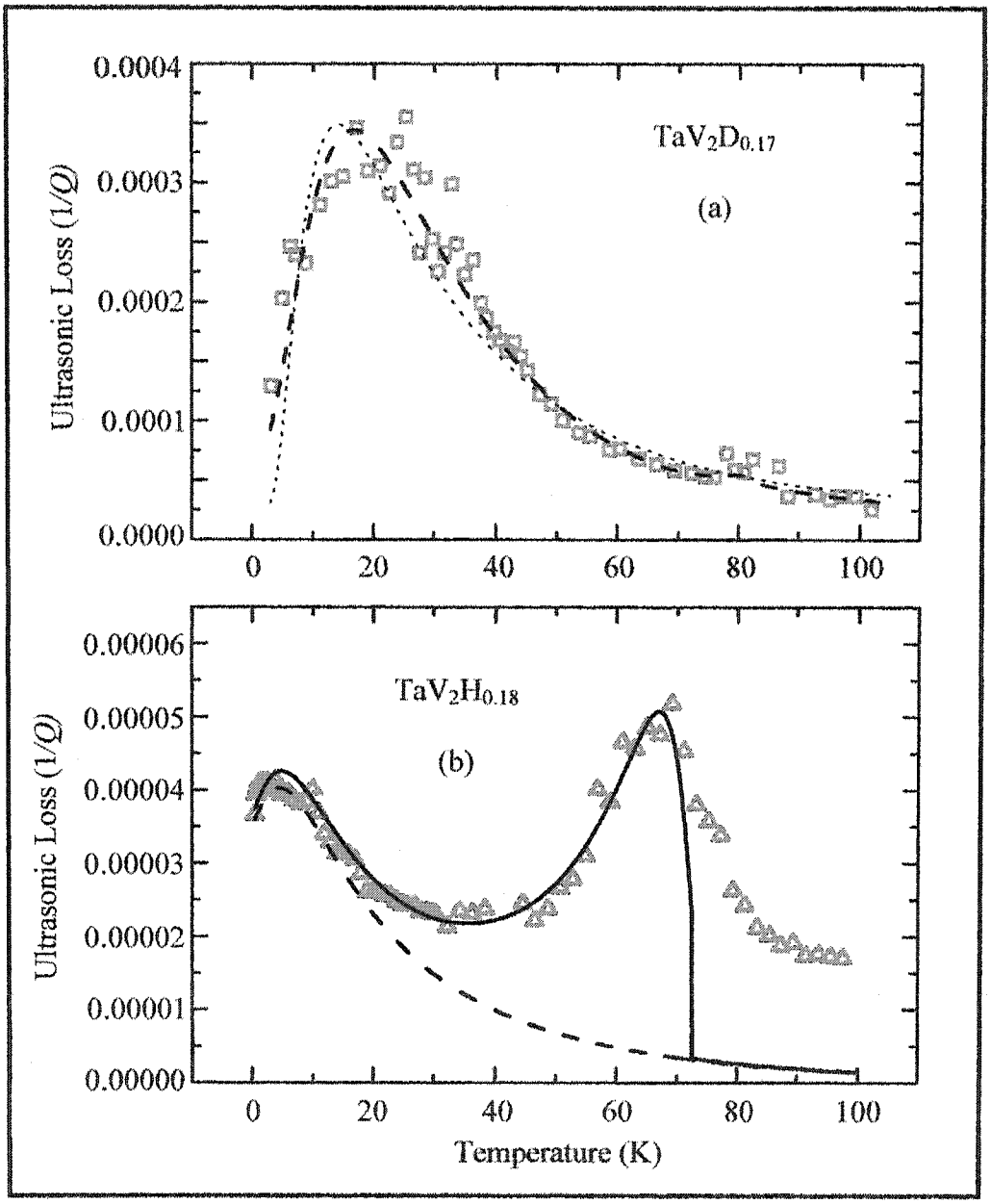

Fig. 3.7 Low-temperature ultrasonic loss for (a) $TaV_2D_{0.17}$ and (b) $TaV_2H_{0.18}$. The dotted line in (a) represents a model of the data using Eqs. (6), (8), (11) and (12) with a single mobilization energy. The dashed lines show fits using a Gaussian distribution of mobilization energies. The solid line in (b) shows contributions from all of the effects we have modeled.

a hexagon of g sites. 3. There is an intermediate temperature peak. This peak occurs at about 70 K for $TaV_2H_{0.18}$ and about 125 K for $TaV_2D_{0.50}$. There is a hint of such a peak at about 80 K for $TaV_2D_{0.17}$. Based on other work,[26,27] we suggest that these peaks are due to an order-disorder transition of H(D) on the interstitial sites.

We now turn to a more detailed analysis and interpretation of the data. Hydrogen hopping has been studied by use of ultrasonic attenuation in many systems. The motion of a hydrogen isotope between neighboring sites can lead to ultrasonic attenuation. Anelastic relaxation[17] occurs when nearby interstitial sites are affected differently by the applied ultrasonic stress causing the hydrogen to relocate to sites of lower energy. When the applied ultrasonic frequency is comparable to the hydrogen hopping rate, the net effect is dissipation of the input energy. As shown in Section 1.3, the ultrasonic loss, $1/Q$, due to anelastic relaxation is given by[18]

$$\frac{1}{Q} = \frac{\Delta c}{c}\frac{\omega\tau_R}{1+\omega^2\tau_R^2}, \tag{8}$$

where $\Delta c/c$ is the relaxation strength, $\omega/2\pi$ is the ultrasonic frequency and τ_R is the relaxation time. The quantity Δc is the difference between the unrelaxed (c_U) and relaxed (c_R) elastic moduli, $\Delta c = c_U - c_R$, and is given by Eq. (6).

For the large attenuation peak at higher temperature a simple single-term Arrhenius expression for the relaxation time,

$$\tau_R = \tau_{R0}\exp\left(\frac{E_a}{k_BT}\right), \tag{9}$$

with activation energy E_a, can be used along with Eqs. (6) and (8) to fit the data satisfactorily as discussed previously.[24] The solid line in Fig. 3.5 is a fit to the high-temperature loss peak using Eqs. (6), (8), and (9). This description is valid over a

range of measurement frequencies and also describes the dispersion in the frequency. As described in Section 1.3, relaxation causes a change in the elastic moduli. This subsequently results in a shift in the resonance frequencies given by

$$\delta f = \frac{\Delta c}{c}\frac{f}{2}\frac{\omega^2\tau_R^2}{1+\omega^2\tau_R^2}. \qquad (10)$$

Data for two different measurement frequencies were simultaneously fit to Eqs. (8) and (9) for this material. The same parameters were successfully used to fit the dispersion in the frequency as well by adding a linear background to Eq. (10). Figure 3.8 shows the frequency of one of the mechanical eigenmodes versus temperature for $TaV_2D_{0.50}$. Included in this figure are the corresponding ultrasonic loss results for the same eigenmode. The solid lines in Fig. 3.8 are theoretical fits to the data using Eqs. (6), (8) and (9) for the loss and Eqs. (6), (9) and (10), with a linear background, for the frequency. The fit parameters for $TaV_2D_{0.50}$ were $\tau_{R0} = 2.2 \times 10^{-12}$ s and $E_a =$ 0.26 eV. These values are in good agreement with NMR results.[8] The fact that a single-term relaxation time describes the data well indicates that one mechanism for motion dominates in this temperature range, the phonon-assisted tunneling between excited states. This interpretation has been described in detail in Refs. 24 and 25.

The fit also determines $n\Gamma^2/(k_B c)$, a quantity related to the relaxation strength as shown in Eq. (6). Using measured values of the aggregate shear modulus for c, the values for $n\Gamma^2/k_B$ were calculated. For the x(D) = 0.5 case, $n = 1.03 \times 10^{28}$ m^{-3}, and $c = 78.4$ GPa (the room temperature value), were used. The quantity $n\Gamma^2/(k_B c)$ was found to be linearly dependent on the concentration, n, for the deuterated samples, as was found for the hydrogenated case.[24] The linear dependence

yields a value of the deformation potential, $\Gamma = 0.17$ eV for D in TaV_2, the same value previously reported for the hydrogenated samples.[24] This linear dependence is an example of the Snoek effect for H(D) in intermetallic compounds. Γ is related to the response of interstitial sites on *different* hexagons to the applied ultrasonic strain. Therefore, it seems reasonable that there is no isotope dependence for Γ. Note that $(1/Q)_{max}$, which is given by $\left(nI^2 / 2k_B cT\right)_{max}$, *does not* depend linearly on the concentration, although nI^2 / k_B does. This difference is due to the strong concentration dependence of the shear elastic constant.[33]

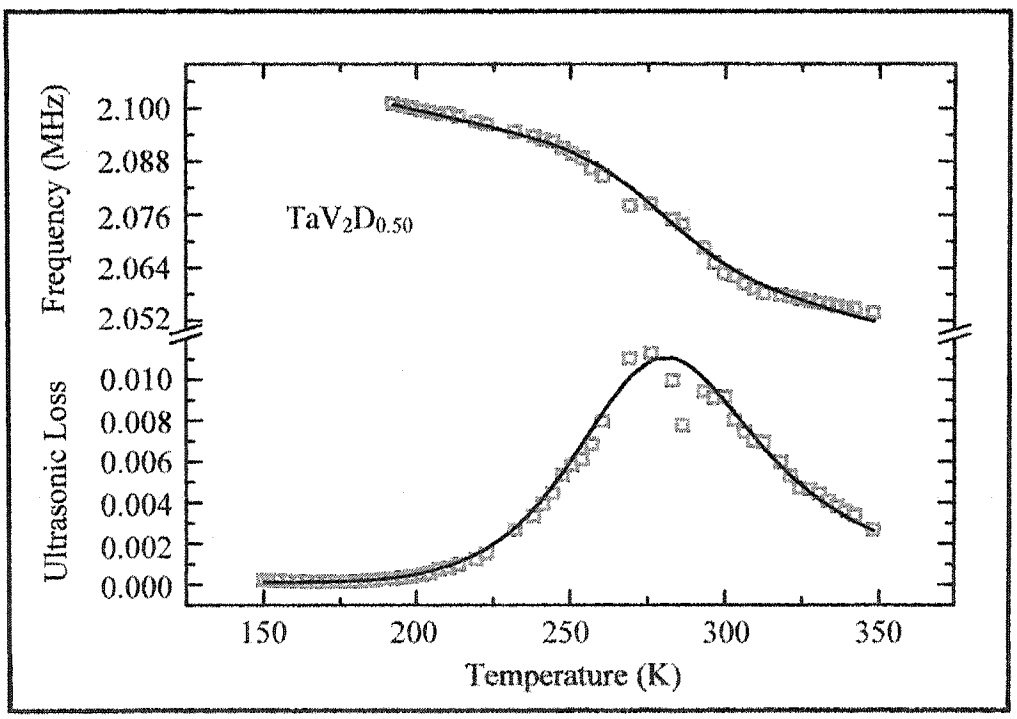

Figure 3.8 Temperature dependence of the resonant frequency and attenuation of a mechanical eigenmode in $TaV_2D_{0.50}$. The solid lines represent theoretical fits to the data with parameters given in the text. A background term linear in temperature was included in the frequency fit.

In contrast to the high-temperature peaks, which are well described as classical Debye peaks with an Arrhenius-type relaxation process, the low-temperature peaks behave quite differently. Skripov *et al.*[8] found that the relaxation time for the low-temperature NMR spin-lattice relaxation data is reasonably well described by the expression

$$\tau_{1} = \tau_{1,0} \exp\left(\frac{-T}{T_0}\right), \tag{11}$$

where T_0 and $\tau_{1,0}$ are fitting parameters. This expression has some justification from quantum diffusion theory, taking into account the effects of barrier fluctuations.[22] We have used this expression to model our low-temperature data. Not only is the relaxation time non-Arrhenius, but the concentration, n, of H(D) atoms contributing to the relaxation strength was found to be dependent on temperature. Evidence has been given for a temperature-dependent mobile population.[11] The suggested approach to the description of $n(T)$ is based on the assumption of some energy gap, E_o, between the static and mobile H(D) states. In this case,

$$n(T) = n_0 \frac{\exp\left(\frac{-E_0}{k_B T}\right)}{1+\exp\left(\frac{-E_0}{k_B T}\right)}, \tag{12}$$

where n_0 is taken as the total H(D) concentration. Indeed, a temperature-dependent population appears to be required to describe our data. Eqs. (11) and (12) with mobilization energy, E_0, can be used along with Eqs. (6) and (8) to provide a reasonable fit to the low temperature data for $TaV_2D_{0.17}$, $TaV_2H_{0.18}$, and $TaV_2D_{0.50}$. An application of this model is shown by the dotted line in Fig. 3.7(a), where a single value of E_o =

1.98 meV has been used in Eq. (12) to fit the data for $TaV_2D_{0.17}$. Consistently better agreement between the model and the data was obtained by using a distribution of energies centered on some mean energy value E_0, *i.e.* by integrating Eq. (8) from 0 to infinity over a Gaussian distribution of mobilization energies. The dashed line in Fig. 3.7(a) shows a fit using a Gaussian distribution with a mean value $E_0 = 3.45$ meV and a Gaussian width $\delta E_0 = 1.29$ meV. Similarly, the dashed lines in Figs. 3.6 and 3.7(b) show fits to the low-temperature peak using the same Gaussian distribution model. The parameters for these fits are given in Table 3.1.

Table 3.1 Parameters of the low-temperature H(D) relaxation for $TaV_2H_{0.18}$, $TaV_2D_{0.17}$ and $TaV_2D_{0.50}$. T_0 and τ_{L0} are the parameters derived using Eq. (11). A temperature-dependent mobile population of H(D) atoms was used in place of the total concentration, with a Gaussian distribution of mobilization energies centered on E_0 with width δE_0.

	τ_{L0} (s)	T_0 (K)	E_0 (meV)	δE_0 (meV)
$TaV_2H_{0.18}$	2.7×10^{-10}	50	1.12	1.20
$TaV_2D_{0.17}$	8.6×10^{-9}	30	3.45	1.29
$TaV_2D_{0.50}$	5.0×10^{-8}	38	7.85	3.35

The intermediate-temperature peaks, attributed to an order-disorder transition, give some contribution to the attenuation in the region of the low-temperature peaks. In order to extract the parameters of the low-temperature motion, a simple model for the order-disorder contribution is discussed in what follows. The full lines in Figs. 3.6 and 3.7(b) show contributions from both the low-temperature motion just discussed and the order-disorder effect. Before discussing the intermediate-temperature peaks, we make some remarks about the parameters used for the low-temperature peaks. It has been supposed that the existence of the mobilization energy E_0 results

from some short-range order among the H(D) atoms. The Gaussian distribution might approximate a spread in the local configurations. For fitting the ultrasonic data, the low-energy side of the Gaussian distribution is much more important than the high-energy side. The reason for this is as follows. Hydrogen isotopes that are in configurations requiring higher mobilization energies will only become mobile at high temperature. At these higher temperatures, the H(D) hopping rate will be so fast, *i.e.* the relaxation time given by Eq. (11) will be so short, that the combined effect of $\omega\tau_L(T)$ and $n(T)$ will contribute little to the ultrasonic attenuation. Neutron scattering experiments have been interpreted in terms of an $n(T)$ that increases linearly at higher temperatures. It is possible that the actual distribution of E_0 is such as to give the observed rise in the ultrasonic attenuation at low temperatures, and the increase in $n(T)$ at higher temperatures needed to explain the neutron scattering experiments.

It is important to note that the condition $\omega\tau_L \approx 1$ is never met in the frequency range of our study (approximately 1 MHz). In fact, $\omega\tau_L \approx 10^{-3}$ at 1 K for $TaV_2H_{0.18}$ and $\omega\tau_L \approx 0.03$ at 15 K for $TaV_2D_{0.17}$. In the $\omega\tau_L << 1$ limit, the ultrasonic loss is given by $1/Q \propto n(T)\omega\tau_L(T)$. Figure 3.9 shows a solid line for $\omega\tau_L(T)$ for $TaV_2D_{0.17}$, and shows a dashed line proportional to $n(T)$. The presence of an attenuation peak is due to these two contributing factors. As the temperature decreases $n(T)$ decreases, but $\omega\tau_L$ increases. These opposite trends are responsible for producing the peak in the attenuation, not the condition $\omega\tau_L \approx 1$. The dotted line in Fig. 3.9 shows the multiplication of $n(T)$ and $\omega\tau_L(T)$, which indeed results in a small peak. Thus, the present results indicate that the rate of the H motion remains well above 1

MHz down to 1 K. This is extremely fast for such low temperatures. The model we have used gives only a weak dependence of peak position on measurement frequency, which is in accord with the experimental results. It would be highly desirable to carry out ultrasonic attenuation experiments on this system at 10 – 100 MHz, which would be an excellent test of the ideas presented here.

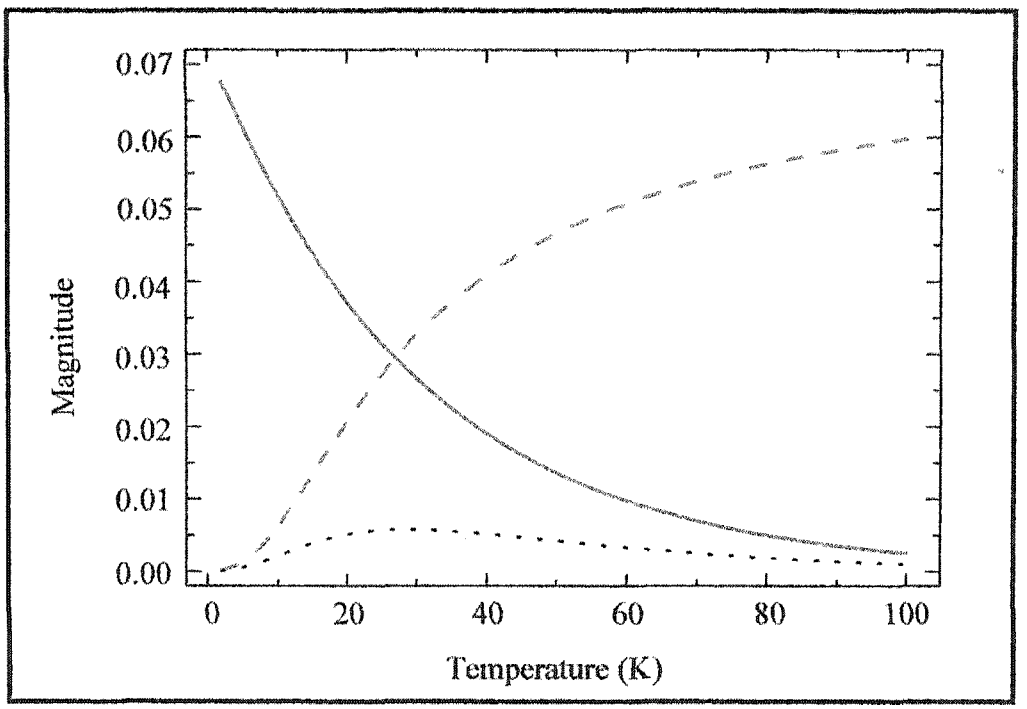

Fig. 3.9 Contributions to the low-temperature ultrasonic attenuation of $TaV_2D_{0.17}$. The solid line is $\omega\tau_L(T)$. The dashed line is proportional to $n(T)$. The dotted line is the multiplication of $\omega\tau_L(T)$ and $n(T)$.

Values of T_0 and τ_{L0} for $TaV_2D_{0.50}$ have been reported[15] from NMR experiments as 38 K and 5 x 10^{-8} s respectively. These values were used to fit our data. The other fitting parameters for the relaxation time in Table 3.1 are in accord with the NMR data. The trends in relaxation time as a function of isotope and of concentration are in good agreement with what has been found for other concentrations at higher

temperatures.[8,15,34] Namely, the H(D) hopping rate is faster for lower concentrations and at least an order of magnitude faster for H than D for a similar concentration.

From the fit of the data to the theoretical expressions, the quantity $n_0 \Gamma_{low}^2 / k_B$ is determined, where Γ_{low} is related to the response of different interstitial sites *within* a hexagon to the applied strain. Assuming that the quantity n_0 is the total concentration of interstitial H(D) atoms, an estimate of $\Gamma_{low} = 0.1$ eV is found for the low-temperature motion for all three cases studied (Figs. 3.6 and 3.7). It is remarkable that the same value is found for all three cases, and indicates a certain self-consistency of the approach. It is reasonable to expect this value to be isotope independent, and to differ somewhat, but not drastically, from the value of Γ found for the response of sites on *different* hexagons (0.17 eV).

We now take a more detailed, yet somewhat qualitative look at the contribution to the ultrasonic loss for each material from the intermediate-temperature peaks, which we consider to be due to an ordering transition. The intent is not to provide an accurate description of this effect, but to provide an approximate description so as to be able to extract the parameters of the local motion giving rise to the low-temperature peak. If we take the small rise at about 80 K in $TaV_2D_{0.17}$ as an indication of such a peak, then a number of features of these peaks are in accord with heat capacity[28] and neutron scattering[26] studies of the order-disorder transition in $TaV_2H(D)_x$ at higher concentrations. 1. For equal concentrations the transition temperature is higher for D than for H. 2. For a given isotope the transition temperature increases with increasing H(D) concentration. 3. For equal concentrations the magnitude of the effect does not depend strongly on the isotope. 4. For a given isotope the

intensities of the superlattice lines indicating the long-range ordering "are found to increase rapidly with increasing x".[26] This strong increase is in accord with the fact that the peak at about 125 K in Fig. 3.6 is much stronger than any possible peak at about 80 K in Fig. 3.7(a).

For long-range ordering below the transition temperature, T_C, the relaxation of the order parameter is described by[35,36] the relaxation time $\tau_C = t_0/(T_C - T)$, in the expression,

$$\frac{1}{Q} = B\frac{\omega\tau_C}{1+\omega^2\tau_C^2}, \tag{13}$$

where t_0 and B are fitting parameters and $\omega/2\pi$ is the ultrasonic frequency. This model only applies below the ordering temperature T_C. *Hence, we make no attempt to account for the contribution of the order-disorder transition to the ultrasonic loss above* T_C. There seems to be no direct evidence for long-range order, such as superlattice lines, at the relatively low H(D) concentrations of our experiments. However, given the strong concentration dependence found for the superlattice lines, it seems that long-range order could exist with a low value of the order parameter at the lower concentrations. Another possibility is that the ordering at the low concentrations is short-range. For short-range ordering the expression for the relaxation time would be slightly different than given above. In any case, we have used Eq. (13) with $\tau_C \propto (T_C - T)^{-1}$ to obtain a qualitative model of our data, in order to take into account the contribution from this peak to the attenuation in the region of the low-temperature peak. The solid lines in Figs. 3.6 and 3.7(b) show the results from adding Eq. (13) to the low-temperature model (indicated by the dashed line), which

was discussed previously. The fitting parameters τ_0, T_C and B for $TaV_2D_{0.50}$ were 2.4 x 10^{-6} s, 140 K and 6 x 10^{-6} respectively, and for $TaV_2H_{0.18}$, 9.3 x 10^{-7} s, 74 K and 1 x 10^{-6} respectively. The amplitude of the order-disorder peak for $TaV_2D_{0.50}$ is approximately 4 x 10^{-4}, an order of magnitude larger than the peak for $TaV_2H_{0.18}$. Assuming the amplitude should be roughly isotope-independent, the transition peak in $TaV_2H_{0.18}$ would indicate that an ordering transition in $TaV_2D_{0.17}$ would have an amplitude of approximately 5 x 10^{-5}. A feature with this amplitude would be virtually lost in the tail of the low-temperature loss peak for this isotope as indicated in Fig. 3.7(a), but is consistent with the bump in the ultrasonic loss around 80 K in the $TaV_2D_{0.17}$ data.

In general, the interpretation of the ultrasonic data is in accord with the parameters and trends found for the NMR experiments, with one exception. Nuclear spin-lattice relaxation measurements on ^{51}V in $TaV_2H(D)_x$ have found a stronger relaxation for D as compared to H for the same concentration of the two isotopes.[8] This result has been interpreted[11] as meaning that a larger fraction of the D atoms participate in the local motion as compared to H at the temperatures of the measurements ($\approx$ 100 K). The present ultrasonic measurements at lower temperatures are in disagreement with this interpretation. The ultrasonic results were fit using a mobilization energy for H that is lower than for D. The result is that the population of mobile H is larger than for D in the temperature range of our measurements. In general, neutron scattering, NMR, and ultrasound results all require a temperature-dependent and possibly isotope-dependent population of mobile H(D) atoms to explain the results. These three experimental probes tend to have maximum sensitivity

to the H(D) motion in different frequency and temperature ranges. It may be that Eq. (12) just provides a convenient means to describe a temperature-dependent population of H(D) atoms. The actual population may have a more complicated dependence on temperature (and isotope), especially if it is related to the order-disorder transition. The origin of the temperature-dependent population remains unclear.

3.2.3 Conclusions

Ultrasonic techniques were used to study hydrogen motion in $TaV_2H_{0.18}$, $TaV_2D_{0.17}$ and $TaV_2D_{0.50}$, providing strong evidence for the local quantum tunneling of hydrogen in Laves-phase materials, motion that remains extremely fast even at very low temperatures. This study also provides details concerning the diffusive motion of hydrogen. The magnitude of the ultrasonic loss for the hexagon-to-hexagon hopping, the rate-limiting step for long-range diffusion, was found to be linear in D concentration, as was previously found for H. The parameter I' describing the coupling between g sites and strain had the value 0.17 eV for both isotopes. The relaxation rate exhibited a small isotope effect and was well described by an Arrhenius-type expression for the H(D) hopping rate. The single-term relaxation time indicates that the mechanism for this motion is dominated by phonon-assisted tunneling between excited states.

In marked contrast to these high-temperature peaks, much weaker peaks were observed at lower temperatures that exhibited totally non-classical behavior. These peaks were attributed to motion within a hexagon of g sites. The relaxation rate was satisfactorily described by a non-classical expression, similar to the results from a barrier fluctuation model in the theory of quantum tunneling. The parameters used to

describe the relaxation rate for $TaV_2D_{0.50}$ were the same as those used to describe NMR spin-lattice relaxation measurements at higher temperatures on the same material. The relaxation rate for $TaV_2D_{0.17}$ was somewhat faster than that for $TaV_2D_{0.50}$, in agreement with the concentration dependence found from NMR experiments. Also in qualitative agreement with NMR measurements, the relaxation rate for H was over an order of magnitude faster than that for D for similar concentrations. Within experimental error the same value of $\Gamma_{low} = 0.1$ eV was found for the low-temperature motion for all three materials.

Previously undetected attenuation peaks were observed and attributed to an order-disorder transition of the H(D) atoms among the interstitial sites. These peaks provide experimental evidence for an earlier suggestion that the temperature-dependent mobile population is related to ordering. The main contribution of the present work is to provide further evidence for the unusual motion of H(D) at low temperatures in the Laves-phase material TaV_2, and to show that this motion seems to be dominated by quantum effects. Our results indicate that the local relaxation of H(D) in this material remains extremely fast down to very low temperatures. Therefore, the familiar situation of thermally-activated motion does not describe our low-temperature results. The motion appears to be due to other effects, such as barrier fluctuations. Similar effects probably hold for other Laves-phase AB_2 materials and perhaps rare-earth materials as well. A consistent picture was used to describe the present results. Unanswered questions include the nature of the mobile H(D) population, and the reason for the apparent disagreement between the present

ultrasonic measurements and previous NMR measurements as to the fraction of H(D) atoms participating in the local motion.

3.3 Ultrasonic Measurements of H(D) Effects on the Laves-Phase Material $ZrCr_2H(D)_x$.

3.3.1 Introduction and Experimental Details

Due to the small mass of the hydrogen atom, quantum-mechanical effects have been observed for the interstitial motion of H(D) in *C*15 Laves-phase materials.[1,23,24] As discussed in Section 3.1, H(D) diffusion exhibits two different frequencies of motion among interstitial sites in these materials. It is expected that the difference between the two characteristic hopping rates decreases with an increase in R_A/R_B. The ratio for $ZrCr_2$ is considerably higher than for previously studied Laves-phases. Therefore, the difference between the fast jump rate and the slow jump rate for hydrogen motion in this material is expected to be small.[14] Previous studies[37] have shown that the hydrogen in $ZrCr_2$ retains a higher long-range diffusivity than any other metal-hydrogen system with comparable hydrogen concentrations. This work[37] also indicated a change in the effective activation energy for the motion below 200 K. These results were interpreted under the framework of quantum diffusion theory, as discussed in Section 3.1, leading to an understanding of this change as due to a change in the dominant mechanism from tunneling between excited states, to phonon-assisted tunneling between ground states. The case of extremely fast diffusive motion and the possibility of clarifying the diffusive mechanisms motivate the present ultrasonic investigation. The aim of the present work is to explore the concentration dependence and isotope effects on the elastic shear modulus

and the ultrasonic loss in $ZrCr_2H(D)_x$. Ultrasonic attenuation measurements indicate peaks in the loss for $ZrCr_2H_{0.09}$, $ZrCr_2H_{0.15}$, $ZrCr_2H_{0.31}$ and $ZrCr_2D_{0.12}$ that were not observed in the hydrogen-free material. These peaks are associated with the long-range motion of H(D). The ultrasonic measurements reported in Section 3.2 on the Laves-phase compound, TaV_2, have indicated a strong isotope effect on the fast, localized motion, with only a weak isotope effect on the hexagon to hexagon motion. It is interesting in the current measurements that a strong isotope effect is observed for the hexagon to hexagon motion, indicating a larger contribution from quantum effects in $ZrCr_2$. This is consistent with what is expected from the results of Renz *et al.*,[37] for our measurement frequencies and temperatures. The shear modulus also has been measured and is reported for the three concentrations, x(H) = 0, 0.09 and 0.15, and x(D) = 0.12. The modulus is found to increase with increasing H concentration.

Button ingots of the *C*15 Laves-phase intermetallic compound $ZrCr_2$ were prepared by A. V. Skripov *et al.*[29] by arc melting appropriate mixtures of the high-purity constituent elements in an argon atmosphere followed by various annealing procedures. Samples of $ZrCr_2H(D)_x$ were prepared as described previously.[29]

The ultrasonic attenuation and resonant frequencies were measured for $ZrCr_2H_{0.09}$, $ZrCr_2H_{0.15}$, $ZrCr_2H_{0.31}$ and $ZrCr_2D_{0.12}$ over the range of 4-295 K. Rectangular parallelepipeds suitable for the ultrasonic measurements were prepared in the same manner as the TaV_2 samples of Section 3.2. Sample edge dimensions were in the range of 0.8-2.3 mm. Lithium-niobate compressional-mode transducers were used to excite and detect the mechanical resonances. Measurements throughout the entire temperature range were made using a commercial ^{4}He cryostat and temperature

controller. As before, the ultrasonic attenuation in the materials was found by fitting the Lorentzian lineshapes of the resonant peaks to determine the quality factor, Q. The ultrasonic loss is then given simply by $1/Q$.

The aggregate elastic shear moduli for the hydrogenated and deuterated samples were determined at room temperature by RUS as was described in detail in Chapter 2. In all cases, the frequencies of the lowest 20 resonances were measured with a typical root-mean-square (rms) difference between the measured and computed values of 0.4 %. The temperature-dependent values were then calculated from the temperature-dependence of a single frequency, 100 % dependent on the shear modulus.

3.3.2 Results and Discussion

Figure 3.10 shows the ultrasonic loss for $ZrCr_2H_{0.09}$, $ZrCr_2H_{0.15}$, $ZrCr_2H_{0.31}$ and $ZrCr_2D_{0.12}$ over the range of 4-295 K. For comparison, the loss is also shown for hydrogen-free $ZrCr_2$. The room temperature frequencies of all modes are approximately 1.5 MHz. Although there is considerable scatter in the low-temperature data, several meaningful features are apparent. For all hydrogenated samples with $x > 0$ an obvious peak was observed centered at approximately 50-75 K. The attenuation in the hydrogen-free material exhibits an almost constant background with no prominent loss peak. It is clear that the magnitude of the effect increases with increasing H concentration. An obvious peak is also observed in the deuterated material, centered at approximately 160 K. These relatively large peaks are associated with H(D) hopping between hexagons, the slower motion responsible for long-range diffusion.

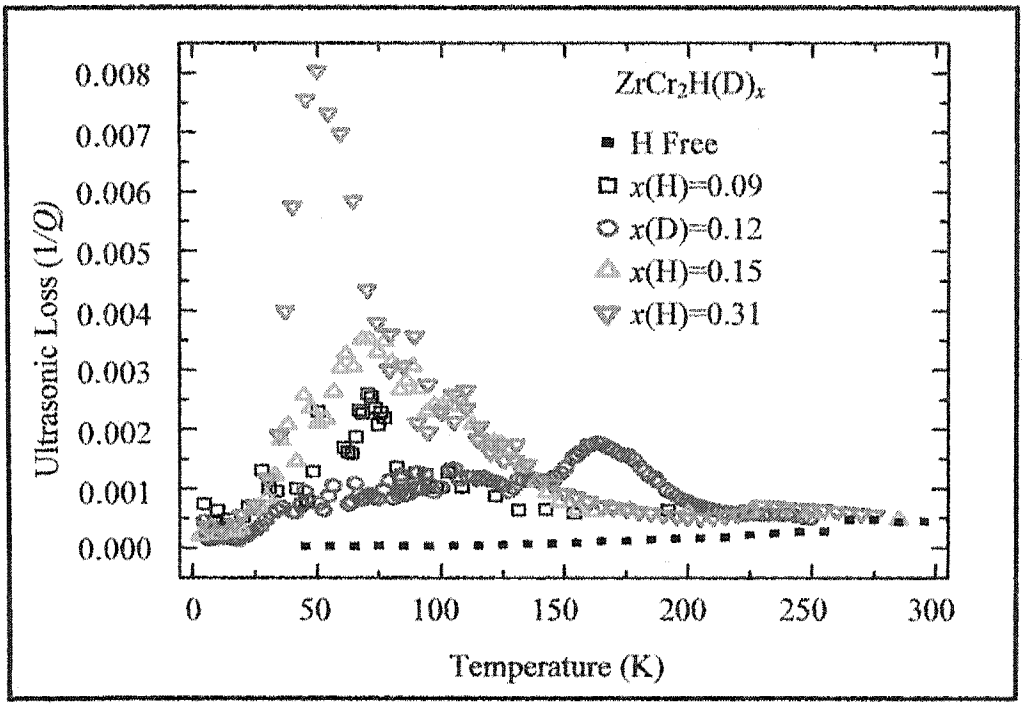

Fig. 3.10 Ultrasonic loss over the temperature range of 4-295 K for $ZrCr_2H(D)_x$ with $x(H) = 0$, 0.09, 0.15 and 0.31 and $x(D) = 0.12$.

Figure 3.11 shows in more detail the loss peaks in $ZrCr_2H_{0.15}$ and $ZrCr_2D_{0.12}$. The peaks indicate a considerable isotope effect. The peak for $ZrCr_2D_{0.12}$ clearly occurs at higher temperatures for approximately the same measurement frequency. This indicates that the D hexagon-to-hexagon jump rate is much lower than that for H. The lower peak height for the deuterated material is almost exactly accounted for by the slightly lower concentration and the fact that it occurs at a higher temperature, assuming a $1 / T$ dependence for the ultrasonic loss. Comparing the temperature at which these peaks occur to the room-temperature peaks in TaV_2 indicates that the long-range motion of H(D) in $ZrCr_2$ is, in fact, much faster than in TaV_2.

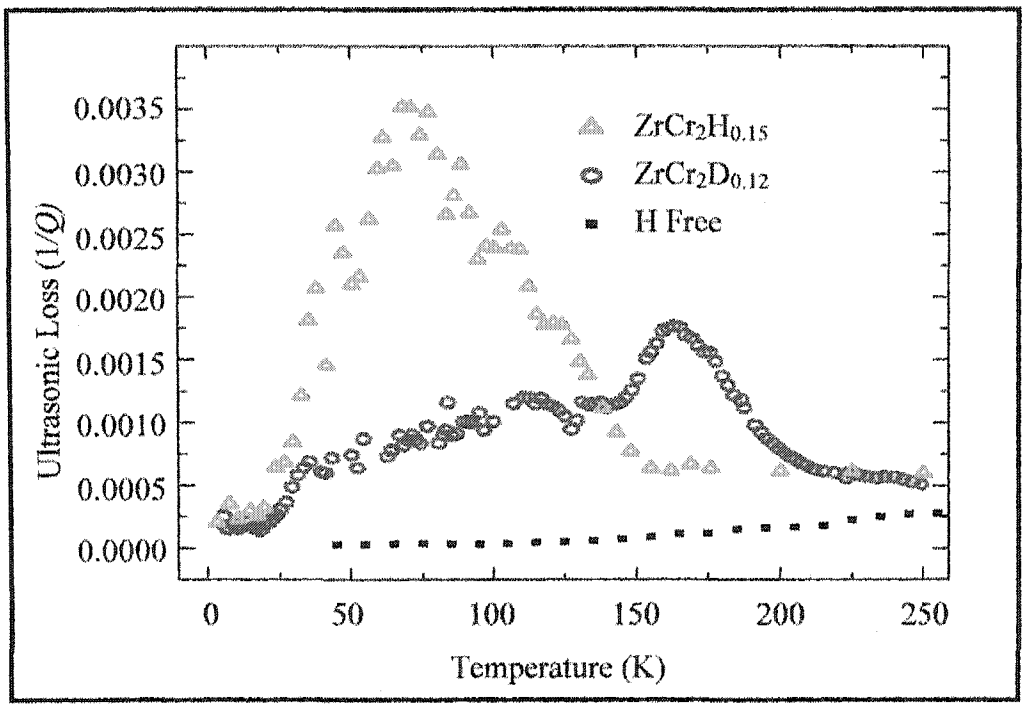

Fig. 3.11 Detail of the ultrasonic loss for $ZrCr_2H_{0.15}$ and $ZrCr_2D_{0.12}$, showing the strong isotope effect. The loss for $ZrCr_2$ is shown for comparison.

The results of Renz *et al.*[37] for $ZrCr_2$ show that the diffusivity of H fit a two-term Arrhenius expression, one term with parameters corresponding to quantum tunneling between excited states and one with parameters corresponding to phonon-assisted tunneling between ground states. The results also suggest that for the temperatures at which our peaks occur, the tunneling between ground states should be the dominant mechanism of the motion. From diffusivity parameters for $ZrCr_2H_{0.30}$, attempt times and activation energies can be calculated for a two-term Arrhenius relaxation time given by

$$\tau_R = \left[\tau_{R0,1}^{-1} \exp\left(\frac{-E_{a,1}}{k_B T}\right) + \tau_{R0,2}^{-1} \exp\left(\frac{-E_{a,2}}{k_B T}\right) \right]^{-1}. \qquad (14)$$

Parameters for the first term, corresponding to tunneling between excited states, are $E_{a,1} = 157$ meV as given in Ref. 37, and $\tau_{R0,1} = 7.26x10^{-13} s$. Parameters for the second term, corresponding to tunneling between ground states, are $E_{a,2} = 39$ meV and $\tau_{R0,2} = 8.43x10^{-10} s$. Using Eq. (14) in Eq. (8), it can be demonstrated that the excited state term is completely negligible for our measurement frequencies and temperatures. Using the ground state term alone, the results are in qualitative agreement with our data for $ZrCr_2H_{0.31}$. Better agreement was found by using an activation energy of $E_{a,2} = 23$ meV in the ground state term. This energy differs somewhat from the value reported in Ref. 37. The solid line in Figure 3.12 shows the results for Eq. (8), using the parameters, $E_a = 23$ meV and $\tau_{R0} = 8.43 \times 10^{-10} s$, in a single-term relaxation time, given by Eq. (9). These parameters produce a peak that compares closely with the $ZrCr_2H_{0.31}$ data as shown in Fig. 3.12. Scatter in the data of Fig. 3.10 due to experimental challenges, together with the presence of some background contributions to the loss, has not allowed us to obtain a reliable fit of the peaks to Eqs. (8) and (9). However, the shape and position of the peaks are consistent with results from using NMR parameters. In this temperature and frequency range, the dominant term in the relaxation is the one associated with ground state tunneling. The theory of quantum diffusion[38,39] indicates that tunneling between ground states is especially sensitive to the mass of the tunneling particle. This is consistent with the large isotope effect seen in the ultrasonic loss data. Due to these factors, it is assumed that at these temperatures and measurement frequencies, the long-range H(D) motion is dominated by quantum tunneling between ground states. A two-term Arrhenius relaxation time previously was found to fit the diffusive H motion in TaV_2 for low H

concentrations.[24,25] However, in the case of TaV_2, tunneling between excited states was the dominant term, with ground state diffusion being negligible for higher hydrogen concentrations and for deuterium. This was consistent with the smaller isotope effect observed for these materials.

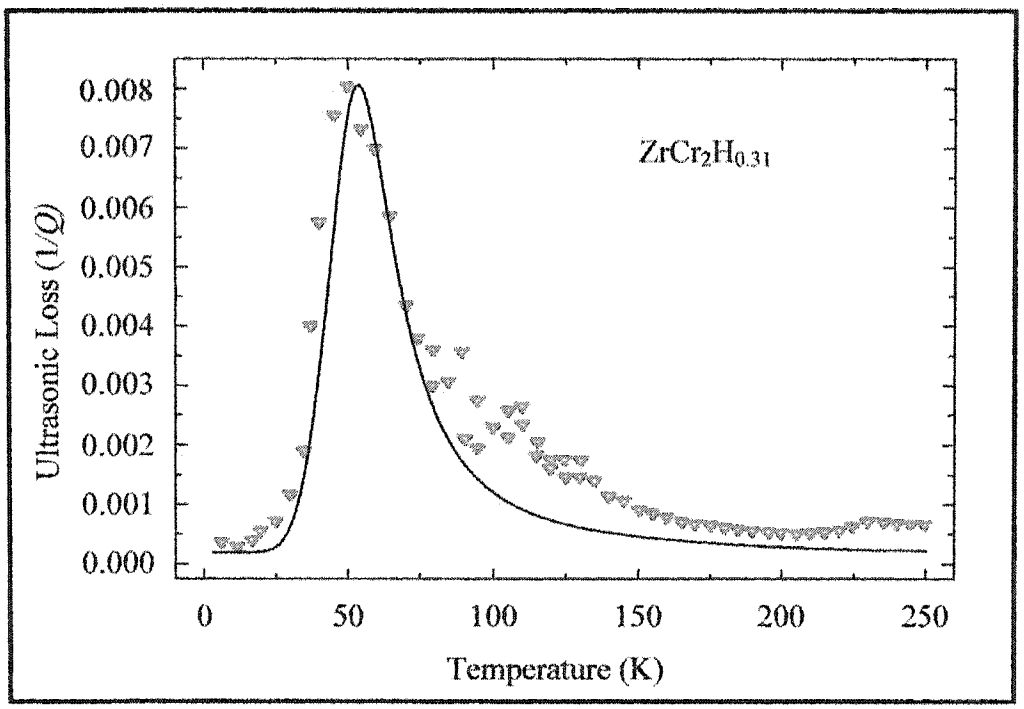

Fig. 3.12 The ultrasonic loss for $ZrCr_2H_{0.31}$. The solid line is a model of the data using Eqs. (8) and (9) with parameters reported in the text.

Figure 3.13 shows the aggregate shear modulus, G, for $ZrCr_2H_{0.09}$, $ZrCr_2H_{0.15}$ and $ZrCr_2D_{0.12}$ over the range of 4-295 K. For comparison, G is also shown for $ZrCr_2$ from previously reported measurements.[40] As mentioned in Section 3.3.1, the temperature-dependence of G for the samples loaded with H(D) is determined by that of a particular resonance frequency, wholly dependent on the shear modulus. A reliable initial fit was not obtained for the highest concentration material. Therefore, G is

not reported for $ZrCr_2H_{0.31}$. For typical materials, the temperature dependence of the elastic constants is such that the moduli approach 0 K with zero slope and decrease monotonically with increasing temperature.[41,42] Fig. 3.13 shows that the moduli of the reported compounds of $ZrCr_2H(D)_x$ behave in a normal fashion over the temperature range of this study. The results also show an increase in the modulus with increasing H content.

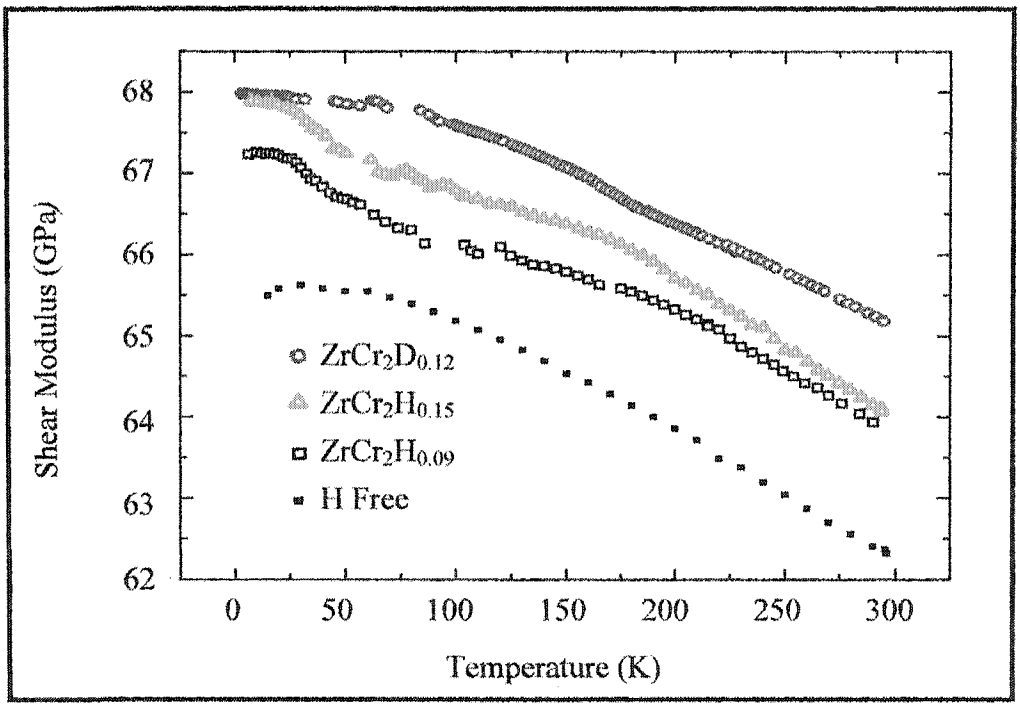

Fig. 3.13 Shear modulus over the temperature range of 4-295 K for $ZrCr_2H_{0.09}$, $ZrCr_2H_{0.15}$ and $ZrCr_2D_{0.12}$. The shear modulus for $ZrCr_2$ is shown for comparison.

Also significant in the shear modulus data is the slight step seen at about 50 K for the hydrogenated materials and at about 160 K for the deuterated sample. As noted in Chapter 1, the theory of relaxation in solids predicts a shift in the real part of the elastic modulus as well as the attenuation effects. The shift is related to the tran-

sition from the relaxed to the unrelaxed elastic moduli as the temperature decreases. The change in the moduli, δc, is given by

$$\delta c = \Delta c \frac{\omega^2 \tau_R^2}{1+\omega^2 \tau_R^2}. \qquad (14)$$

The shifts in G occur at temperatures comparable to the temperatures of peaks in the attenuation. The fractional change in the elastic constant, $\Delta c/c$, can be estimated from Fig. 3.13. $\Delta c/c$ is related to the maximum value of the ultrasonic loss. The maximum value occurs when the quantity $\omega\tau_R \approx 1$, resulting in the relationship, $(1/Q)_{max} = (1/2)\ \Delta c/c$. Using values taken from Fig. 3.13, we estimate for $(1/Q)_{max}$, 0.0035 for $ZrCr_2H_{0.09}$, 0.0036 for $ZrCr_2H_{0.15}$ and 0.0013 for $ZrCr_2D_{0.12}$. These are in remarkably close agreement with values for $(1/Q)_{max}$ taken from Fig. 3.10 of 0.0026 for $ZrCr_2H_{0.09}$, 0.0035 for $ZrCr_2H_{0.15}$ and 0.0017 for $ZrCr_2D_{0.12}$. This agreement supports the interpretation of these peaks as due to H(D) relaxation.

3.3.3 Conclusions

Ultrasonic measurements were made on the *C*15 Laves-phase material $ZrCr_2H(D)_x$ over the temperature range of 4-295 K. Concentrations of hydrogen and deuterium were $x(H) = 0.09$, 0.15 and 0.31 and $x(D) = 0.12$ respectively. Attenuation peaks associated with H(D) motion between *g*-site hexagons were observed in all of these materials for measurement frequencies of approximately 1.5 MHz. The peaks were centered at 50-75 K for H motion, while the peak for D motion was centered at 160 K. This strong isotope effect has been interpreted in terms of quantum mechanical mechanisms of diffusion. The dominant mechanism for these temperatures appears to be tunneling transitions between ground states. These results are

consistent with NMR results for $ZrCr_2$ at higher temperatures. The shear modulus of $ZrCr_2H_{0.09}$, $ZrCr_2H_{0.15}$ and $ZrCr_2D_{0.12}$ was also measured. The overall temperature-dependence was similar to that of typical metals. A small shift was observed in the modulus for each material at a temperature corresponding to the relevant peak in the ultrasonic loss, which is consistent with the interpretation that these peaks were due to H(D) relaxation.

This study, together with the studies reported in Section 3.2, provides insight into the complicated behavior of hydrogen motion in Laves-phase intermetallic compounds. Quantum mechanical motion with an Arrhenius-type appearance was observed for the long-range motion in each material. It has been shown that the particular mechanism that dominates is dependent on the system and the temperature of the measurements. For our measurement temperatures, the long-range motion of hydrogen in TaV_2 is primarily tunneling between excited states while that in $ZrCr_2$ is primarily tunneling between ground states. The local motion of hydrogen in TaV_2 remains extremely fast down to very low temperatures and does not have an Arrhenius-type appearance. This motion may be due to barrier fluctuations. A consistent picture was used to describe the ultrasonic results on the $TaV_2H(D)_x$ and the $ZrCr_2H(D)_x$ systems.

References

[1] A. V. Skripov, Defect and Diffusion Forum, **224-225**, 75 (2004).

[2] J. Shinar, D. Davidov and D. Shaltiel, Phys. Rev. B **30**, 6331 (1984).

[3] R. Hempelmann, D. Richter, O. Hartmann, E. Karlsson and R. Wäppling, J. Chem. Phys. **90**, 1935 (1989).

[4] C. U. Maier and H. Kronmüller, J. Phys.: Condens. Matter **4**, 4409 (1992).

[5] H. Reule, M. Hirscher and H. Kronmüller, Phil. Mag. B **76**, 929 (1997).

[6] M. Kemali, C. E. Buckley, D. K. Ross, S. M. Bennington and S. F. Parker, Physica B **234-236**, 906 (1997).

[7] A. V. Skripov, J. C. Cook, C. Karmonik, and V. N. Kozhanov, Phys. Rev. B **60**, 7238 (1999).

[8] A. V. Skripov, S. V. Rychkova, M. Yu. Belyaev, and A. P. Stepanov, J. Phys.: Condens. Matter **2**, 7195 (1990).

[9] A. V. Skripov, M. Yu. Belyaev, S. V. Rychkova, and A. P. Stepanov, J. Phys.: Condens. Matter **3**, 6277 (1991).

[10] A. V. Skripov, J. C. Cook, C. Karmonik, and R. Hempelmann, J. Phys.: Condens. Matter **8**, L319 (1996).

[11] A. V. Skripov, J. C. Cook, D. S. Sibirtsev, C. Karmonik, and R. Hempelmann, J. Phys.: Condens. Matter **10**, 1787 (1998).

[12] A. V. Skripov, M. Pionke, O. Randl, and R. Hempelmann, J. Phys.: Condens. Matter **11**, 1489 (1999).

[13] A. V. Skripov, J. C. Cook, C. Karmonik, and V. N. Kozhanov, Phys. Rev. B **60**, 7238 (1999).

[14] A. V. Skripov, J. C. Cook, T. J. Udovic, and V. N. Kozhanov, Phys. Rev. B **62**, 14099 (2000).

[15] A. V. Skripov, A. V. Soloninin and V. N. Kozhanov, Solid State Commun. **122**, 497 (2002).

[16] J. H. Westbrook, ed., *Intermetallic Compounds* (Wiley, New York, 1967).

[17] A. S. Nowick and B. S. Berry, *Anelastic Relaxation in Crystalline Solids* (Academic Press, New York, 1972).

[18] A. Migliori and J. L. Sarrao, *Resonant Ultrasound Spectroscopy* (Wiley, New York, 1997).

[19] J. Jackle, L. Piche, W. Arnold and S. Hunklinger, J. Non-Crystal. Solids **20**, 365 (1976).

[20] D. Emin, M. I. Baskes, and W. D. Wilson, Z. Phys. Chem., NF **114**, 231 (1979).

[21] C. P. Flynn and A. M. Stoneham, Phys. Rev. B **1**, 3966 (1970).

[22] Yu. Kagan, J. Low Temp. Phys. **87**, 525 (1992).

[23] K. Foster, R.G. Leisure, and A.V. Skripov, J. Phys.: Condens. Matter **11**, 799 (1999).

[24] K. Foster, J. E. Hightower, R. G. Leisure, and A. V. Skripov, J. Phys.: Condens. Matter **13**, 7327 (2001).

[25] K. Foster, R. G. Leisure, and A. V. Skripov, Phys. Rev. B **64**, 214302 (2001).

[26] P. Fischer, F. Fauth, A. V. Skripov, A. A. Podlesnyak, L. N. Padurets, A. L. Shilov, and B. Ouladdiaf, J. Alloys Comp. **253-254**, 282 (1997).

[27] A. L. Shilov, L. N. Padurets, Zh. V. Dobrokhotova, and N. T. Kuznetsov, Russ. J. Inor. Chem. **45**, 1401 (2000).

[28] A. V. Skripov, A. V. Mirmelshtein, and M. Yu. Belyaev, Solid State Commun. **81**, 689 (1992).

[29] A. V. Skripov, M. Yu. Belyaev, S. V. Rychkova, and A. P. Stepanov, J. Phys.: Condens. Matter **1**, 2121 (1989).

[30] A. Migliori, J. L. Sarrao, W. M. Vissher, T. M. Bell, M. Lei, Z. Fisk, and R. G. Leisure, Physica B **183**, 1 (1993).

[31] R. G. Leisure and F. A. Willis, J. Phys.: Condens. Matter **9**, 6001 (1997).

[32] A. B. Bhatia, *Ultrasonic Absorption: An Introduction to the Theory of Sound Absorption and Dispersion in Gases, Liquids and Solids* (Oxford University Press, London, 1967).

[33] K. Foster, J. E. Hightower, R. G. Leisure, and A. V. Skripov, Phys. Rev. B **65**, 094108 (2002).

[34] A. L. Buzlukov and A. V. Skripov, J. Alloys Comp., to be published.

[35] A. P. Levanyuk, S. A. Minyukov and M. Vallade, J. Phys. I France **2**, 1949 (1992).

[36] Walther Rehwald, Adv. Phys. **22**, 721 (1973).

[37] W. Renz, G. Majer, A. V. Skripov and A. Seeger, J. Phys.: Condens. Matter **6**, 6367 (1994).

[38] D. Emin, M. I. Baskes and W. D. Wilson, Z. Phys. Chem., Neue Folge **114**, 231 (1979).

[39] Y. Fukai, *The Hydrogen-Metal System* (Springer, Berlin, 1993).

[40] K. Foster, J. E. Hightower, R. G. Leisure and A. V. Skripov, Phil. Mag. B **80**, 1667 (2000).

[41] J. A. Garber, A. V. Granatao, Phys. Rev. B **11**, 3990 (1975).

[42] G. A. Alers in: *Physical Acoustics, Vol. IV*, W. P. Mason, ed. (Academic Press, New York, 1966).

Chapter 4

A Resonant Ultrasound Spectroscopy Study of the Elastic Properties of the Hydrogen-Absorbing Compounds $TiCr_{1.8}$ and $LaAl_xNi_{5-x}$

- 4.1 Background
- 4.2 Temperature Dependence of the Elastic Moduli of Polycrystalline $TiCr_{1.8}$.
- 4.3 Temperature Dependence of the Elastic Moduli of Polycrystalline $LaAl_xNi_{5-x}$.
- References

4.1 Background

Many of the hydrogen-absorbing intermetallic compounds are of great interest for the reversible absorption of hydrogen. Among the benefits of reversibility is the use of such materials to supply hydrogen as the negative electrode in battery applications. The stability of the formed hydride is determined by the hydrogen equilibrium pressure at a given temperature.[1] This equilibrium pressure, or plateau pressure, is the hydrogen pressure in the relatively flat region of the pressure-composition (PC) isotherm for hydrogenation. Figure 4.1 shows theoretical PC isotherms for the absorption of hydrogen in intermetallic compounds. In the α-phase, at low H content, the hydrogen forms a single-phase solid-solution. As the H/M concentration is increased, there is a two-phase domain in which the α-phase is saturated and hydride formation takes place.

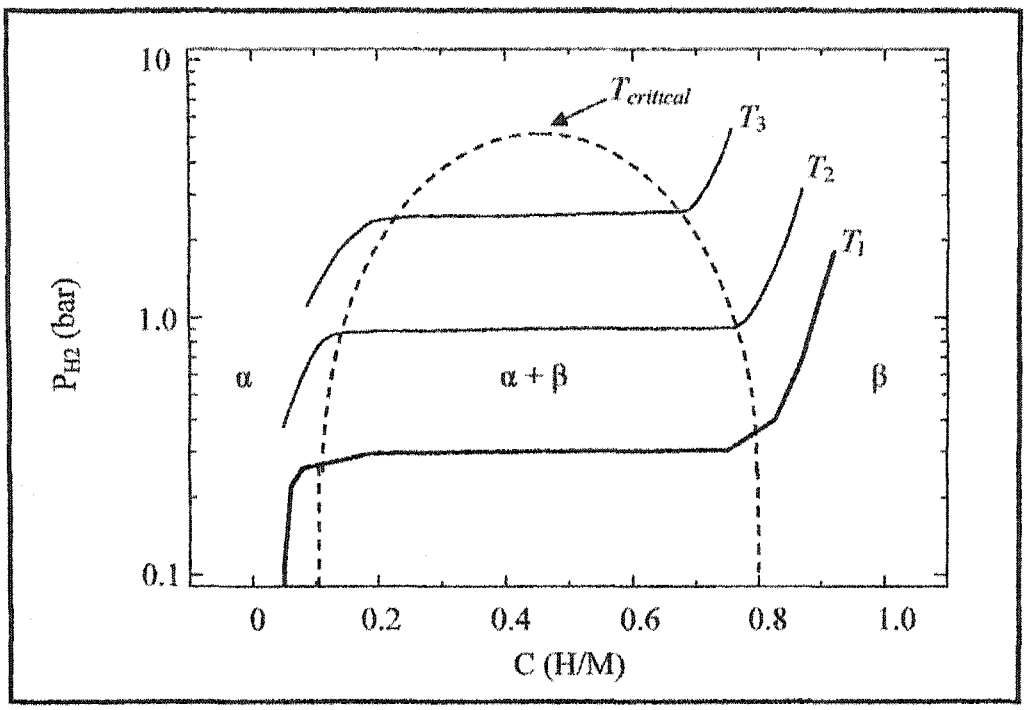

Fig. 4.1 Typical pressure-composition isotherms for the absorption and of hydrogen in hydrogen-absorbing compounds. Isotherms at and above the critical temperature have no two-phase region, α + β.

The elastic constants of these materials are important for a variety of reasons. Specifically for metal-hydride materials, the elastic constants are useful for an evaluation of the elastic contribution to the hydrogen-hydrogen interaction energy[2] and the elastic energy associated with the precipitation of hydrides.[3,4] For an isotropic material with free surfaces, the long-range, average elastic interaction energy of one interstitial hydrogen atom with the strain field of all the other hydrogen atoms is[5]

$$U_{elastic} = -\gamma \frac{P^2 \rho}{B} \tag{1}$$

where B is the bulk modulus, P is an element of the dipole moment tensor, ρ is the density of H atoms, and

$$\gamma = \frac{2(1-2\nu)}{3(1-\nu)} \tag{2}$$

with ν being Poisson's ratio. This result can be expressed in a more convenient form for the present analysis, in which elastic properties are determined. First,

$$\rho = \frac{n_H}{V} \tag{3}$$

where n_H is the number of hydrogen atoms in a volume V. For a homogeneous distribution of centers of dilatation, the dipole moment tensor is $P_{ij} = P\delta_{ij}$. The hydrogen atoms produce a change in volume given by[6]

$$\frac{\Delta V}{V} = \frac{\rho P}{B}. \tag{4}$$

Solving for P gives

$$P = \frac{V}{n_H}\frac{n_H v_H}{V} B = B v_H \tag{5}$$

where we have used $\Delta V = n_H v_H$, with v_H being the volume associated with each of the n_H hydrogen atoms. Substituting Eqs. (3) and (5) into (1) and using $V = n_M v_o$, with v_o being the volume associated with each of the n_M metal atoms, gives

$$U_{elastic} = -u_{elastic}\left(\frac{n_H}{n_M}\right) \tag{6}$$

with

$$u_{elastic} = \gamma B \frac{v_H^2}{v_o} \tag{7}$$

Alefeld[5] shows that the factor γ accounts for the fact that the self-energy of the H atom interacting with its own stress field should be omitted. Eq. (7) shows that the

elastic interaction energy is dependent on Poisson's ratio and on the bulk modulus, two elastic parameters that may be obtained from resonant ultrasound spectroscopy measurements.

In addition to the elastic contributions to the interactions among the dissolved H atoms, there is expected to be an electronic contribution. For low H concentrations, the total interaction may be written[2]

$$U = -(u_{elastic} + u_{electronic})\left(\frac{n_H}{n_M}\right). \tag{8}$$

As discussed in Reference 2, the electronic term is expected to consist of a part that depends only on the total number of extra electrons brought into the metal by the added H atoms and a part that depends on the local electronic structure. The elastic energy of hydride formation will be discussed in the following sections for the particular cases of $TiCr_{1.8}$ and $LaAl_xNi_{5-x}$.

At the most fundamental level, the adiabatic elastic constants are given by the second derivative of the internal energy with respect to strain and thus are related to interatomic potentials. They are also related to thermal properties through the Debye theory. The long-wavelength vibrational contribution to the heat capacity at low temperature, T, is given by

$$c_v = \frac{2\pi^2 k_B^4 T^3}{5\hbar^3 c_0^3} = \frac{12\pi^4}{5}\left[\frac{N}{V}\right]k_B\left[\frac{T}{\theta_D}\right]^3 \tag{9}$$

where k_B is Boltzmann's constant. Eq. (9) effectively defines the Debye temperature, θ_D, which is given by

$$\theta_D = \left[6\pi^2 \frac{N}{V}\right]^{1/3} \frac{\hbar}{k_B} c_0 \tag{10}$$

where N/V is usually taken[7,8] as the number of atoms per unit volume, and the average sound velocity, c_0, is given by the expression

$$\frac{1}{c_0^3} = \frac{1}{3}\left[\frac{1}{c_l^3} + \frac{2}{c_t^3}\right]. \tag{11}$$

The longitudinal and transverse sound velocities, c_l and c_t respectively, can be calculated from the polycrystalline elastic moduli, C_{11} and G, using the following relationships:

$$c_l = \sqrt{\frac{C_{11}}{\rho}}, \qquad c_t = \sqrt{\frac{G}{\rho}} \tag{12}$$

where ρ in this case is the density of the metal. These thermal parameters will be calculated in the following sections for $TiCr_{1.8}$ and $LaAl_xNi_{5-x}$.

4.2 Temperature Dependence of the Elastic Moduli of Polycrystalline $TiCr_{1.8}$.

4.2.1 Introduction and Experimental Details

A substantial effort is being made by various research groups to understand metal-hydrogen systems at a fundamental level. In that connection, the pressure-composition isotherms of the hydrides of $TiCr_{\approx 2}$ were recently measured.[9,10] The critical temperature of this system is rather low, which means that it is possible, at reasonable temperatures (up to 400 K) and hydrogen pressures (a few hundred atmospheres), to measure the PC isotherms above the critical temperature. As indicated in Fig. 4.1, isotherms above the critical temperature bypass the two-phase

region, $\alpha + \beta$. Fitting statistical thermodynamic models to the data is much simplified if the complications of the α - β phase separation are avoided. The results of such experiments and fitting indicated that the H-H interaction in the $TiCr_{1.8}$ - H_2 system changed sign at about 400 K, being attractive below this temperature and repulsive above. Contributing to the H-H interaction is the long-range, elastic interaction. In order to evaluate the long-range elastic interaction, the elastic constants are needed. This section reports on the measurement of the elastic moduli of $TiCr_{1.8}$ over the temperature range of 3-410 K and gives the elastic interaction energy.

The $TiCr_{1.8}$ sample was prepared by O. Beeri and M. H. Mintz at the Nuclear Research Center of the Negev in Beer Sheva, Israel. Details of the sample preparation have been described previously.[9,10] The present measurements were carried out on $TiCr_{1.8}$ that had the cubic, *C*15 Laves-phase structure. This structure has been described in detail in Chapter 4. The elastic moduli were measured using the technique of Resonant Ultrasound Spectroscopy (RUS).[11,12,13] As described in detail in Chapter 2, with the RUS technique, piezoelectric transducers are used to excite a large number of the lowest frequency vibrational eigenmodes for samples of well-defined shapes, such as rectangular parallelepipeds. For the present study, a low-speed diamond saw was used to cut an approximate parallelepiped from the intermetallic, polycrystalline ingot. This sample was then hand-polished into an accurate rectangular parallelepiped suitable for the ultrasonic measurements. The edge dimensions of the sample were 1.640 mm, 1.014 mm, and 1.142 mm. The determination of elastic constants by RUS was described in detail in Chapter 2. For

the entire temperature range investigated, the frequencies of the lowest 20 resonances were measured with a typical rms difference between measured and computed frequencies of 0.30 %. For materials with isotropic symmetry, only two independent moduli are required to fully define the elasticity of the system. The aggregate elastic moduli C_{11} and C_{44} were derived directly from the measured frequencies. C_{44} is simply the usual polycrystalline shear modulus G. Other aggregate elastic parameters such as the bulk modulus, Young's modulus, and Poisson's ratio can be calculated from C_{11} and C_{44}. These relationships were given in Chapter 1, Eq. (5). The temperature-dependent measurements below room temperature were made using a commercial ^{4}He cryostat and temperature controller. Measurements above room temperature were made using a commercial oven. Below 295 K the temperature was measured with a calibrated silicon diode thermometer. Above 295 K the temperature was measured with a platinum resistance thermometer.

4.2.2 Results and Discussion

By direct measurement of dimensions and mass, the room-temperature density of bulk $TiCr_{1.8}$ was found to be 5.987 g/cm^3 ± 0.3 %. The lattice parameter of $TiCr_{1.8}$ is reported[14] to be 0.6939 nm at 25 °C. Obviously, not all the sites in the AB_2, $C15$ structure are occupied by A and B atoms in the usual way for $TiCr_{1.8}$. We can use the measured value of the density to infer something about the $TiCr_{1.8}$ structure. Using the mass of one $TiCr_{1.8}$ unit, the volume of one unit cell and the measured density, we can calculate the number of $TiCr_{1.8}$ units in one unit cell. The result is 8.52, from which we get 8.52 Ti atoms, 15.34 Cr atoms and 0.14 vacant sites in a unit cell. These numbers are in contrast to those for the usual AB_2 unit cell, which would

normally have 8 A atoms and 16 B atoms. If we assume that the Ti sites are fully occupied by Ti atoms and some of the nominally Cr sites are occupied by Ti in the AB_2 C15 structure, these numbers correspond to 0.9 % of the Cr sites being vacant, and 3.3 % of the Cr sites being occupied by Ti atoms. The atomic size of the Ti atoms is approximately equal to that of the Cr atoms. One would expect, for Laves-phases with a small atomic size difference between the A atoms and the B atoms, that there would be anti-site substitutions more readily than constitutional vacancies.[15] The calculation above agrees with this expectation.

Figure 4.2 shows the polycrystalline bulk and shear moduli of $TiCr_{1.8}$ over the temperature range of 3–410 K. Figure 4.3 shows Young's modulus and Figure 4.4 shows Poisson's ratio for $TiCr_{1.8}$. Error bars on the graphs represent an estimate of the absolute accuracy of the results based on the agreement between calculated and measured resonance frequencies, and errors in density measurements. The accuracy is higher for the shear modulus than for the bulk modulus, as mentioned in Section 2.4. Especially for the bulk modulus, the estimated error is much larger than any random scatter in the data. This is because the errors from the density and the RUS fit are systematic across the entire temperature range. The sample dimensions and density are needed to calculate the elastic constants deduced from the measured frequencies. Because thermal expansion data are not presently available for $TiCr_{1.8}$ the results have not been corrected for thermal contraction; the room temperature dimensions and density were used in the analysis. Taking into account the direct dimensional effects as well as the indirect effect through the density, the computed C_{ij} vary inversely with the dimensions. Transition metals have a total thermal

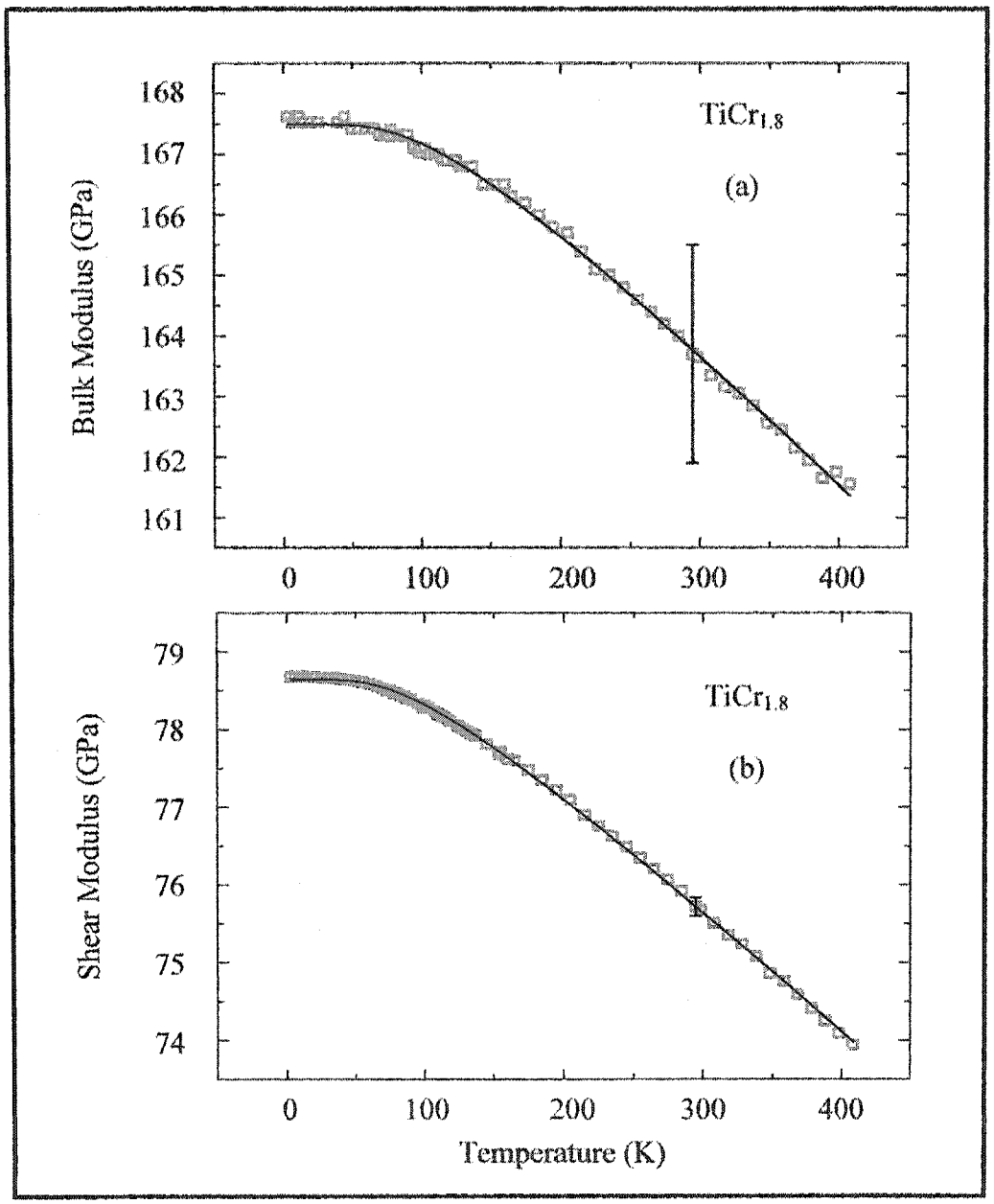

Fig. 4.2 Elastic moduli of polycrystalline $TiCr_{1.8}$ vs. temperature: (a) bulk modulus; (b) shear modulus. The solid lines represent a fit of the semi-empirical Varshni expression to the data, with fit parameters given in the text. Error bars represent an estimate of the absolute error.

contraction of less than 0.2 % on cooling from room temperature to 3 K.[16] In particular, titanium has a total thermal contraction of 0.153 % and chromium, from room temperature to 25 K, has a total thermal contraction of 0.098 %.[17] Furthermore, the thermal expansion of alloys does not seem to differ much from that of the constituent elements. Assuming that $TiCr_{1.8}$ behaves similarly, correcting for thermal contraction would add at most 0.2 % to the low-temperature values. Similarly, the values at 410 K would be at most 0.2 % lower with corrections for thermal expansion above room temperature.

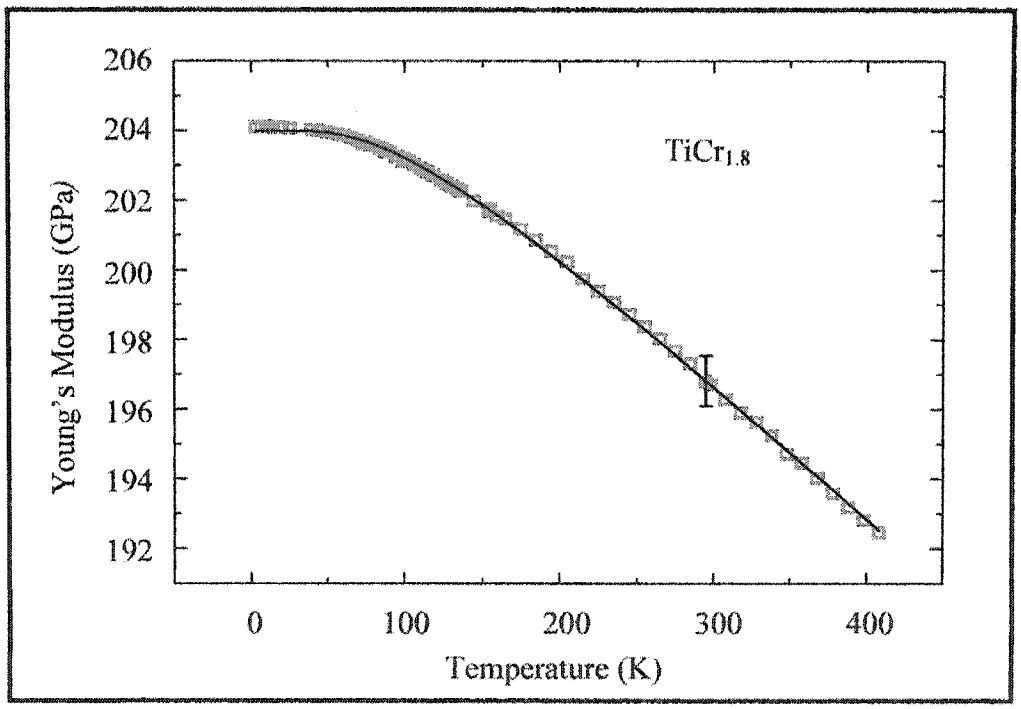

Fig. 4.3 Young's modulus of polycrystalline $TiCr_{1.8}$ vs. temperature. The solid line represents a fit of the semi-empirical Varshni expression to the data, with fit parameters given in the text.

The temperature dependence of the elastic moduli was discussed in detail in Section 2.5. Taking into account the various contributions to the temperature dependence, the overall result, for typical materials, is that the elastic moduli approach 0 K with zero slope and decrease monotonically with increasing temperature.[18,19] This simple picture is not applicable to materials undergoing phase transitions[20,21] or to materials with more complicated electronic structures.[22,23,24] Figures 4.2 and 4.3 show that the moduli of $TiCr_{1.8}$ behave in a normal fashion, becoming linear in temperature at high temperature. Figure 4.4 gives Poisson's ratio ν, which increases very slightly with increasing temperature. Both the value of $\nu \approx 0.30$ and the observed temperature dependence are characteristic of metals.[25]

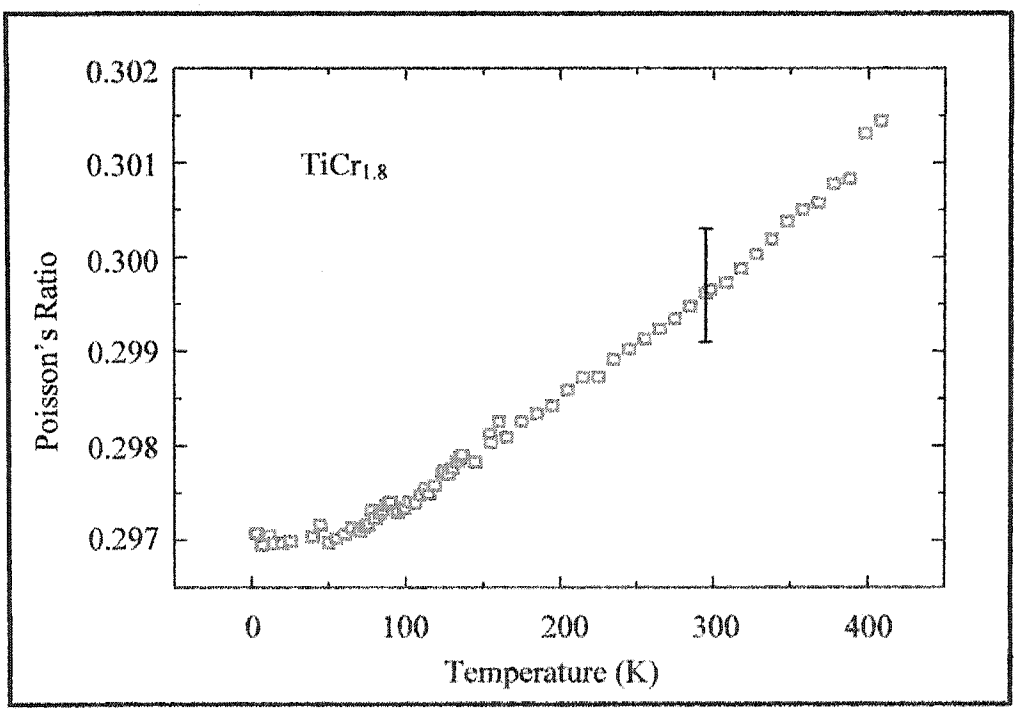

Fig. 4.4 Poisson's ratio of polycrystalline $TiCr_{1.8}$ vs. temperature.

The temperature dependence of the elastic constants of many materials is described successfully by the semi-empirical Varshni expression,[26]

$$C(T) = C(0) - \frac{s}{\exp(t/T) - 1} \tag{13}$$

where $C(0)$, s, and t are three adjustable parameters with $C(0)$ being the value of the elastic constant C at zero temperature. The solid lines in Figs. 4.2 and 4.3 represent the fit of Eq. (13) to the data. The fitting parameters $C(0)$, s, and t for the bulk modulus are 167.5 GPa, 7.2 GPa, and 318 K; for the shear modulus 78.6 GPa, 4.3 GPa, and 265 K; and, for Young's modulus 204.0 GPa, 10.8 GPa, and 271 K, respectively. As Figs. 4.2 and 4.3 show, this simple expression gives a good account of the temperature dependence of the moduli. This provides additional evidence that the temperature dependence of the polycrystalline elastic moduli of $TiCr_{1.8}$ resembles that of many other materials.

One of the applications of this study lies in the realm of the hydrogen storage properties of $TiCr_{1.8}$. In particular, one can use the bulk modulus in a calculation of the hydrogen interaction energy. We now evaluate $u_{elastic}$ for $TiCr_{1.8}$. In addition to the elastic moduli, v_H and v_o are needed. The partial molar volume of H in $TiCr_{1.8}$ was measured by Lynch *et al.*[27] to be $\bar{V}_H = 1.51\,\mathrm{cm}^3$. Thus, $v_H = \bar{V}_H / N_A = 2.51 \times 10^{-30}\ \mathrm{m}^3$. Using the lattice parameter for $TiCr_{1.8}$ of 0.6939 nm and 23.86 as the number of metal atoms in the unit cell as inferred from the density, results in $v_o = 1.40 \times 10^{-29}\ \mathrm{m}^3$. Figure 4.5 presents $u_{elastic}$ as a function of temperature. The factor $\gamma = 0.38$ in the present case and depends only very weakly on temperature. As can be seen from Fig. 4.5, $u_{elastic}$ has only a weak temperature dependence, essentially that of the bulk modulus. It has the value of approximately 0.175 eV per H atom in the

range of room temperature and above. Taking into account the negative sign of Eq. (8), this value represents a *negative* contribution to the enthalpy of formation.

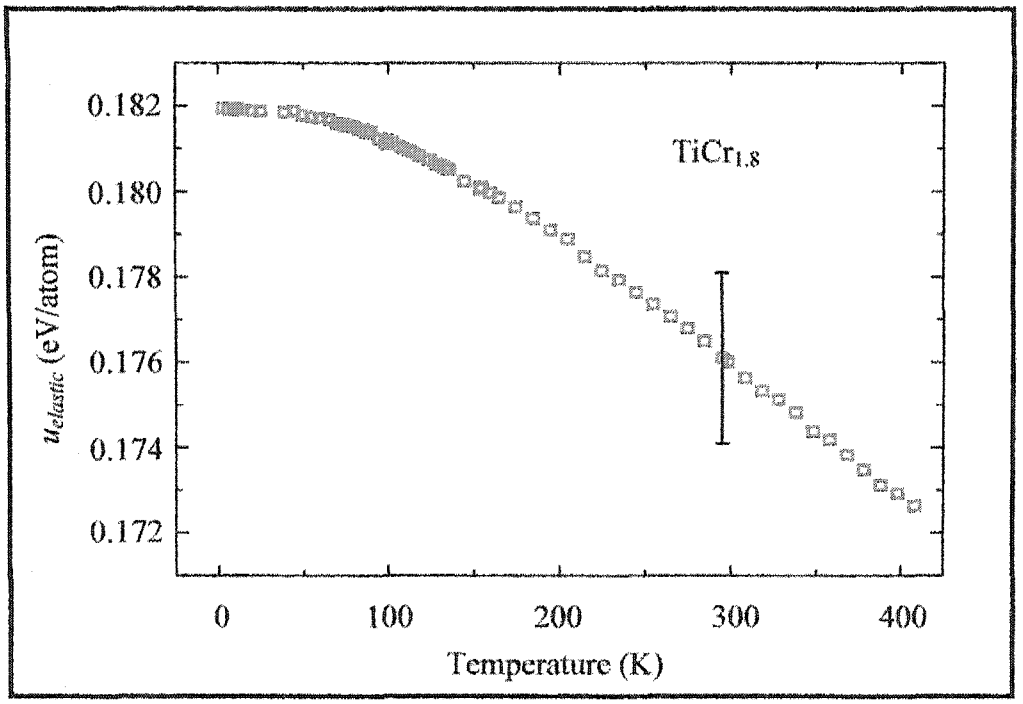

Fig. 4.5 Parameter describing the long-range elastic interaction energy of one interstitial hydrogen atom with the stress fields of all the other hydrogen atoms, calculated from Eq. (7) using the elastic parameters of Figs. 4.2 and 4.4.

The experimental results for the enthalpy of formation, ΔH, in $TiCr_{1.8}$ are expressed as

$$\Delta H = a_H + b_H (n_H / n_m) . \tag{14}$$

The result[10] is $-b_H = 0.0586$ eV per H atom. The experimental b_H includes the elastic interaction as well as electronic effects. Comparing the experimental result for b_H with that for the elastic interaction gives $u_{electronic} = -0.116$ eV per H atom. Taking into account the sign of Eq. (8) indicates that the electronic effects result in a *positive* contribution to the enthalpy of formation. The electronic effect may be somewhat

larger than what is reported here, because the factor γ probably underestimates the elastic contribution at short range.[28] One positive contribution to b_H is due to the filling of states at the Fermi level by the extra electrons brought into the metal by the hydrogen atoms. In a simple band-filling picture, this effect gives a positive contribution to the heat of formation proportional to $1/N(E_F^M)$ where $N(E_F^M)$ is the density of states of the host metal at the Fermi level.[2] The density of states for *C*15 $TiCr_2$ has been calculated,[29] yielding a value of 1.29 states / eV. Taking spin into account, *if* each hydrogen atom contributed one electron to the conduction band, then it would take two hydrogen atoms to raise the energy by 0.77 eV. This represents a positive contribution to the heat of formation that is proportional to 0.39 eV per H atom. This value is obviously too high, indicating that this picture is undoubtedly oversimplified. Short-range effects due to the local electronic structure are surely important.

Fitting statistical thermodynamic results to the measured pressure-composition isotherms in the $TiCr_{1.8} - H_2$ system indicated[10] that the H-H interaction parameter changed sign as a function of temperature, being attractive below about 400 K and repulsive above that temperature. The present results indicate that this sign reversal is not due to any unusual behavior of the elastic moduli. It must be said, however, that the moduli of the hydride could be qualitatively different from those of the host metal reported here.

As mentioned in Section 4.1, other parameters related to thermal properties can be calculated from the elastic constant measurements. The values of B and G at 3 K give $c_o = 4.05 \times 10^3$ m/s for the average sound velocity in the material. Using this

value in Eq. (10), the Debye temperature, calculated from the 3 K moduli, is found to be 500 K. The acoustic contribution to the low-temperature specific heat is found to be $c_v / T^3 = 1.84$ J/m^{3}K^4. The Debye theory gives an accurate account of the long-wavelength acoustic contribution to the specific heat at low temperatures. Calorimetric measurements, of course, include all contributions - phonon, electronic, and any other effects.

4.2.3 Conclusions

The elastic moduli of polycrystalline $TiCr_{1.8}$ have been measured over the temperature range of 3–410 K. The temperature dependence resembles that of ordinary metals, approaching 0 K with zero slope and decreasing linearly with temperature at higher temperatures. The moduli measurements, along with other data from the literature, were used to calculate the long-range, elastic interaction between absorbed hydrogen atoms. This interaction is weakly temperature dependent, having essentially the temperature dependence of the bulk modulus. Expressed as a linear function of the H/(Ti + Cr) ratio, the interaction parameter decreases from 0.182 eV per H atom at 3 K to 0.172 eV per H atom at 410 K and represents a negative contribution to the enthalpy of formation of the hydride. The elastic interaction does not appear to be responsible for the reversal of the sign of the H-H interaction parameter found in fitting pressure-composition isotherms to statistical thermodynamics models. Comparison of the elastic contribution to thermodynamic measurements indicates a positive electronic contribution of the heat of formation of about 0.116 eV per H atom near room temperature. The Debye temperature, calculated from the low-temperature elastic moduli, was found to be 500 K.

4.3 Temperature Dependence of the Elastic Moduli of Polycrystalline $LaAl_xNi_{5-x}$

4.3.1 Introduction and Experimental Details

The intermetallic compound $LaNi_5$ is of great importance for hydrogen storage applications,[30] especially for use as an electrode in metal-hydride batteries. Alloys such as LaM_xNi_{5-x} where M represents a metal atom that substitutes for Ni, are commonly used because the basic properties can be altered in favorable ways by such substitution. One such property is the plateau pressure, discussed in Section 4.1. The $LaAl_xNi_{5-x}$ system exhibits a unit cell expansion and concomitant decrease in plateau pressure upon the substitution of Al for Ni.[31,32,33] We have previously measured and reported the room-temperature elastic constants of these alloys and found that the elastic constants decrease with increasing x.[34] This section reports ultrasonic measurements of the elastic moduli of polycrystalline $LaAl_xNi_{5-x}$ over the temperature range of 3-415 K. Temperature dependent measurements of the elastic constants provide useful information. Theoretical calculations of the moduli are usually made for zero temperature, thus low-temperature experimental results provide a better test of theory. The temperature dependence of the moduli reflects the anharmonic nature of the interatomic potentials and thus provides a challenge for theorists. Finally, practical uses of these materials often occur at temperatures other than room temperature.

$LaAl_xNi_{5-x}$ (x = 0, 0.25, 0.50, 1) compounds were prepared by O. Yeheskel and I. Jacob at Ben-Gurion University of the Negev in Beer Sheva, Israel. The materials were prepared by arc-melting the elemental constituents (> 99.9 % purity)

on a water-cooled copper hearth under argon atmosphere. Attainment of single-phase $CaCu_5$-type intermetallic compounds was confirmed in all cases by x-ray diffraction analysis. The attenuation of the ultrasonic signals in the as-cast samples, or in samples treated by standard annealing procedures, was so great that it prevented any meaningful analysis of the corresponding experimental data. Subsequently, the brittle $LaAl_xNi_{5-x}$ pellets were ground to powder less than 36 μm (~ 400 mesh) in size. About five grams of each powder were wrapped in a thin Mo foil and the "cigarette"-like sample was inserted into a low-carbon steel tube. One end of the tube was welded and the samples were degassed at 225 °C at approximately 2 x 10^{-2} mbar for one hour. The second end of the stainless steel tube was welded at the termination of the degassing procedure. The tube was then introduced into a special chamber that was filled with argon at 1000 bar. Electrical current concomitantly heated the stainless steel tube to 1050 °C for two hours. The tube softened under these conditions and transmitted the external pressure to the wrapped intermetallic powders, which, at the end of this hot isostatic pressing (HIP) procedure, were found to be solid bulk pieces. The many cracks and micro-cracks, easily observed in the as-cast or standard-annealed samples, vanished after the HIP. The intermetallic compounds that underwent HIP treatment were also examined by x-ray diffraction. Slight changes of the lattice constants were observed. The slight changes may be a result of the drastic procedure the samples underwent, or of some minute Ni segregation. Densities were measured by the liquid displacement (Archimedes) method. The liquid density was corrected for temperature variation. The accuracy of the density measurement is estimated to be ± 0.4 %.

The elastic moduli were measured using the technique of Resonant Ultrasound Spectroscopy (RUS), in the same manner as described in Section 4.2. The HIP samples were hand-polished into accurate rectangular parallelepipeds suitable for the ultrasonic measurements. The resulting edge dimensions were in the range of 1 to 2 mm for the various $LaAl_xNi_{5-x}$ samples. Figure 4.6 shows a section of an RUS spectrum for the $LaAlNi_{4.0}$ sample, taken at 10 K. Two resonances are shown. The clean spectrum and relatively high Q-values (narrow lines) indicate the high quality of the specimen. High Q-values were typical of all the samples studied. The elastic

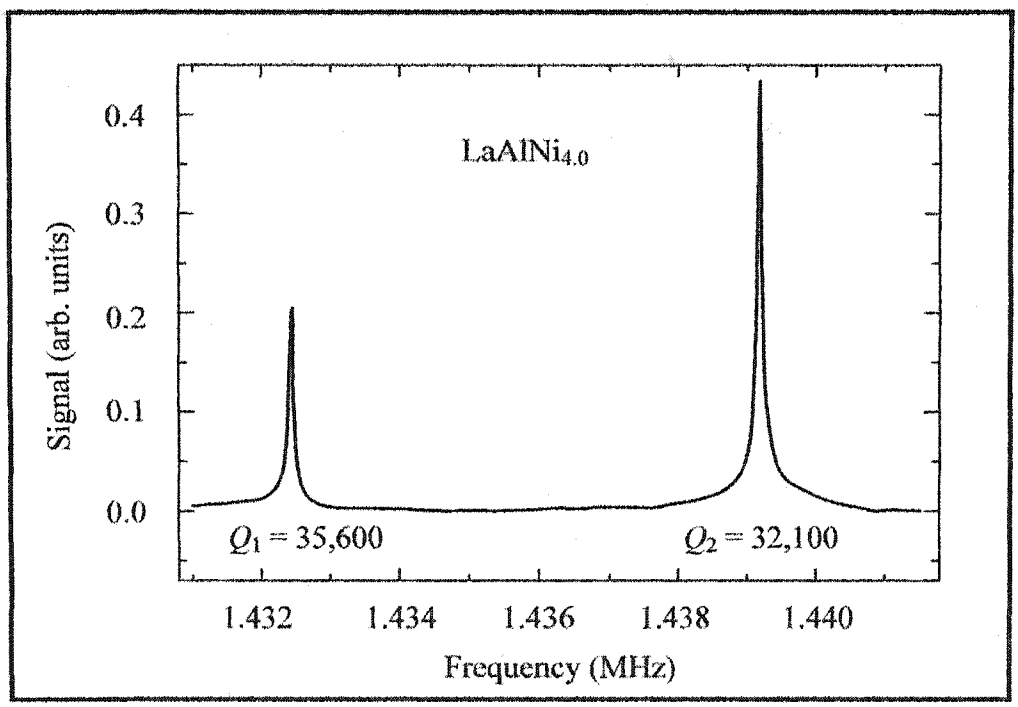

Fig. 4.6 Section of an RUS spectrum for $LaAlNi_4$ at 10 K showing two resonances.

constants were calculated from the measured frequencies as described in detail in Chapter 2. For the entire temperature range investigated, the frequencies of the lowest 25 resonances were measured with a typical rms difference between measured

and computed frequencies of 0.20 % or less. The aggregate elastic moduli C_{11} and C_{44} were derived directly from the measured frequencies. From these two moduli the polycrystalline shear modulus (G), bulk modulus (B), Young's modulus (E), and Poisson's ratio (ν), were computed using the relationships given in Chapter 1, Eq. (5). The measurements below room temperature were made using a commercial ^{4}He cryostat and temperature controller. Lithium-niobate compressional-mode transducers were used to excite and detect mechanical resonances. Measurements above room temperature were made using a commercial oven and temperature controller.

4.3.2 Results and Discussion

For all of the studied materials, a theoretical density was calculated from the measured lattice constants. By comparing this density with that measured by the Archimedes method, a porosity, δ, was calculated. Room temperature lattice constants, measured room temperature densities and theoretical x-ray densities have been reported previously[34] for all of the materials. The porosity for the $LaAl_xNi_{5-x}$ samples ranged from 0 to 2.0%. Although the porosity is relatively low, it was decided to make a correction for this effect so that the dependence of the moduli on x would not be distorted by the different porosities. The measured bulk and shear moduli were corrected in the following way. In the limit of low porosity, different theoretical expressions give the same result for the correction.[35,36] For small porosity the void-free bulk and shear moduli, B and G, may be written as

$$B \cong B_p\left(1+\delta\frac{3B_p+4G_p}{4G_p}\right) \tag{15}$$

and

$$G \cong G_p\left(1+\delta\frac{15B_p+20G_p}{9B_p+8G_p}\right), \tag{16}$$

where B_p and G_p are the moduli measured in the porous material.

The porosity corrections throughout the entire temperature range of the experiment were made in the same manner. Taking into account both the rms error in the RUS fit and that estimated for the density measurements, the resulting overall error in the absolute values of the moduli were estimated. These errors are represented as error bars on the graphs presented below. The relative error for each material is, of course, quite small and is essentially indicated by the scatter in the data.

Figure 4.7 shows the porosity-corrected shear modulus over the range of 3-415 K for $LaAl_xNi_{5-x}$ (x = 0, 0.25, 0.50, 1.0). Figure 4.8 shows the porosity-corrected bulk modulus over the same range. With the RUS technique, the low-frequency modes are more dependent on shear than on compression, resulting in a higher uncertainty in the bulk modulus than in the shear, represented by the error bars in the figures. As noted previously, the other elastic moduli can be calculated from any two that are known. Figures 4.9 and 4.10 show Young's modulus and Poisson's ratio for all of the alloys. Because thermal expansion data below room temperature are not available for the $LaAl_xNi_{5-x}$ alloys, the results have not been corrected for thermal contraction; the room temperature dimensions and density were used in the analysis as well as the room temperature porosity. The sample dimensions and density are needed to calculate the elastic constants deduced from the measured frequencies. Taking into account the direct dimensional effects as well as the indirect effect

through the density, the computed C_{ij} vary inversely with the dimensions. As mentioned in Section 4.2, transition metals typically have a total thermal contraction of less than 0.2% on cooling from room temperature to 3 K.[16] Aluminum has a total thermal contraction of less than 0.5% on cooling from room temperature to 0 K.[17] Furthermore, the thermal expansion of alloys does not seem to differ much from that of the constituent elements. Assuming that the $LaAl_xNi_{5-x}$ alloys behave similarly, correcting for thermal contraction would add at most 0.5% to the low-temperature values. Similarly, the values at 415 K would be at most 0.5% lower with corrections for thermal expansion above room temperature.

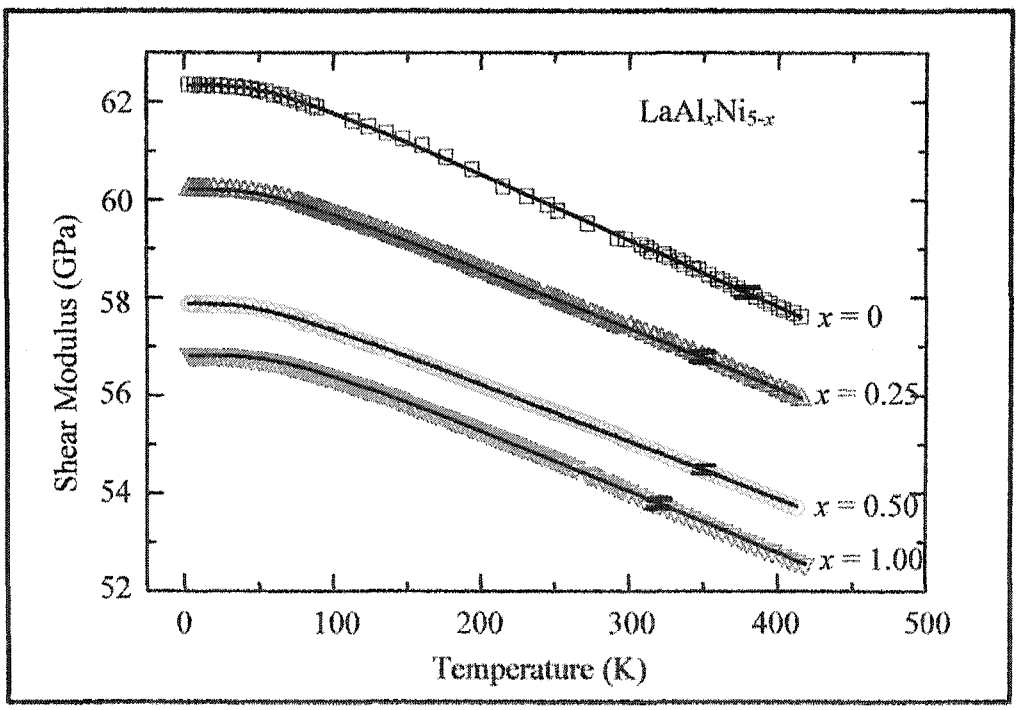

Fig. 4.7 Shear modulus versus temperature for $LaAl_xNi_{5-x}$. The solid lines represent a fit of the semi-empirical Varshni expression to the data. The fitting parameters are given in Table 4.1.

As described in Section 4.2, the adiabatic elastic constants are given by the second derivatives of the internal energy with respect to strain; thus, the temperature dependence of the lattice and electronic energies directly affects the temperature dependence of the C_{ij}. The overall result, for typical materials, is that the elastic moduli approach 0 K with zero slope and decrease monotonically with increasing temperature. Figs. 4.7, 4.8 and 4.9 show that the moduli of $LaAl_xNi_{5-x}$ behave in a normal fashion over the temperature range of the study, becoming linear in temperature at high temperature. Figure 4.10 gives Poisson's ratio, ν, which increases very slightly with increasing temperature. Both the value of $\nu \approx 0.30$ and the observed temperature dependence are characteristic of metals.[25,37]

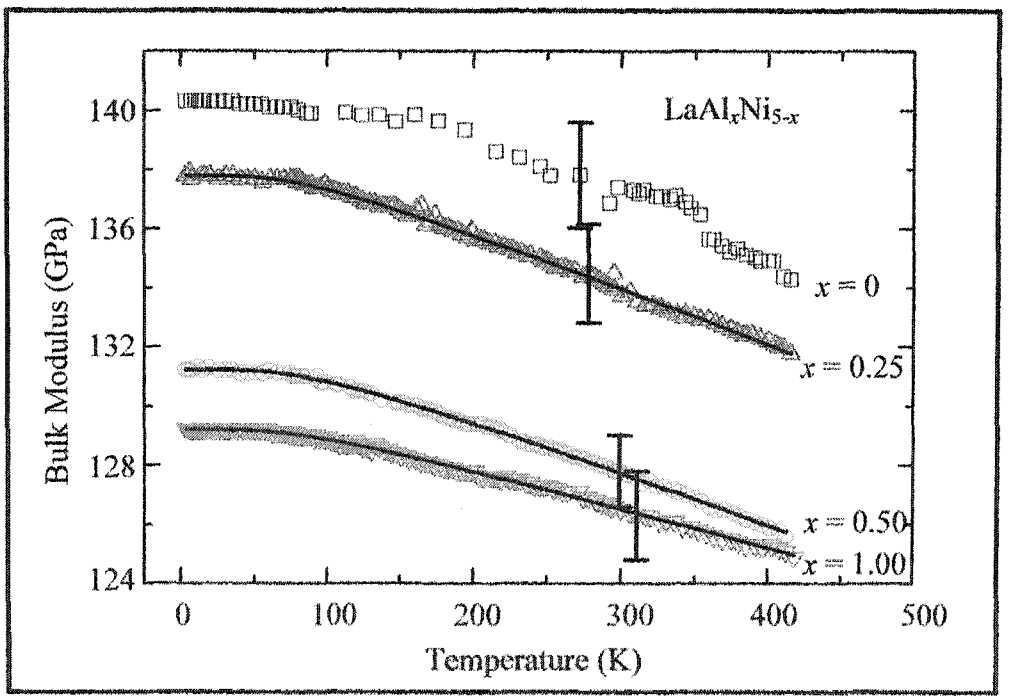

Fig. 4.8 Bulk modulus versus temperature for $LaAl_xNi_{5-x}$. The solid lines represent a fit of the semi-empirical Varshni expression to the data. The fitting parameters are given in Table 4.1.

In a purely harmonic lattice the elastic constants would be independent of temperature. Thus, in a qualitative sense, the temperature dependence reflects the anharmonic interactions. An examination of Figs. 4.7 – 4.9 shows that alloying $LaNi_5$ with Al has only a weak effect on the temperature dependence of the moduli, which indicates that the anharmonic interactions contributing to the elastic moduli must be similar in the two materials.

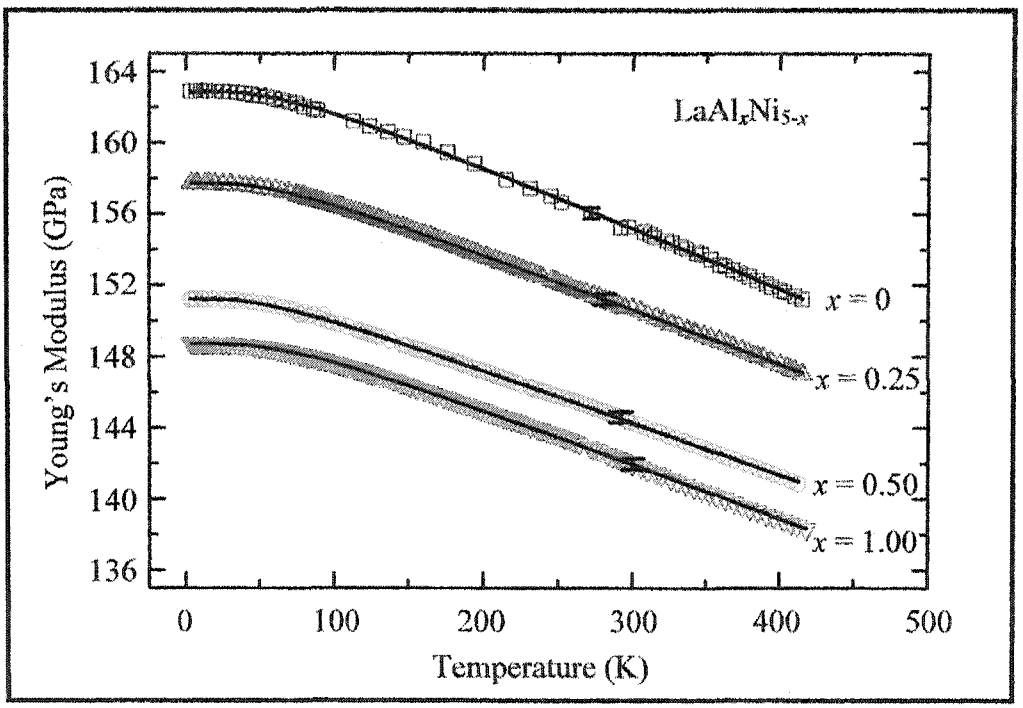

Fig. 4.9 Young's modulus versus temperature for $LaAl_xNi_{5-x}$. The solid lines represent a fit of the semi-empirical Varshni expression to the data. The fitting parameters are given in Table 4.1.

The solid lines in Figs. 4.7, 4.8 and 4.9 represent Varshni fits from Eq. (13) to the data for $LaAl_xNi_{5-x}$. The fitting parameters are reported in Table 4.1. Due to scatter in the bulk modulus for $LaNi_5$, a reliable Varshni fit was not obtained for this material. As the figures show, this simple expression does give a good account of the

temperature dependence of the moduli for the Al alloys. This provides additional evidence that the temperature dependence of the polycrystalline elastic moduli of $LaAl_xNi_{5-x}$ resembles that of many other materials. The moduli change at most 5 % on cooling from room temperature to 3 K.

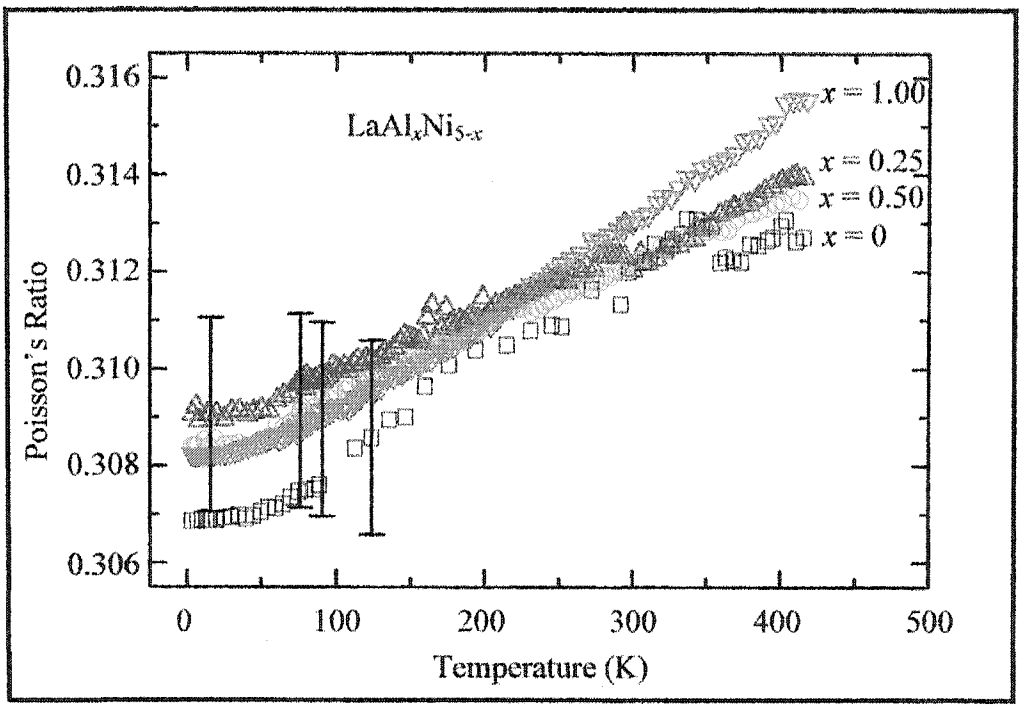

Fig. 4.10 Poisson's ratio versus temperature for $LaAl_xNi_{5-x}$.

The present measurement of the $x = 0$ polycrystalline value of the room temperature shear modulus is 59.2 GPa. The theoretical polycrystalline value is 53 GPa.[38] The single-crystal elastic constants of $LaNi_5$ have also been measured[39] from which a polycrystalline average[37] shear modulus of 55.5 GPa is calculated. All of these numbers appear to be in satisfactory agreement with each other. The corresponding measured value of the room temperature bulk modulus is 136.9 GPa. This value is in good agreement with the compressibility measurements of Brouha and

Buschow[40] for $LaNi_5$, which give a bulk modulus of 139 GPa. As Fig. 4.8 shows, Al substitution results in a decrease of the bulk modulus. Brouha and Buschow studied the $LaCo_xNi_{5-x}$ system. Their results indicated that the bulk modulus decreased with increasing x for Co substitution as well. The magnitude of the effect appears to be comparable for Co and Al substitution. The theoretical modulus[38] for polycrystalline $LaNi_5$ is 125 GPa, which is regarded as good agreement with our experimental value. The polycrystalline value calculated from the experimental single-crystal results[39] is 126.8 GPa. Neither the estimated measurement errors nor the density of the single-crystal were reported in Ref. 39, so that a further comparison with the single-crystal values is difficult.

Table 4.1 Fit parameters for the semi-empirical Varshni expression of Eq. (13) for $LaAl_xNi_{5-x}$. Fits were performed for the shear and Young's moduli with $x = 0$, 0.25, 0.50 and 1.00 and for the bulk moduli with $x = 0.25$, 0.50 and 1.00.

	x	$C(0)$ (GPa)	s (GPa)	t (K)
Shear	0	62.34	2.23	160.6
	0.25	60.21	1.96	157.6
	0.50	57.87	1.68	141.2
	1.00	56.82	2.46	190.6
Bulk	0.25	137.8	4.68	239.7
	0.50	131.2	4.73	257.2
	1.00	129.2	3.22	236.9
Young's	0	162.8	6.23	178.7
	0.25	157.7	5.14	164.2
	0.50	151.2	4.51	150.5
	1.00	148.7	6.12	194.3

Pressure-composition isotherms for hydride phase formation, introduced in Section 4.1, can be described by a lattice gas model with hydrogen-hydrogen interactions.[2,41] The major contribution to this interaction is usually taken to be the elastic interaction energy, $u_{elastic}$, which was derived in Section 4.2. Using the data

for the elastic moduli at room temperature, along with data for the lattice expansion upon absorption of hydrogen,[33,42] $u_{elastic}$ was calculated for $LaAl_xNi_{5-x}$. The results are presented in Table 4.2. The critical temperature for the isotherms is given by

$$T_c = \frac{ur}{4k_B} \tag{17}$$

where u is the total hydrogen-hydrogen interaction which includes $u_{elastic}$ and r is the number of interstitial sites per metal atom. The effective r is often somewhat less than the number of sites that might in principle be available[41] because occupancy of some sites blocks occupancy of nearby sites. The problem is particularly complicated in $LaAl_xNi_{5-x}$ because r may also depend on x. If we take u as $u_{elastic}$ (or directly proportional to $u_{elastic}$) then, as can be seen from the values recorded in Table 4.2, T_c decreases with increasing x only above $x = 0.25$. As is obvious from Fig. 4.1, the width of the pressure plateau decreases as the isotherm approaches T_c. Therefore a lowering of the critical temperature would also appear to shorten the length of the plateau, and hence decrease the hydrogen absorption capacity. The apparent unchanging value of $u_{elastic}$ between $x = 0$ and 0.25 should be regarded with caution. It arises because the available data indicate that v_H increases with x in this region, while it is a slowly decreasing function of x otherwise. It is intriguing to note, however, that E. Akiba *et al.*[43] have observed an increase of the hydrogen capacity in $LaAl_xNi_{5-x}$ when x increases from 0 to 0.25. H. Diaz *et al.*[44] have also reported an increase of the hydrogen capacity (and increase in the length of the plateau pressure) in the $x = 0.1$ compound relative to the $x = 0$ compound. A significant decrease in the hydrogen absorption capacity in $LaAl_xNi_{5-x}$ occurs for $x > 0.25$. Our results seem to be consistent with the idea that the hydrogen capacity may increase up to $x = 0.25$, but

decrease above that value. The elastic interaction energy, being dependent on the bulk modulus, is also weakly temperature-dependent, as was shown in Fig. 4.5 for $TiCr_{1.8}$.[45]

The values of C_{11} and G at 3 K have been used to calculate c_0, θ_D, and the vibrational contribution to the low-temperature specific heat, c_v/T^3, for $LaAl_xNi_{5-x}$. These values are reported in Table 4.2. The Debye temperature ranges from 370 to 375 K, which is in good agreement with heat capacity measurements[46] where the results ranged from 351 to 358 K for the same range of x. The difference between the two sets of Debye temperatures is at most 6.8%. (The present acoustic values, based on the low-temperature moduli, are about 3 % higher than those reported earlier based on the room-temperature moduli.[34] The present values are to be preferred.) The heat

Table 4.2 The elastic interaction energy calculated from room temperature values and the average sound velocity, Debye temperature and acoustic contribution to the low-temperature specific heat, calculated from the 3 K elastic moduli for $LaAl_xNi_{5-x}$.

x	$u_{elastic}$ (eV)	c_0 (m/s)	θ_D (K)	c_v/T^3 (J/(mol K^4))
0	0.232	3.07×10^3	375	2.21×10^{-4}
0.25	0.232	3.06×10^3	373	2.25×10^{-4}
0.50	0.194	3.04×10^3	370	2.31×10^{-4}
1.00	0.187	3.11×10^3	375	2.21×10^{-4}

capacity measurements[46] report values for the electronic specific heat constant, λ, at low-temperature. These values can be used along with our values for the phonon contribution, $A = c_v/T^3$, to find the total specific heat,

$$c(T) = \lambda T + AT^3. \qquad (18)$$

As would be expected, the first term dominates at very low temperature with the second term crossing over and dominating at a few Kelvin (5 K for $LaNi_5$).

4.3.3 Conclusions

Using a hot isostatic pressing technique, polycrystalline samples of $LaAl_xNi_{5-x}$ suitable for ultrasonic measurements have been produced. The elastic moduli of samples with x ranging from 0 to 1 were determined over the range of 3-415 K. The results were corrected for porosity so that values expected for the fully-dense material were found. The temperature-dependence resembles that of ordinary metals, with no indication of a phase change or unusual electronic effects. Poisson's ratio was independent of x within experimental error and remained nearly temperature-independent with a value around 0.31. The Debye temperatures were calculated from the 3 K moduli and were in good agreement with values reported from heat capacity measurements. The acoustic contribution to the low-temperature specific heat was also calculated and compared with the electronic contribution reported in the literature.

For both of the materials, $TiCr_{1.8}$ and $LaAl_xNi_{5-x}$, the elastic interaction energy of one interstitial hydrogen atom with the strain field of all the other hydrogen atoms was calculated. The critical temperature of hydride formation is proportional to this energy. The information reported here should prove useful to theorists in calculations of electronic structure and should add to the fundamental understanding of the processes of hydride formation.

References

[1] F. Cuevas, J. -M. Joubert, M. Latroche and A. Percheron-Guégan, Appl. Phys. A **72**, 225 (2001).

[2] Y. Fukai, *The Metal-Hydrogen System* (Springer, Berlin, 1993).

[3] J. D. Eshelby, Proc. R. Soc. London Ser. A **241**, 376 (1957).

[4] J. D. Eshelby, in *Progress in Solid Mechanics*, I. N. Sneddon and R. Hill, eds. (North-Holland, Amsterdam, 1961).

[5] G. Alefeld, Ber. Bunsen-Gesellschaft **76**, 746 (1972).

[6] H. Peisl, in *Hydrogen in Metals I*, G. Alefeld and J. Völkl, eds. (Springer-Verlag, Berlin, 1978).

[7] G. Alers, in: *Physical Acoustics, Vol. IIIB*, W. P. Mason, ed. (Academic Press, New York, 1965).

[8] O. L. Anderson, in: *Physical Acoustics, Vol. IIIB*, W. P. Mason, ed. (Academic Press, New York, 1965).

[9] O. Beeri, D. Cohen, Z. Gavra, J.R. Johnson, M.H. Mintz, J. Alloys Comp. **267**, 113 (1998).

[10] O. Beeri, D. Cohen, Z. Gavra, J.R. Johnson, M.H. Mintz, J. Alloys Comp. **293-295**, 14 (1999).

[11] A. Migliori, J. L. Sarrao, W. M. Visscher, T.M. Bell, Ming Lei, Z. Fisk, and R. G. Leisure, Physica B **183**, 1 (1993).

[12] A. Migliori and J. L. Sarrao, *Resonant Ultrasound Spectroscopy*, (Wiley, New York, 1997).

[13] R. G. Leisure and F. A. Willis, J. Phys.: Condens. Matter **9**, 6001 (1997).

[14] J. R. Johnson and J. J. Reilly, Inorganic Chem. **17**, 3103 (1978).

[15] J. H. Zhu, P. K. Liaw, C. T. Liu, Proceedings of the 13th Annual Conference on Fossil Energy Materials, 4.7 (1999).

[16] G. K. White, *Experimental Techniques in Low-Temperature Physics*, (Clarendon Press, Oxford, 1959).

[17] Y. S. Touloukian, R. K. Dirby, R. E. Taylor, P. D. Desai, in *Thermophysical Properties of Matter Vol. 12*, (IFI/Plenum, New York, 1975).

[18] J. A. Garber and A. V. Granatao, Phys. Rev. B **11**, 3990 (1975).

[19] G. A. Alers, in *Physical Acoustics Vol. IV Part A*, W. P. Mason ed. (Academic Press, New York, 1966).

[20] W. L. Rehwald, Adv. Phys. **22**, 721 (1973).

[21] F. Willis and R. G. Leisure, Phys. Rev. B **54**, 9077 (1996).

[22] C. Weinmann and S. Steinemann, Sol. State. Commun. **15**, 281 (1974).

[23] K. Foster, J. E. Hightower, R. G. Leisure, and A. V. Skripov, Phil. Mag. B **80**, 1667 (2000).

[24] K. Foster, J. E. Hightower, R. G. Leisure, and A. V. Skripov, Phys. Rev. B **65**, 094108 (2002).

[25] H. M. Ledbetter, in *Materials at Low Temperatures*, R. P. Reed and A. F. Clark, eds. (Metals Park, Ohio: American Society for Metals, 1983), p.1.

[26] Y. P. Varshni, Phys. Rev. B **2**, 3952 (1970).

[27] J. F. Lynch, J. R. Johnson and J. J. Reilly, Z. Phys. Chem. N. F. **117**, S. 229 (1979).

[28] Y. Fukai, private communication.

[29] M. Sluiter and P. E. A. Turchi, Phys. Rev. B **43**, 12251 (1991).

[30] L. Schlapbach, in *Hydrogen in Intermetallic Compounds II* (Springer, Berlin, 1992).

[31] M. L. Wasz, P. B. Desch and R. B. Schwarz, Phil. Mag. A **74**, 15 (1996).

[32] J. –C. Achard, A. –J. Dianoux, C. Lartrigue, A. Percheron-Guégan and F. Tasset, in *The Rare Earths in Modern Science and Technology*, G. J. McCarthy, H. B. Silber and J. J. Rhyne, eds. (New York, 1982).

[33] J. –M. Joubert, M. Latroche, R. Cerný, R. C. Bowman, Jr., A. Percheron-Guégan and K. Yvon, J. Alloys Compd. **293-295**, 124 (1999).

[34] M. Bereznitsky, A. Ode, J. E. Hightower, O. Yeheskel, I. Jacob and R. G. Leisure, J. Appl. Phys. **91**, 5010 (2002).

[35] J. K. Mackenzie, Proc. Phys. Soc. B **63**, 2 (1950).

[36] H. Ledbetter, M. W. Austin, S. A. Kim and Ming Lei, J. Mater. Res. **2**, 786 (1987).

[37] G. Simmons and H. Wang, *Single Crystal Elastic Constants and Calculated Aggregate Properties* (MIT Press, Cambridge, MA, 1971).

[38] L. G. Hector, Jr., J. F. Herbst and T. W. Capehart, J. Alloys Compd. **353**, 74 (2003).

[39] K. Tanaka, S. Okazaki, T. Ichitsubo, T. Yamamoto, H. Inui, M. Yamaguchi and M. Koiwa, Intermetallics **8**, 613 (2000).

[40] M. Brouha and K. H. J. Buschow, J. Phys. F: Met. Phys. **5**, 543 (1975).

[41] G. Song, M. Geitz, A. Abromeit and H. Zabel, Phys. Rev. B **54**, 14093 (1996).

[42] Y. Nakamura and E. Akiba, J. Alloys Compd. **308**, 309 (2000).

[43] E. Akiba, H. Hayakawa, Y. Ishido, K. Namura, S. Shin and T. Minesawa, *Materials Research Society Meeting on Advanced Materials Vol. 2* (MRS, Pittsburgh, PA, 1989) p. 39.

[44] H. Diaz, A. Percheron-Guégan, J. C. Achard, C. Chatillon and J. C. Mathieu, in *Hydrogen in Energy Systems*, T. N. Veziroglu and W. Seifritz, eds. (Pergamon, New York, 1979).

[45] J. E. Atteberry, D. S. Agosta, R. G. Leisure, O. Beeri and M. H. Mintz, J. Alloys Compd. **365**, 68 (2004).

[46] Y. Chung, T. Takeshita, O. D. McMasters and K. A. Gschneidner Jr., J. Less-Common Met. **74**, 217 (1980).

Chapter 5

Conclusions

Resonant ultrasound spectroscopy (RUS) has been used to study four different hydrogen-absorbing intermetallic compounds. A fundamental study of the properties of hydrogen motion within a host metal lattice was undertaken on two different $C15$ Laves-phase compounds. The H motion within these materials has shown unusual behavior, with two frequencies of motion and strong effects on the frequency upon the substitution of deuterium for hydrogen. These results were obtained by determining the ultrasonic attenuation as a function of temperature from low temperatures (~0.5 K) up to room temperature and above. The hydrogen-absorbing compound, $TiCr_{1.8}$, was studied in order to investigate the elastic contribution to the hydrogen-hydrogen interaction energy, an important parameter for the stability of a metal-hydride. In a similar study, the technologically important intermetallic compound, $LaNi_5$, was studied along with alloys having Ni substituted with various amounts of Al. The temperature-dependence of several polycrystalline elastic moduli were determined from 3-410 K for $TiCr_{1.8}$ and from 3-415 K for the La-Al-Ni alloys and used to estimate the temperature-dependence of the elastic energy and various parameters derived through Debye theory.

Earlier work on TaV_2 loaded with several different H and D concentrations prompted the further study of this interesting system. Ultrasonic techniques were

used to study H(D) motion in $TaV_2H_{0.18}$, $TaV_2D_{0.17}$ and $TAV_2D_{0.50}$, providing strong evidence for the local quantum tunneling of hydrogen in Laves-phase materials, motion that remains extremely fast even at very low temperatures. This study also provides details concerning the diffusive motion of hydrogen. The magnitude of the ultrasonic loss for the hexagon-to-hexagon hopping, the rate-limiting step for long-range diffusion, was found to be linear in D concentration, as was previously found for H. The parameter describing the coupling between inter-hexagon *g* sites and strain had the value 0.17 eV for both isotopes. The relaxation rate for H(D) motion exhibited a small isotope effect and was well described by an Arrhenius-type expression. The single-term relaxation time indicated that the mechanism for this motion is dominated by phonon-assisted tunneling between excited states, for temperatures above ~ 200 K.

In marked contrast to these high-temperature peaks, much weaker peaks were observed at lower temperatures that exhibited totally non-classical behavior. These peaks were attributed to motion within a hexagon of *g* sites. The relaxation rate was satisfactorily described by a non-classical expression, similar to the results from a barrier fluctuation model in the theory of quantum tunneling. The parameters used to describe the relaxation rate for $TaV_2D_{0.50}$ were the same as those used to describe NMR spin-lattice relaxation measurements at higher temperatures on the same material. The relaxation rate for $TaV_2D_{0.17}$ was somewhat faster than that for $TaV_2D_{0.50}$, in agreement with the concentration dependence found from NMR experiments. Also in qualitative agreement with NMR measurements, the relaxation rate for H was over an order of magnitude faster than that for D for similar concentrations. Within

experimental error, the same value of 0.1 eV was found for all three materials for the coupling parameter between intra-hexagon g sites and strain. No information about this coupling parameter was previously available.

Previously undetected attenuation peaks, not associated with the local or long-range motion of H(D), were observed at intermediate temperatures in the $TaV_2H(D)_x$ materials and attributed to an order-disorder transition of H(D) atoms among the interstitial sites. These peaks provide experimental evidence for an earlier suggestion that the temperature-dependent mobile population is related to ordering.

Along with NMR results in publication, these are the first parameters reported for H(D) motion in TaV_2 at such low concentrations. The ultrasonic measurements are particularly well-suited for studies of low-concentration interstitial atom diffusion, being extremely sensitive to anelastic relaxation. The low-temperature loss peak due to the local motion of hydrogen had not been seen previously. Although this indicated a strong isotope effect, it was only possible to speculate as to why this peak had not been seen. The current study has taken advantage of the sensitivity of the measurements by succeeding in lowering the overall background loss and decreasing the scatter in the data. The resulting observation of the low-temperature peak for $TaV_2H_{0.18}$ provides convincing details concerning the local motion of hydrogen, including parameters for the extremely fast hydrogen motion and a consistent explanation of the strong isotope effect.

Ultrasonic measurements also were made on the Laves-phase compound $ZrCr_2H(D)_x$ over the temperature range of 5-295 K. Concentrations of hydrogen and deuterium were $x(H) = 0.09$, 0.15 and 0.31 and $x(D) = 0.12$ respectively. Attenuation

peaks associated with H(D) motion between *g*-site hexagons were observed in all of these materials for measurement frequencies of approximately 1.5 MHz. The peaks were centered at 50-75 K for H motion, while the peak for D motion was centered at 160 K. This strong isotope effect has been interpreted in terms of quantum mechanical mechanisms of diffusion. In the temperature range of our measurements, the dominant mechanism appears to be tunneling transitions between ground states. A two-term Arrhenius process has been proposed to explain NMR results for $ZrCr_2$ at higher temperatures, with one term corresponding to tunneling between ground states and the other to tunneling between excited states. The current results provide strong confirmation of the idea of a two-term Arrhenius process. Tunneling between ground states has been discussed theoretically for a two-level system, which is an appropriate description of an interstitial atom such as hydrogen occupying either of two nearby sites. However, there has been very little evidence indicating the existence of this mechanism for motion. The current results provide strong evidence for this novel mode of hydrogen diffusion. The shear modulus of $ZrCr_2H_{0.09}$, $ZrCr_2H_{0.15}$ and $ZrCr_2D_{0.12}$ was also measured. The overall temperature-dependence was similar to that of typical metals. A small shift was observed in the modulus for each material at a temperature corresponding to the relevant peak in the ultrasonic loss, which is consistent with the interpretation that these peaks were due to H(D) relaxation. These are the first measurements comparing hydrogen motion to deuterium motion in $ZrCr_2$. The observed isotope effects are a clear indication of quantum behavior in the long-range diffusive motion of H(D) in this Laves-phase material.

The results for TaV_2 and $ZrCr_2$ provide insight into the complicated behavior of hydrogen motion in Laves-phase intermetallic compounds. Quantum mechanical motion with an Arrhenius-type appearance was observed for the long-range motion in each material. It has been shown that the particular mechanism that dominates is dependent on the system and the temperature of the measurements. NMR results for $ZrCr_2H_x$ over the range of 130-430 K revealed a change in the activation energy below 200 K, and thus a change in the dominant diffusion mechanism. Our measurements, in the range of 4-200 K, confirmed this interpretation with tunneling between ground states being the dominant mechanism for the long-range motion of hydrogen in $ZrCr_2$. The short-range motion of hydrogen in TaV_2 remains extremely fast down to very low temperatures and does not have an Arrhenius-type appearance. This motion may be due to barrier fluctuations. A consistent picture was used to describe the results in the $TaV_2H(D)_x$ and the $ZrCr_2H(D)_x$ systems.

In a more applied study, the elastic moduli of polycrystalline $TiCr_{1.8}$ were measured over the temperature range of 3–410 K. The temperature-dependence resembled that of ordinary metals, approaching 0 K with zero slope and decreasing linearly with temperature at higher temperatures. The modulus measurements, along with other data from the literature, were used to calculate the long-range, elastic interaction between absorbed hydrogen atoms. This interaction is weakly temperature dependent, having essentially the temperature-dependence of the bulk modulus. Measurements such as these are becoming increasingly important for a complete understanding of hydrogen-metal materials. The use of the elastic moduli, measured in this work, to evaluate elastic energy contributions to hydrogen-hydrogen

interactions is a valuable addition to the growing emphasis on a fundamental understanding of these systems. Expressed as a linear function of the H/(Ti + Cr) ratio, the interaction parameter decreases from 0.182 eV per H atom at 3 K to 0.172 eV per H atom at 410 K and represents a negative contribution to the enthalpy of formation of the hydride. Comparison of the elastic contribution to thermodynamic measurements indicated a positive electronic contribution of the heat of formation of about 0.116 eV per H atom near room temperature. This information should be useful to theorists who do electronic structure calculations. The Debye temperature, calculated from the low-temperature elastic moduli, was found to be 500 K.

Temperature-dependent measurements also were made on polycrystalline $LaAl_xNi_{5-x}$ with x ranging from 0 to 1. The elastic moduli were determined over the range of 3-415 K. The results were corrected for porosity so that values expected for the fully-dense material were found. The temperature-dependence resembled that of ordinary metals, with no indication of a phase change or unusual electronic effects. The similar temperature-dependence observed in each of the studied materials indicates that the anharmonic nature of the interatomic potentials for each material is similar as well. The present measurements of the $x = 0$ polycrystalline room-temperature shear and bulk moduli were 59.2 GPa and 136.9 GPa, respectively. Theoretical values for the shear and bulk moduli are regarded to be in good agreement with our experimental values. Poisson's ratio remained nearly temperature-independent with a value around 0.31. The Debye temperatures were calculated from the 3 K moduli and were in good agreement with values reported from heat capacity measurements. The acoustic contribution to the low-temperature specific heat was

also calculated and compared with the electronic contribution reported in the literature. The effect of Al substitution in $LaNi_5$ is to expand the lattice, decrease the bulk modulus and lower the plateau pressure. The results of this work should prove useful in discerning trends or correlations that could help in the selection of new metal-hydride materials.

These four studies illustrate the power of resonant ultrasound spectroscopy to investigate fundamental physical properties and to contribute to an understanding of materials that have technological importance. This dissertation increases the understanding of quantum mechanical effects observed in the diffusion of light interstitial atoms. It also reports various elastic and thermal parameters that influence the productivity and viability of hydrogen-absorbing compounds currently used in technology.